

XX(125786.1)



CINVESTAV

*Centro de Investigación y de Estudios Avanzados del IPN
Unidad Guadalajara*

Modelado de Líneas de Transmisión No Uniformes para el Análisis de Transitorios

Electromagnéticos

**CINVESTAV
IPN
ADQUISICION
DE LIBROS**

Tesis que presenta
Pablo Gómez Zamorano

Para obtener el grado de
Doctor en Ciencias

En la Especialidad de
Ingeniería Eléctrica
CINVESTAV I.P.N.
SECCION DE INFORMACION
Y DOCUMENTACION

Guadalajara, Jalisco, Agosto 2005

CLASIF.: TK165,58.566.2005
ADQUIS.: SSI - 381
FECHA: 28 VI. 2006
PROCED.: DON-2006
\$

ID, 125370 - 2001



CINVESTAV

*Centro de Investigación y de Estudios Avanzados del IPN
Unidad Guadalajara*

Non Uniform Transmission Line Modeling for Electromagnetic Transient Analysis

CINVESTAV

IPN

**ADQUISICION
DE LIBROS**

Thesis submitted by
Pablo Gómez Zamorano

For the degree of
Doctor of Sciences

In the specialty of
Electrical Engineering

Guadalajara, Jalisco, August 2005

Modelado de Líneas de Transmisión No Uniformes para el Análisis de Transitorios Electromagnéticos

**Tesis de Doctorado en Ciencias
Ingeniería Eléctrica**

Por

Pablo Gómez Zamorano

Ingeniero Mecánico Electricista
Universidad Autónoma de Coahuila
1994-1999

Maestro en Ciencias en Ingeniería Eléctrica
Centro de Investigación y de Estudios Avanzados del I.P.N.
2000-2002

Becario de CONACyT expediente No. 157984

Director de Tesis

Dr. Pablo Moreno Villalobos

CINVESTAV del IPN Unidad Guadalajara, Agosto 2005

Non Uniform Transmission Line Modeling for Electromagnetic Transient Analysis

**Doctor of Sciences Thesis
Electrical Engineering**

By
Pablo Gómez Zamorano

Mechanical and Electrical Engineer
Universidad Autónoma de Coahuila
1994-1999

Master of Sciences in Electrical Engineering
Centro de Investigación y de Estudios Avanzados del I.P.N.
2000-2002

Thesis Advisor
Dr. Pablo Moreno Villalobos

CINVESTAV del IPN Unidad Guadalajara, August 2005

Resumen

En esta tesis se discute la dependencia frecuencial y espacial de líneas de transmisión, así como el efecto de campos electromagnéticos incidentes.

Se consideran y comparan dos métodos en el dominio de la frecuencia para el análisis de líneas multiconductoras no uniformes. El primer método se basa en la conexión cascada de matrices cadena o ABCD de secciones de línea uniforme. El segundo método consiste en la solución de un sistema lineal variante en espacio con los elementos de la matriz cadena como estados del sistema. Para resolver este sistema se evalúan varias técnicas de integración numérica.

Adicionalmente, el modelo de líneas de transmisión no uniformes en el dominio de la frecuencia se extiende a la inclusión del efecto de campos incidentes. El procedimiento consiste en calcular fuentes equivalentes concentradas, las cuales se conectan al extremo receptor de la línea sin excitación. Para obtener las soluciones en el dominio del tiempo se aplica la Transformada Numérica de Laplace.

Finalmente se presenta un nuevo modelo en el dominio del tiempo para analizar líneas monofásicas no uniformes con parámetros eléctricos dependientes de la frecuencia. Este modelo está basado en la síntesis de una línea uniforme equivalente a partir de la matriz cadena de una línea no uniforme. Las dependencias frecuencial y espacial de la línea se incorporan a los parámetros transitorios de la línea uniforme (resistencia y conductancia). Las ecuaciones resultantes de la línea de transmisión se resuelven empleando el Método de Características.

Se incluyen varios ejemplos de aplicación, los cuales se validan mediante comparaciones con resultados obtenidos empleando el ATP/EMTP y resultados experimentales publicados por otros autores.

Abstract

In this thesis, the frequency and space dependence of the electrical parameters of transmission lines are discussed, as well as the effect of incident electromagnetic fields.

First, two methods in the frequency domain for analyzing non-uniform multiconductor lines are considered and compared. The first one is based on the cascaded connection of chain or ABCD matrices of uniform line segments. The second method consists of solving a space variant linear system with the chain matrix elements as system states. To solve this system, several techniques of numerical integration are evaluated.

In addition, the frequency domain model for non-uniform transmission lines is extended to include the effect of incident fields. The procedure consists of computing equivalent lumped sources which are connected at the receiving end of the unexcited line. To obtain the time domain solutions, the Numerical Laplace Transform is used.

Finally, a new time domain model for analyzing single-phase non-uniform lines with frequency dependent electrical parameters is presented. This model is based on synthesizing an equivalent uniform line from the chain matrix of a non-uniform line. The space and frequency dependence are incorporated into the uniform line's transient parameters (resistance and conductance). The resultant transmission line equations are solved using the Method of Characteristics.

Several application examples are included and validated through comparisons with results obtained with the ATP/EMTP and experimental measurements published elsewhere.

Acknowledgments

Special thanks to...

...God, for letting me reach this point of my life.

...my thesis advisor, Dr. Pablo Moreno, for all his help and encouragement, and especially for his friendship.

...Dr. José Luis Naredo for introducing me to the world of electromagnetic transients and for his wise counsel and support.

...the other members of the comitee: Dr. Abner Ramirez, Dr. Juan Manuel Ramirez and Dr. Ricardo Mota for their invaluable suggestions.

...my colleagues and friends from CINVESTAV, as well as the academic and administrative staff.

...my siblings Lauren and Ruben for their love and support, and my niece Marian for thinking that I'm 4 years old too.

...my aunts Guadalupe Zamorano and Guadalupe Chaparro for all their assistance and care.

...my dear girlfriend Erika for her inspiring and loving presence in my life and for being so supportive and patient when I was only thinking about transmission lines.

...the National Council of Science and Technology (CONACyT) for the financial support to complete my graduate studies.

Lastly, and most importantly, I wish to thank my parents, Pablo Gomez and Yolanda Zamorano, for their unconditional love and for always being there for me. To them I dedicate this thesis.

Index

Resumen	i
Abstract	ii
Acknowledgments	iii
Index	iv
List of Figures	vii
List of Tables	ix
1 Introduction	1
1.1 Background	1
1.2 Problem Statement	4
1.3 Scope	5
2 Non-uniform Lines	6
2.1 Introduction	6
2.2 Solution to the line equations	7
2.3 Cascaded Connection of Chain Matrices	9

2.4	Derivation of the Chain Matrix	10
2.4.1	Taylor Series Expansion	11
2.4.2	Modal Decomposition	12
2.4.3	Padè Approximation	12
2.4.4	Sylvester Formula	13
2.5	Applications	13
2.5.1	River Crossing	14
2.5.2	Tower Model Using Non-uniform Lines	16
2.6	Conclusions	17
3	Field Excited Lines	20
3.1	Introduction	20
3.2	Incident Field Representation	21
3.2.1	Distributed Sources	21
3.2.2	Lumped Sources	22
3.2.3	Modified Nodal Analysis	23
3.3	Applications	24
3.3.1	Field excited Distribution Line with Propagation in the $-y$ Direction	25
3.3.2	Incident Field with Propagation in the x Direction	26
3.4	Conclusions	27
4	Time Domain Analysis of Non-uniform Lines	28
4.1	Introduction	28
4.2	Transient Parameters of a Non-uniform Line	29
4.3	Telegrapher Equations in Time Domain	30
4.4	Method of Characteristics	31
4.5	Numerical Solution	33
4.5.1	Numerical Treatment of the Recursive Convolutions	33
4.5.2	Internal Points	35
4.5.3	Boundary Points	39
4.5.4	Applications	41
4.6	Numerical Solution with One Internal Point	46

4.6.1	Internal Point	46
4.6.2	Boundary Points	49
4.6.3	Applications	51
4.7	Conclusions	52
5	Conclusions	54
5.1	Summary of Results	54
5.2	Recommendations for Future Research	55
6	References	57
Appendix A : The Numerical Laplace Transform		63
A.1	Introduction	63
A.2	Analysis of Errors	63
A.3	Discretization of the Laplace Transform Pair	67
Appendix B : Computation of the Line Electrical Parameters		68
B.1	Introduction	68
B.2	Longitudinal Impedance Matrix	68
B.2.1	Geometric Impedance	68
B.2.2	Earth Return Impedance	70
B.2.3	Conductor Impedance	71
B.3	Transversal Admittance Matrix	71
Appendix C : Published Work		72

List of Figures

Figure 2.1. Cascaded connection of chain matrices.	10
Figure 2.2. River crossing profile.	14
Figure 2.3. Voltage at phase B of the receiving node.	16
Figure 2.4. Voltage at phase B of the receiving node.	16
Figure 2.5. Waveform of the current source injected to the tower.	17
Figure 2.6. (a) Transmission tower. (b) Tower representation with non-uniform line segments.	18
Figure 2.7. Voltage at the injection point of the tower..	18
Figure 3.1. Field excited NUL configuration	22
Figure 3.2. Representation of a field excited line segment	22
Figure 3.3. Field excited line representation through equivalent sources.	24
Figure 3.4. Representation of a transmission line with incident field excitation through MNA.	24
Figure 3.5. Induced voltages at the ends of the line central conductor.	25
Figure 3.6. Induced voltages at the ends of the line central conductor	26
Figure 3.7. Induced voltages at the ends of the line central conductor.	26
Figure 4.1. Characteristics grid – Internal points.	36
Figure 4.2. Characteristics grid: (a) source boundary, (b) load boundary.	39
Figure 4.3. Voltage at the receiving end of the line.	42
Figure 4.4. Transient resistance for the sagging between towers (in ohms).	42
Figure 4.5. Transient conductance for the sagging between towers (in Siemens).	42
Figure 4.6. Voltage at the left hand side of the river crossing profile.	43
Figure 4.7. Transient resistance for the river crossing (in Ohms).	43
Figure 4.8. Transient conductance for the river crossing (in Siemens).	43
Figure 4.9. Winding representation using line segments.	44

Figure 4.10. Voltage at node B of the winding.	44
Figure 4.11. Transient resistance for the machine winding (in Ohms).	45
Figure 4.12. Transient conductance for the machine winding (in Siemens).	45
Figure 4.13. Characteristics grid with one internal point.	47
Figure 4.14. Comparison of methods.	52
Figure 4.15. Configuration of the NUL.	52
Figure 4.16. Voltage at the receiving end of the line.	53
Figure A.1. Errors obtained with 4 different windows (1 cycle).	65
Figure A.2. Errors obtained with 4 different windows (3 cycles).	65
Figure A.3. Errors obtained with $c = 2\Delta\omega$ (Wilcox).	66
Figure A.4. Errors obtained with $c = \ln(N^2)/T$ (Wedepohl).	66
Figure B.1. Method of images.	69
Figure B.2. Representation of the complex penetration depth: (a) earth return (b) conductor.	70

List of Tables

Table 2.1. Results of Method 1.	15
Table 2.2. Results of Method 2.	15
Table 2.3. Tower Data	18
Table 4.1. Winding Data	45

1 Introduction

1.1 Background

The fundamental causes of electromagnetic transients in power systems are switching operations, faults and lightning. The consequential phenomena are traveling waves in transmission lines or cables and oscillations due to the energy interchange between inductances and capacitances of the system. Electromagnetic transients cause overvoltages that can be dangerous to the power system. Characteristics of these overvoltages, such as amplitude, frequency and point of occurrence have an effect on the insulation design of transmission lines, the selection of equipment and the system operation. Therefore, a deep knowledge of these disturbances is very important for designing and coordinating the protection of power systems.

For systems of less than 230 kV, the insulation level is determined primarily for protection against lightning; for systems between 230 and 700 kV, both lightning and switching events are considered for the insulation design; and for systems above 700 kV, switching overvoltages are the fundamental factor in the selection of the insulation level.

Typical examples of switching transients are the energization or reclosure of transmission lines, as well as faults occurrence and clearance. In the case of lightning transients, these can be due to direct or indirect strokes. Direct strokes usually affect the conductors and towers of transmission systems. In a well designed transmission system, ground conductors are the ones normally hit by direct lightning strokes. However, when the phase conductors are hit by the stroke, the consequent overvoltages can be in the order of 1 MV, and even if the ground wires are the only ones affected by the stroke, the electromagnetic induction can generate large overvoltages. On the other hand, indirect strokes, this is, strokes that hit the proximity of the transmission line, produce incident electromagnetic fields and since these events are more common than the direct strokes, the consequent overvoltages are one of the most important issues for the design and coordination of distribution systems.

Modeling of transmission lines for the analysis of electromagnetic transients has been a topic of large significance and expansion in the last decades. Early line models were based on the lossless case, for which the line equations are just a particular case of the Wave Equation. D'Alembert solution to this equation in terms of traveling waves is well known and is the basis for the Bergeron model, which was originally developed for analyzing hydraulic systems in 1949 and was later adapted to transmission lines [1].

In 1968, Dommel developed a program based on the Bergeron model for the solution of electromagnetic transients in time domain [2]. This is the well known "Electromagnetic Transient Program" (EMTP) which allows a highly efficient simulation of transient conditions in power systems, as well as the inclusion of control elements. Later on, alternative versions to the EMTP emerged, as the "Alternative Transient Program" (ATP) developed by Meyer in 1974 and the "Electromagnetic Transients for Direct Current" (EMTDC) initially developed by Woodford in 1975.

As an electromagnetic wave propagates along a transmission line, its shape suffers a gradual distortion due to the fact that the different frequency components of the wave travel at different speeds and with different attenuations. Hence, one of the most important aspects in modeling transmission lines has been the inclusion of these frequency dependent effects for time domain transient studies. Since the early 1970's, several approaches have been developed, and some of them have found their use in general simulation programs such as ATP and EMTDC.

The first two works that included the frequency dependence of the electrical parameters on a single-phase transmission line for time domain analysis were presented by Budner [3] and Snelson [4] in 1970 and 1972, respectively. Both models are based on a 2-port representation and the solution of the propagation equations is carried out by means of long convolutions between weighting functions of the transfer matrix and the corresponding voltages and currents.

In 1974, Meyer and Dommel applied the technique of long convolutions, developed by Snelson, to include frequency dependence in the transmission line model of the EMTP [5]. Since this program is based on the trapezoidal integration rule, the convolutions are numerically solved using this rule. Semlyen and Dabuleanu proposed in 1975 a method of recursive solution; this technique, along with modal analysis using real and constant transformation matrices, was applied to the modeling of multiconductor lines [62].

In 1982, J. R. Marti proposed a model in which both line terminals are connected to a network representing its characteristic impedance for an specific frequency range [6]. With this technique, difficulties in the accurate determination of the weighting functions are greatly reduced. The characteristic impedance and the propagation function are synthesized using rational functions whose poles and zeros are obtained using Bode's method. However, the modal

transformation matrices are considered as real and constant, which precludes the application of this method in representing unbalanced or untransposed lines for which the transformation matrices are highly frequency dependent. To overcome this problem, L. Marti proposed in 1988 a technique to take into account the frequency dependence of the modal transformation matrices [7]. Unfortunately, the method was implemented for underground cables and its extension to overhead lines has not been successful to this day.

Gustavsen and Semlyen introduced in 1998 a powerful technique called Vector Fitting [8]. This technique allows the rational fitting of frequency domain responses of a matrix column-by-column, which results in substantial computer time savings. Besides, the poles and residues can be complex, which is very useful when fitting non-smooth functions, such as the elements of the transformation matrix and the modal characteristic admittance.

In 1999, Morched *et al.* combined the idempotent decomposition technique, presented by Wedepohl in 1982 [9] and completely developed by Marcano and L. Marti in 1997 [10], with Vector Fitting to create the “Universal Line Model” [11]. This model has shown a high precision in the analysis of homogeneous lines with frequency dependence and is nowadays the most advanced model included in commercial programs. However, it has been shown that even this model can present errors when simulating systems with strong frequency dependence [12].

Parallel to time domain analysis, frequency domain analysis of electromagnetic transients has been used as an alternative for several years. The main reason is that the frequency dependence of the line parameters is taken into account in a straightforward way. Initial works in frequency domain were presented by Day *et al.* in 1965 [13] and Wedepohl *et al.* in 1970 [14]. These works were based on the numerical evaluation of the Laplace transform to obtain the frequency response of transmission systems. The implementation of the Cooley-Tukey algorithm [15] – also known as Fast Fourier Transform (FFT) – introduced a significant advance in the numerical computation of the Laplace transform.

An alternative method for the numerical evaluation of the Laplace transform was introduced by Hosono in 1982, through the approximation of the exponential term by a finite series [63]. This method was developed for wave optic applications and was later applied to transient analysis of transmission lines [21, 25, 64]. However, it requires fixing the value of several variables depending on the specific application.

An important limitation of the frequency domain analysis is its inherent linearity. However, in previous works the principle of superposition has been used to analyze non linear conditions such as switching events and the inclusion of non linear elements in transmission systems with important results [12, 16-18].

1.2 Problem Statement

In the analysis of electromagnetic transients, such as those due to switching, the transmission line can be assumed as uniform and take into account only its frequency dependence. However, when analyzing fast transients such as those due to lightning or faults in substation groundings, the line non-uniformities can be as important as the frequency dependence. Examples of non-uniform lines (NUL's) are: overhead lines with sagging conductors between towers, lines entering substations, river crossing lines and vertical conductors.

The non-uniform line problem has been treated in time domain using several techniques. One of the first attempts to solve this problem was proposed by Menemenlis and Chun in 1982 [19]. Their work is based on traveling waves and the Lattice Diagram for single-phase lossless lines. In 1991, Ishii, *et al.* proposed a non-uniform model applied to transmission towers, in which each section of the tower is represented by a frequency dependent line connected to a constant resistance shunted with a constant inductance [20]. A method based on the approximation of the parameter variations by means of exponentials was developed in the frequency domain by Oufi, *et al.* in 1994 [21] and in time domain by Nguyen, *et al.* in 1997 [22], both for single-phase lines.

In 1999, Gutierrez, *et al.* used the finite differences method known as the Method of Characteristics to solve the PDE's of a frequency independent NUL [23]. Davila *et al.* extended this method in 2002 to consider both frequency and space dependence [24].

In 2001, Mamis and Köksal presented a single-phase non-uniform line model in the frequency domain based on the cascaded connection of the chain matrices of uniform line sections [25]. In 2003, Semlyen presented the NUL problem as a space variant linear system whose numerical integration yields the chain matrix of an entire NUL [26]. Applying this technique, Ramirez and Semlyen presented a time domain model for multiphase NUL's with frequency dependence, based on the concept of traveling waves [27].

Another important problem in transient studies is the effect of lightning induced overvoltages on transmission systems. The field-to-line coupling phenomenon has attracted great interest over the last few years. The formulations of Taylor [28], Agrawal [29], and Rachidi [30] represent the three most important approaches for modeling such coupling phenomena.

A straightforward way of solving the multiconductor line equations is by using the Finite Difference Time Domain method (FDTD) [29, 31-33]. However, in order to analyze complex electrical circuits with incident field effects, there is a need for models that are suitable for their incorporation into general purpose circuit simulators. One way to solve this problem was

adopted by Taylor in 1965 [28] and extended to multiconductor lines by Paul in 1976 [34]. This method consists in dividing the transmission line in several segments and including voltage and current sources between contiguous segments. A more practical representation in the frequency domain, which is based on connecting equivalent lumped voltage and current sources at the line receiving end, was presented by Paul in 1994 [35] and implemented for non-uniform field excited single phase lines by Omid *et al.* in 1997 [36]. Regarding time domain methods, a SPICE model based on decoupling the multiconductor line equations for the lossless case was proposed by Paul in 1994 [37]. In addition, Khazaka *et al.* presented in 1998 a method based on complex frequency hopping for the analysis of field coupling effects in high speed circuits [38]. This method uses model reduction techniques [39-42]. More recently, Erdin *et al.* reported the development of a SPICE macro-model based on a closed-form rational approximation of the exponential matrix and on a semi-analytic rational approximation of the involved forcing functions [43].

1.3 Scope

As presented in the previous sections, a lot of work has been done in order to take into account the frequency dependence of the parameters of transmission systems, as well as in the modeling of non-uniform lines and the inclusion of the effect of incident electromagnetic fields in both time and frequency domains. Some of these research works are quite recent and still in experimental stage. Therefore, it is still necessary to establish a general methodology to solve these problems in a straightforward and accurate way.

In this thesis, the methods presented by Mamis *et al.* [25] and Semlyen [26] to analyze non-uniform transmission lines in frequency domain are considered and compared. Then, the effect of incident electromagnetic fields on the non-uniform line is included by means of equivalent lumped sources, extending the work done in [34] for single phase lines to the case of multiconductor lines. To obtain the time domain solutions, the Numerical Laplace Transform is applied. In addition, a new time domain model for analyzing single phase non-uniform transmission lines with frequency dependent electrical parameters is presented. The model is based on the Method of Characteristics and the synthesis of an equivalent uniform transmission line from the chain matrix of a non-uniform line. The frequency and the space dependence of the electrical parameters of the non-uniform line are introduced into the equivalent uniform line by means of a transient resistance and a shunt transient conductance.

2 Non-uniform Lines

2.1 Introduction

When analyzing electromagnetic transients in transmission lines, the computation of electrical parameters is of crucial importance. In several practical cases, these parameters are functions not only of frequency, but also of space. This means, the line geometry varies with its length. This type of line is known as non-uniform. In the analysis of electromagnetic transients, such as those due to switching, one can assume the line as uniform and take into account only its frequency dependence. However, when analyzing fast transients such as those due to lightning or faults in substation groundings, line non-uniformities can be as important as the frequency dependence.

The Non-Uniform Line (NUL) problem has been treated in time domain using different techniques. In well known programs, such as the EMTP or SPICE, modeling of non-uniform lines is performed, in general, by discretization of the line in a number of segments considered as uniform lines. Since these programs use the nodal method to obtain the system solution, line discretization yields a bus admittance matrix of a large order. Besides, the time consumed by the user to generate the study case can be considerable, and a modification of the line non-uniformity may require the reconstruction of the entire case. Finite difference methods represent other approach to analyze NUL in time domain. Particularly, the Method of Characteristics is preferred, due to its effectiveness to solve propagation equations of hyperbolic type, such as the transmission line equations [23, 24]. However, the inclusion of frequency dependence in this method and the extension to the multiconductor case are still in an experimental stage.

In this Chapter, two methods for analyzing non-uniform multiconductor transmission lines in the frequency domain are considered. The first one is based on the cascaded connection of chain matrices of uniform line segments. In the second method, a space variant linear system is solved, with the chain matrix elements as system states. To obtain the solution in time domain,

the Numerical Laplace Transform (NLT) is applied. Several application examples are analyzed and comparisons with the ATP/EMTP and with experimental measurements published elsewhere are provided.

2.2 Solution to the line equations

For a multiphase non-uniform transmission line or cable, the modified Telegrapher's equations proposed by Radulet, *et al.*, can be expressed as follows [44]:

$$-\frac{\partial \mathbf{v}(x,t)}{\partial x} = \mathbf{L}_G(x) \frac{\partial \mathbf{i}(x,t)}{\partial t} + \frac{\partial}{\partial t} \int_0^t \mathbf{r}'(x,t-\tau) \mathbf{i}(x,\tau) d\tau \quad (2.1a)$$

$$-\frac{\partial \mathbf{i}(x,t)}{\partial x} = \mathbf{C}_G(x) \frac{\partial \mathbf{v}(x,t)}{\partial t} + \frac{\partial}{\partial t} \int_0^t \mathbf{g}'(x,t-\tau) \mathbf{v}(x,\tau) d\tau \quad (2.1b)$$

where $\mathbf{v}(x,t)$ and $\mathbf{i}(x,t)$ are the voltage and current vectors of the line, $\mathbf{L}_G(x)$ and $\mathbf{C}_G(x)$ are the geometric inductance and capacitance matrices, $\mathbf{r}'(x,t)$ and $\mathbf{g}'(x,t)$ are the transient series resistance and shunt conductance matrices, respectively. In the case of overhead transmission lines, the matrix $\mathbf{g}'(x,t)$ can be neglected. Taking this into account and applying the Laplace transform to (2.1)

$$\frac{d\mathbf{V}(x,s)}{dx} = -s[\mathbf{L}_G(x) + \mathbf{R}'(x,s)]\mathbf{I}(x,s) \quad (2.2a)$$

$$\frac{d\mathbf{I}(x,s)}{dx} = -s\mathbf{C}_G(x)\mathbf{V}(x,s) \quad (2.2b)$$

where $\mathbf{R}'(x,s)$ is the Laplace domain image of $\mathbf{r}'(x,t)$ computed as [45]

$$\mathbf{R}'(x,s) = \frac{\mathbf{Z}_E(x,s) + \mathbf{Z}_C(x,s)}{s} \quad (2.3)$$

being $\mathbf{Z}_E(x,s)$ and $\mathbf{Z}_C(x,s)$ the earth return and conductor impedance matrices, respectively. From (2.2), the voltage and current propagations along a multiconductor transmission line in the frequency domain can be described by the following equation:

$$\frac{d}{dx} \begin{bmatrix} \mathbf{V}(x,s) \\ \mathbf{I}(x,s) \end{bmatrix} = \begin{bmatrix} \mathbf{0} & -\mathbf{Z}(x,s) \\ -\mathbf{Y}(x,s) & \mathbf{0} \end{bmatrix} \begin{bmatrix} \mathbf{V}(x,s) \\ \mathbf{I}(x,s) \end{bmatrix} \quad (2.4)$$

where $\mathbf{Z}(x,s)$ and $\mathbf{Y}(x,s)$ are the longitudinal impedance and transversal admittance matrices per unit-length, respectively, computed as

$$\mathbf{Z}(x, s) = \mathbf{Z}_G(x, s) + \mathbf{Z}_E(x, s) + \mathbf{Z}_C(x, s) \quad (2.5a)$$

$$\mathbf{Y}(x, s) = s\mathbf{C}_G(x) \quad (2.5b)$$

$\mathbf{V}(x, s)$ and $\mathbf{I}(x, s)$ are the voltage and current vectors in the Laplace domain at any point x of the line, respectively. Matrices \mathbf{Z} and \mathbf{Y} can be divided into their real and imaginary parts:

$$\mathbf{Z}(x, s) = \mathbf{R}(x, s) + s\mathbf{L}(x, s) \quad (2.6a)$$

$$\mathbf{Y}(x, s) = \mathbf{G}(x, s) + s\mathbf{C}(x, s) \quad (2.6b)$$

with $\mathbf{R}(x, s)$, $\mathbf{L}(x, s)$, $\mathbf{C}(x, s)$ and $\mathbf{G}(x, s)$ being the per unit-length resistance, inductance, capacitance and conductance matrices, respectively. For a short enough transmission line segment, the coupled first order differential equations defined in (2.4) can be converted to uncoupled second order equations:

$$\frac{d^2}{dx^2} \begin{bmatrix} \mathbf{V}(x, s) \\ \mathbf{I}(x, s) \end{bmatrix} = \begin{bmatrix} \mathbf{Z}(x, s)\mathbf{Y}(x, s) & \mathbf{0} \\ \mathbf{0} & \mathbf{Y}(x, s)\mathbf{Z}(x, s) \end{bmatrix} \begin{bmatrix} \mathbf{V}(x, s) \\ \mathbf{I}(x, s) \end{bmatrix} \quad (2.7)$$

Solution of system (2.7) is given by

$$\mathbf{V}(x, s) = \exp(-\Psi x)\mathbf{C}_1 + \exp(\Psi x)\mathbf{C}_2 \quad (2.8a)$$

$$\mathbf{I}(x, s) = \mathbf{Y}_0 [\exp(-\Psi x)\mathbf{C}_1 - \exp(\Psi x)\mathbf{C}_2] \quad (2.8b)$$

where Ψ is the phase domain constant propagation matrix of the line segment, defined as

$$\Psi = \mathbf{M}\sqrt{\lambda}\mathbf{M}^{-1} \quad (2.9)$$

\mathbf{M} and λ are the eigenvector and eigenvalue matrices of the matrix product $\mathbf{Z}(x, s) \cdot \mathbf{Y}(x, s)$, respectively, and \mathbf{Y}_0 is the characteristic admittance matrix of the line segment, computed as follows:

$$\mathbf{Y}_0 = \mathbf{Z}(x, s)^{-1}\Psi \quad (2.10)$$

Constant voltage vectors \mathbf{C}_1 and \mathbf{C}_2 in (2.8) are computed considering a uniform line segment of length Δx and applying the terminal conditions at $x - \Delta x$ and x . Evaluating (2.8) at the sending end ($x - \Delta x$) gives

$$\mathbf{C}_1 = \frac{1}{2} \left[\mathbf{V}_0(x - \Delta x, s) + \mathbf{Y}_0^{-1} \mathbf{I}(x - \Delta x, s) \right] \quad (2.11a)$$

$$\mathbf{C}_2 = \frac{1}{2} \left[\mathbf{V}_0(x - \Delta x, s) - \mathbf{Y}_0^{-1} \mathbf{I}(x - \Delta x, s) \right] \quad (2.11b)$$

Finally, substituting, (2.11) in (2.8) and evaluating at the receiving end (x), it yields (in hyperbolic form)

$$\begin{bmatrix} \mathbf{V}(x, s) \\ \mathbf{I}(x, s) \end{bmatrix} = \mathbf{\Phi}(\Delta x, s) \begin{bmatrix} \mathbf{V}(x - \Delta x, s) \\ \mathbf{I}(x - \Delta x, s) \end{bmatrix} \quad (2.12)$$

where

$$\mathbf{\Phi}(\Delta x, s) = \begin{bmatrix} \cosh(\Psi \Delta x) & \mathbf{Y}_0^{-1} \sinh(\Psi \Delta x) \\ \mathbf{Y}_0 \sinh(\Psi \Delta x) & \cosh(\Psi \Delta x) \end{bmatrix} \quad (2.13)$$

A detailed procedure for the computation of the matrices $\mathbf{Z}(x, s)$ and $\mathbf{Y}(x, s)$ from the physical and geometrical parameters of an aerial line is provided in Appendix B.

2.3 Cascaded Connection of Chain Matrices

The 2-port line representation given by 2.12 is known as chain or ABCD matrix and can be used to construct a model for non-uniform transmission lines (NULs). The procedure consists of

- (a) dividing the non-uniform line in several segments,
- (b) computing the chain matrix of each segment, considering them as uniform lines and
- (c) putting together all the chain matrices into an equivalent matrix for the whole line.

Dividing process of the line is shown in Fig. 2.1. Each line segment has different electrical parameters in accordance with the line parameters variation. After dividing the transmission line, the entire equivalent chain matrix is obtained as the product, in the appropriate order, of the whole set of chain matrices, as follows:

$$\begin{bmatrix} \mathbf{V}(L, s) \\ \mathbf{I}(L, s) \end{bmatrix} = \mathbf{\Phi}^{(M)} \dots \mathbf{\Phi}^{(i)} \dots \mathbf{\Phi}^{(1)} \begin{bmatrix} \mathbf{V}(0, s) \\ \mathbf{I}(0, s) \end{bmatrix} \quad (2.14)$$

or in compact form

$$\begin{bmatrix} \mathbf{V}(L, s) \\ \mathbf{I}(L, s) \end{bmatrix} = \left[\prod_{i=1}^M \mathbf{\Phi}^{(M+1-i)} \right] \begin{bmatrix} \mathbf{V}(0, s) \\ \mathbf{I}(0, s) \end{bmatrix} \quad (2.15)$$

being L the line length and $\mathbf{\Phi}^{(i)}$ the chain matrix for the i -th line segment.

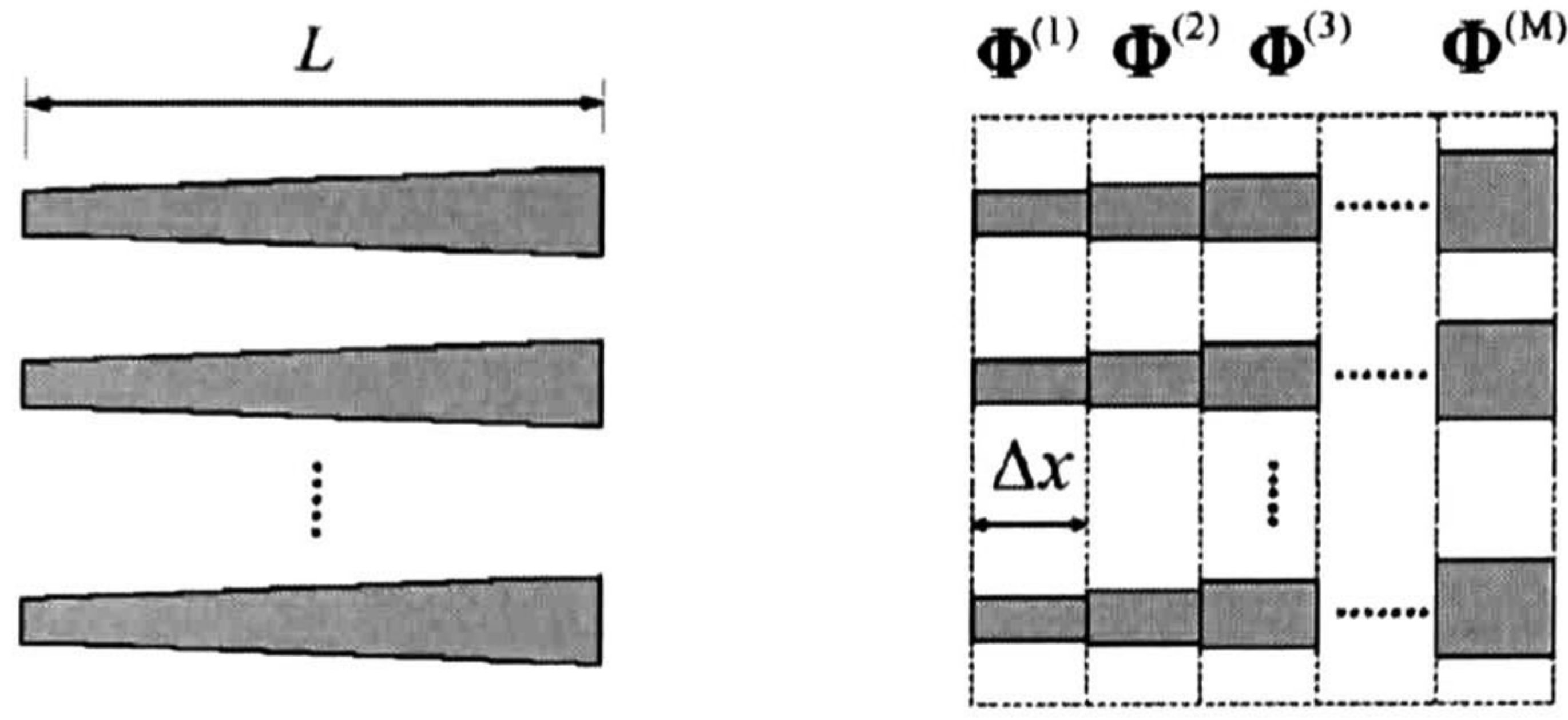


Figure 2.1. Cascaded connection of chain matrices.

It is evident that the procedure's precision depends on the number of segments used to approximate the non-uniform line. A convenient choice of the line segment Δx can be done by complying with the Courant-Fredrichs-Lewi (CFL) condition [46], which can be expressed as follows:

$$\Delta x \geq \nu \Delta t \quad (2.16)$$

where ν is the wave propagation velocity that corresponds to the fastest propagation mode.

2.4 Derivation of the Chain Matrix

An alternative method to analyze non-uniform lines can be obtained from (2.4) and (2.15). According to these equations, the chain matrix must satisfy the following differential equation [26]:

$$\frac{d\Phi(x, s)}{dx} = \mathbf{P} \Phi(x, s), \quad \Phi(0, s) = \mathbf{U} \quad (2.17)$$

where

$$\mathbf{P} = \begin{bmatrix} \mathbf{0} & \mathbf{Z}(x, s) \\ \mathbf{Y}(x, s) & \mathbf{0} \end{bmatrix} \quad (2.18)$$

Equation (2.17) defines a space variant linear system whose states are the elements of the chain matrix. General solution of (2.17) for a uniform line segment is given by

$$\Phi(x + \Delta x, s) = \exp(\mathbf{P}\Delta x) \Phi(x, s) \quad (2.19)$$

Iterative solution of (2.19) involves the computation of the exponential of a matrix. Several techniques have been proposed to solve this problem [47, 48]. The following are applied in this work:

- (a) Taylor Series Expansion.
- (b) Modal decomposition.
- (c) Padè Approximation.
- (d) Sylvester Formula.

2.4.1 Taylor Series Expansion

Equation (2.19) can be expressed as an infinite power series [47, 48], as follows:

$$\Phi(x + \Delta x, s) = \left[\sum_{i=0}^{\infty} \frac{(\Delta x \mathbf{P})^i}{i!} \right] \Phi(x, s) \quad (2.20)$$

In order to perform the numerical evaluation of (2.20), the series is approximated with a finite number of terms. If the first two terms are used, the approximation is equivalent to the numerical integration of the differential equation by the application of the Euler Method:

$$\Phi(x + \Delta x, s) = (\mathbf{U} + \Delta x \mathbf{P}) \Phi(x, s) \quad (2.21)$$

Equation (2.21) is iteratively solved from $x = 0$ to $x = L - \Delta x$, with initial condition $\Phi(0, s)$ defined in (2.17). Similarly, if the first 3 terms of the series are used, the approximation obtained is equivalent to the Heun Method. The problem of this method is that, in some cases, it presents numerical oscillations. To avoid this, a damping factor is included [49], obtaining the following equation:

$$\Phi(x + \Delta x, s) = \left[\mathbf{U} + \Delta x \mathbf{P} + \frac{(1 - \alpha) \Delta x^2 \mathbf{P}^2}{2!} \right] \Phi(x, s) \quad (2.22)$$

It can be seen that when $\alpha = 0$, equation (2.22) becomes the conventional Heun Method, while when $\alpha = 1$, Euler Method is obtained. Therefore, a convenient value of the damping factor to avoid oscillations is in the range $0 < \alpha \leq 1$. If more terms are used in the power series approximation of the matrix exponential, the n -th order Runge Kutta Method is obtained:

$$\Phi(x + \Delta x, s) = \left[\mathbf{U} + \Delta x \mathbf{P} + \frac{\Delta x^2}{2!} \mathbf{P}^2 + \dots + \frac{\Delta x^n}{n!} \mathbf{P}^n \right] \Phi(x, s) \quad (2.23)$$

2.4.2 Modal Decomposition

If \mathbf{P} is a diagonalizable matrix, modal decomposition theory can be applied to obtain [47, 48]

$$\mathbf{P} = \mathbf{M}_p \boldsymbol{\lambda}_p \mathbf{M}_p^{-1} \quad (2.24)$$

where columns of \mathbf{M}_p are the eigenvectors of matrix \mathbf{P} and $\boldsymbol{\lambda}_p$ is a diagonal matrix whose elements are the eigenvalues of \mathbf{P} . The expression $\exp(\mathbf{P}\Delta x)$ in (2.19) is solved using the following property:

$$f(\mathbf{P}) = \mathbf{M}_p f(\boldsymbol{\lambda}_p) \mathbf{M}_p^{-1} \quad (2.25)$$

Therefore, equation (2.19) can be written as

$$\Phi(x + \Delta x, s) = \mathbf{M}_p \exp(\boldsymbol{\lambda}_p \Delta x) \mathbf{M}_p^{-1} \Phi(x, s) \quad (2.26)$$

2.4.3 Padè Approximation

Padè approximation of the exponential function of a matrix \mathbf{P} is, by definition, the rational function [47, 48]

$$R_{mn}(\mathbf{P}) = [D_{mn}(\mathbf{P})]^{-1} N_{mn}(\mathbf{P}) \quad (2.27)$$

Equation (2.27) is equivalent to the power series expansion of $\exp(\mathbf{P})$ using terms to the power $m + n$. Therefore, its coefficients are determined solving the algebraic equations given by

$$\exp(\mathbf{P}) = \sum_{i=0}^{\infty} \frac{\mathbf{P}^i}{i!} = R_{mn}(\mathbf{P}) + O(\mathbf{P}^{m+n+1}) = [D_{mn}(\mathbf{P})]^{-1} N_{mn}(\mathbf{P}) + O(\mathbf{P}^{m+n+1}) \quad (2.28)$$

The solution of (2.28) is given by

$$N_{mn}(\mathbf{P}) = \sum_{i=0}^m \frac{(m+n-i)!n!}{(m+n)!i!(m-i)!} \mathbf{P}^i \quad (2.29a)$$

$$D_{mn}(\mathbf{P}) = \sum_{i=0}^n \frac{(m+n-i)!m!}{(m+n)!i!(n-i)!} (-\mathbf{P})^i \quad (2.29b)$$

Choosing $m = n$, the diagonal Padè approximation is obtained. This choice has the advantage that it yields a higher order approximation with the same amount of computation than the conventional form. Therefore, in this case

$$R_{mm}(\mathbf{P}) = [N_{mm}(-\mathbf{P})]^{-1} N_{mm}(\mathbf{P}) \quad (2.30)$$

with

$$N_{mm}(\mathbf{P}) = \sum_{i=0}^m \frac{(2m-i)!m!}{(2m)!i!(m-i)!} \mathbf{P}^i = \sum_{i=0}^m c_i \mathbf{P}^i \quad (2.31)$$

where the coefficients c_i can be computed by means of the following recursive expression:

$$c_i = c_{i-1} \frac{m+1-i}{i(2m+1-i)}, \quad c_0 = 1 \quad (2.32)$$

2.4.4 Sylvester Formula

Consider the characteristic equation of a matrix \mathbf{P} of size $n \times n$ [47, 48]

$$|\lambda \mathbf{I} - \mathbf{P}| = (\lambda - \lambda_1)(\lambda - \lambda_2) \cdots (\lambda - \lambda_n) = 0 \quad (2.33)$$

being $\lambda_1, \lambda_2, \dots, \lambda_n$ the n eigenvalues of \mathbf{P} (all different). The Lagrange interpolation polynomial of a function $f(\lambda)$ is given by

$$r(\lambda) = \sum_{k=1}^n \frac{(\lambda - \lambda_1) \cdots (\lambda - \lambda_{k-1})(\lambda - \lambda_{k+1}) \cdots (\lambda - \lambda_n)}{(\lambda_k - \lambda_1) \cdots (\lambda_k - \lambda_{k-1})(\lambda_k - \lambda_{k+1}) \cdots (\lambda_k - \lambda_n)} f(\lambda_k) \quad (2.34)$$

From (2.30), the Lagrange interpolation polynomial of the matrix \mathbf{P} is as follows:

$$f(\mathbf{P}) = r(\mathbf{P}) = \sum_{k=1}^n \frac{(\mathbf{P} - \lambda_1 \mathbf{I}) \cdots (\mathbf{P} - \lambda_{k-1} \mathbf{I})(\mathbf{P} - \lambda_{k+1} \mathbf{I}) \cdots (\mathbf{P} - \lambda_n \mathbf{I})}{(\lambda_k - \lambda_1) \cdots (\lambda_k - \lambda_{k-1})(\lambda_k - \lambda_{k+1}) \cdots (\lambda_k - \lambda_n)} f(\lambda_k) \quad (2.35)$$

and from (2.31), it can be written

$$\exp(\mathbf{P} \Delta x) = \sum_{k=1}^n \frac{(\mathbf{P} - \lambda_1 \mathbf{I}) \cdots (\mathbf{P} - \lambda_{k-1} \mathbf{I})(\mathbf{P} - \lambda_{k+1} \mathbf{I}) \cdots (\mathbf{P} - \lambda_n \mathbf{I})}{(\lambda_k - \lambda_1) \cdots (\lambda_k - \lambda_{k-1})(\lambda_k - \lambda_{k+1}) \cdots (\lambda_k - \lambda_n)} \exp(\lambda_k \Delta x) \quad (2.36)$$

2.5 Applications

The methods presented in previous sections were validated by means of two application examples. In the first one, a highly non-uniform 3-phase line was analyzed. As second example, a 500 kV transmission tower was modeled using a series of interconnected non-uniform line segments. Results were compared with ATP/EMTP and experimental measurements published elsewhere. Simulations with the NLT and ATP were performed on a Pentium® IV PC (1.6 GHz, 128 MB of RAM).

2.5.1 River Crossing

As first application example, a highly non-uniform transmission line is analyzed. The problem consists of a river crossing 3-phase line, as shown in Fig. 2.2. This example was extracted from [45]. The line is formed by 3 conductors in horizontal configuration with equal radius of 2.54cm. Distance between conductors is 10m. A unit step voltage source was connected to the 3 phases at the sending node, while the receiving end was left open. The results were analyzed when using the presented techniques. Accuracy and computation efficiency of each method was evaluated comparing the results with those obtained using Padè approximation and dividing the line in a large number of segments (600), considering this result as the base solution. Error was computed as follows:

$$err = \left| \frac{V_2(t) - V(t)}{\max[V(t)]} \right| \quad (2.37)$$

where $V(t)$ is the voltage obtained with the base solution and $V_2(t)$ is the approximation applying one of the following two methods:

1. Cascaded connection of chain matrices.
2. Derivation of chain matrix.

Tables 2.1 and 2.2 show the computer times (using MATLAB®) needed to obtain errors smaller than 0.1 and 0.05. Besides, the number of line segments required by each method to obtain the indicated errors is listed. For this evaluation, 256 samples and an observation time of 25 μ s were used. Complying with (2.16), the number of uniform line segments in cascade connection used for the simulation with the NLT was 18. The simulation in the ATP was done using 18 uniform transmission lines. In order to take into account the frequency dependence of the electrical parameters of each line in the ATP simulation, the J. Marti model was used [6]. Fig. 2.3 shows the voltage at phase B of the receiving node as obtained with both programs.

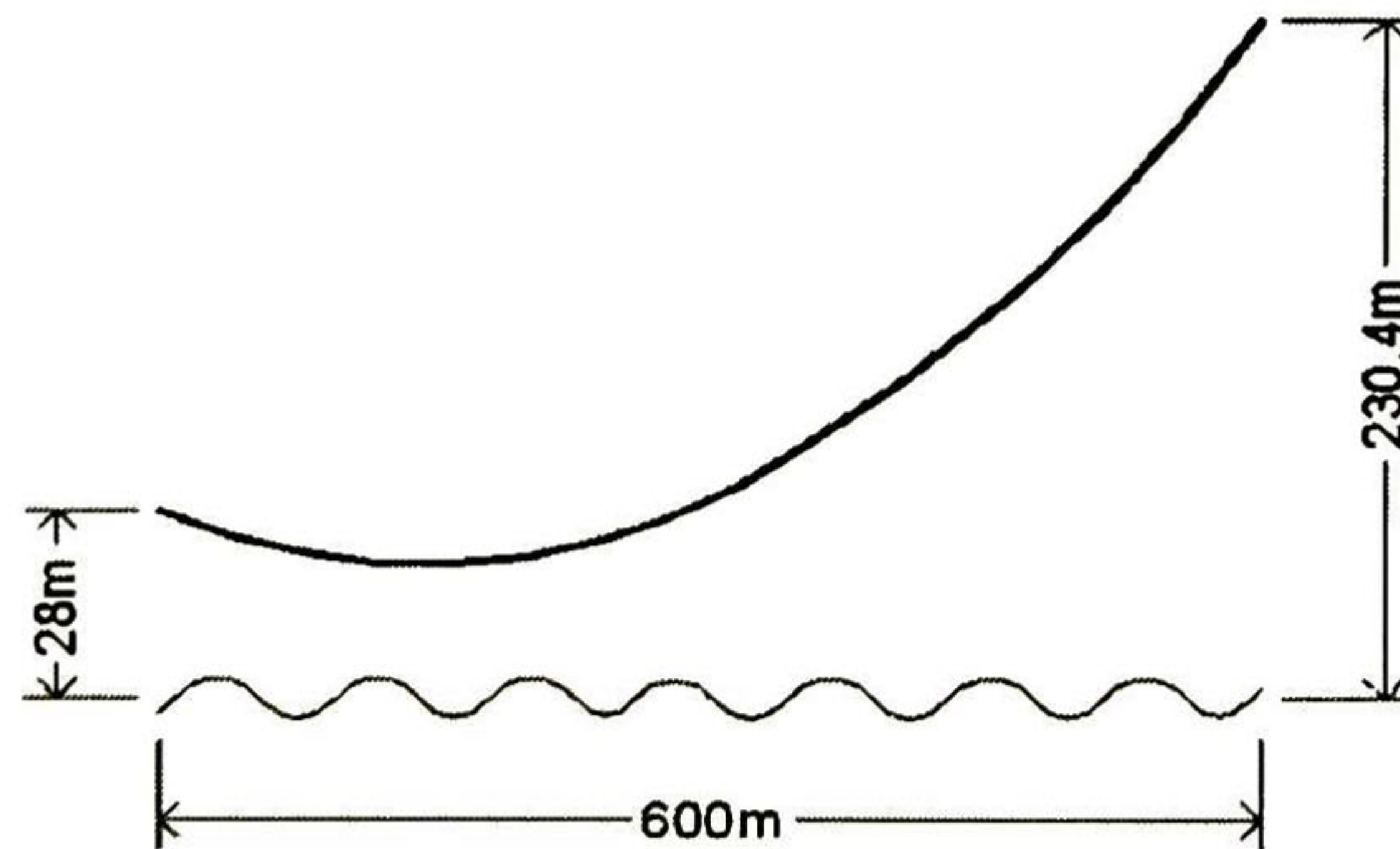


Figure 2.2. River crossing profile.

Table 2.1. Results of Method 1.

	err < 0.1		err < 0.05	
	Computer time (sec)	Segments	Computer time (sec)	Segments
Cascaded Connection	6.64	18	6.64	18

Table 2.2. Results of Method 2.

	err < 0.1		err < 0.05	
	Computer time (sec)	Segments	Computer time (sec)	Segments
Euler	115.18	670	356.79	2050
Heun	39.49	180	99.20	440
Runge Kutta IV	32.52	75	37.52	85
Runge Kutta VI	28.18	35	52.29	65
Modal Decomposition	16.54	35	27.24	65
Padè Aprox.	10.44	35	19.50	65
Lagrange - Sylvester	33.01	35	62.45	65

Using the ATP this case took 3.45 seconds. It should be mentioned that an additional 2.66 seconds for each line segment was required by the J. Martí fitting routine (a total of 2.66×18 seconds). The complete simulation with the NLT MATLAB® program took 6.64 seconds. It should also be stressed that the presented computer times may not be directly compared since they correspond to different platforms.

The example was repeated including 2 ground wires separated 10 m from each other and located 5 m above the phase conductors (radius = 1.25cm, resistivity = $2 \times 10^{-7} \Omega\text{-m}$, relative permeability = 1000). Results using frequency dependent electrical parameters and constant electrical parameters are shown in Fig. 2.4. As seen in the figure, several spikes arise when frequency dependence is not included in the simulation. Computer times when using frequency dependent parameters were very close to those of constant parameters, with difference of about 2%. This is because most of the computation time is mainly consumed by the total chain matrix calculation.

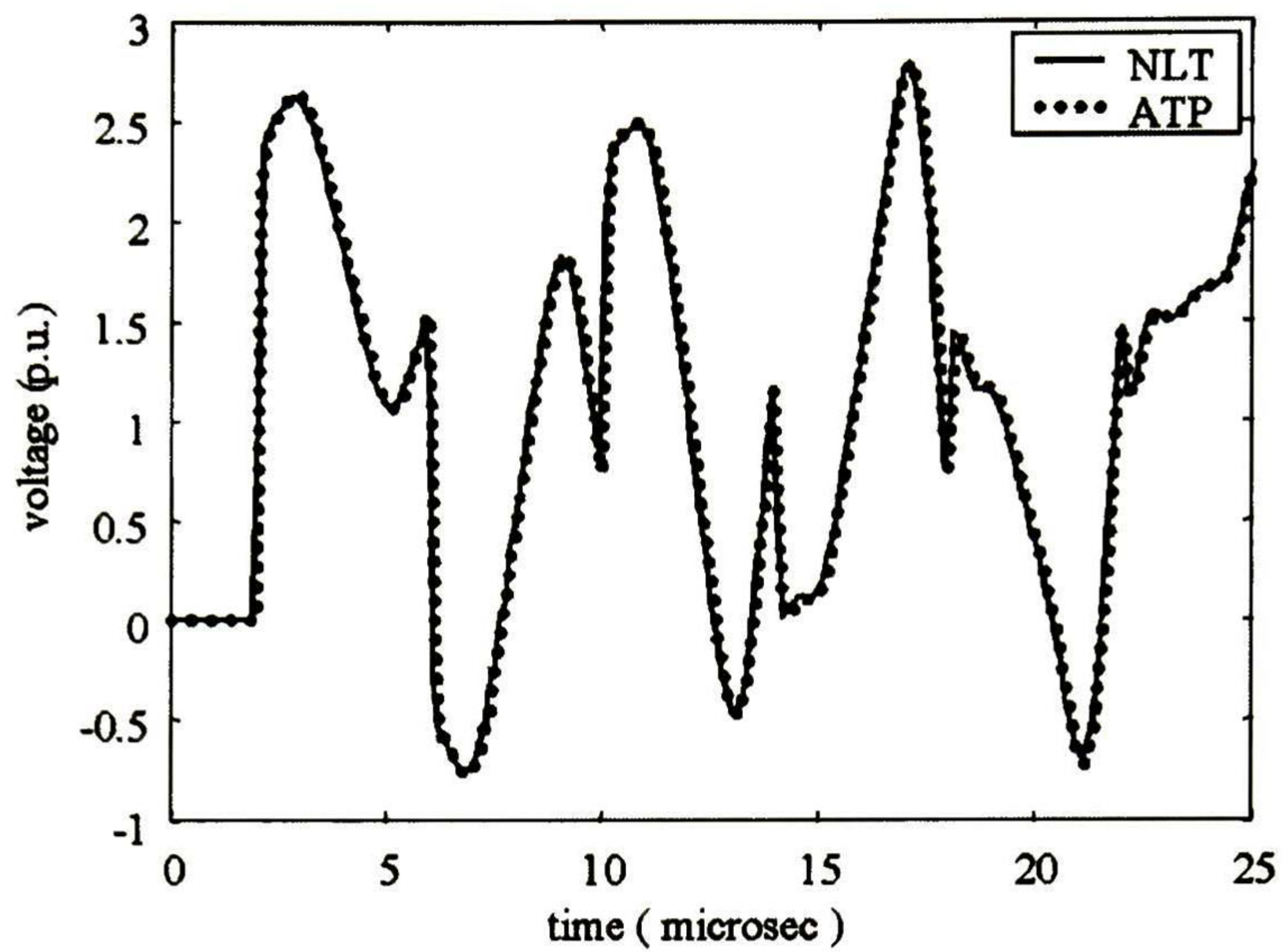


Figure 2.3. Voltage at phase B of the receiving node.

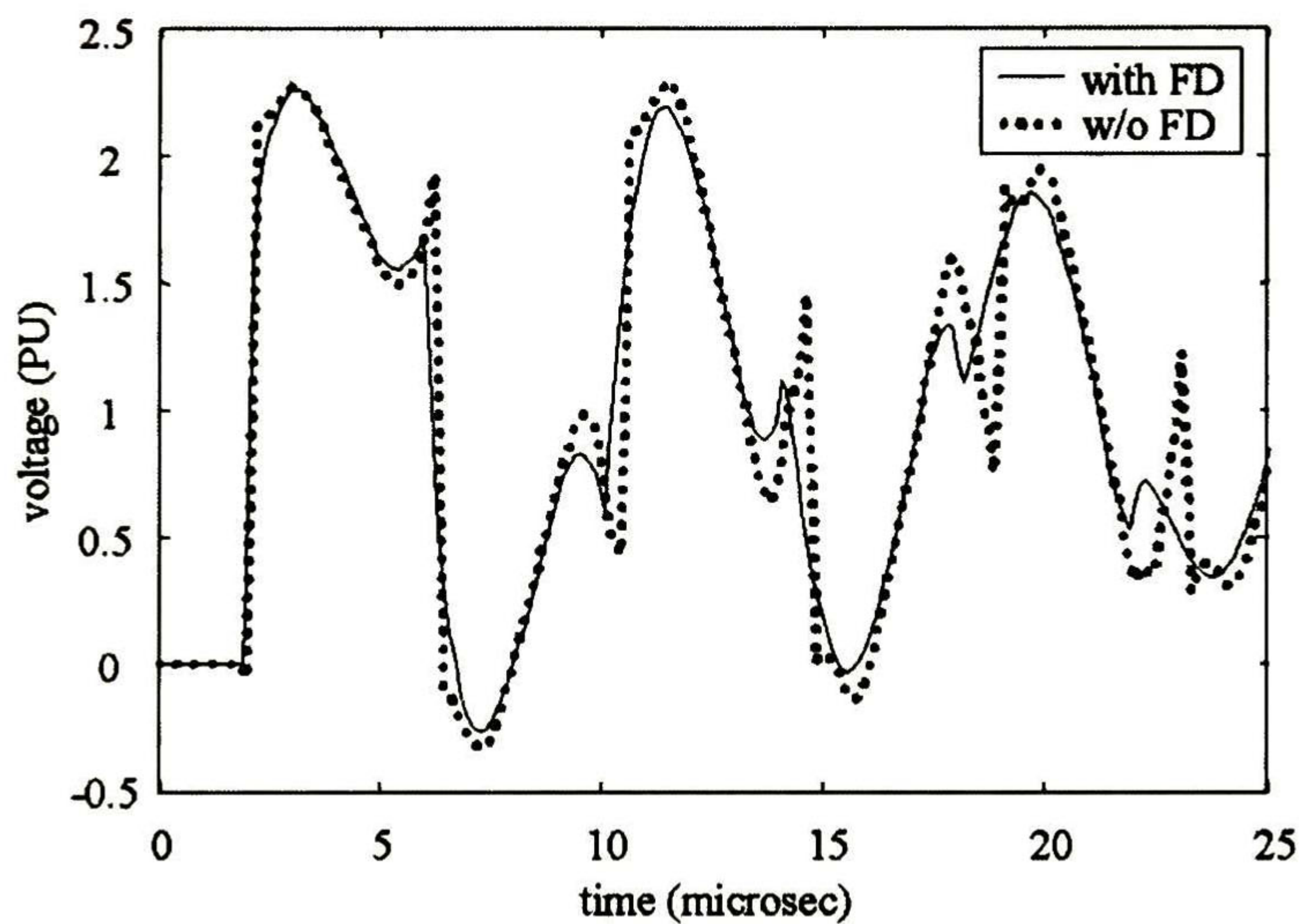


Figure 2.4. Voltage at phase B of the receiving node.

2.5.2 Tower Model Using Non-uniform Lines

As second application example, an experiment reported in [20] was simulated. In this experiment, measurements on a 500kV transmission tower were performed. A rectangular current pulse, with a rise time of $20\eta\text{s}$ and duration of $4\mu\text{s}$, was injected to one of the tower arms through a coaxial cable. In [20] the actual waveform of the source output was not reported; a measurement of the current flowing into the top of the tower was provided instead. Therefore,

the simulation was performed injecting at the top of the tower the current waveform shown in Fig. 2.5. A schematic of the tower with its main dimensions is shown in Fig. 2.6a. The tower model was constructed with a series of interconnected non-uniform transmission line segments, as presented in Fig. 2.6b. The horizontal lines were modeled as a connection of several uniform segments, whose electrical parameters can be calculated from the well known formulas detailed on Appendix B. On the other hand, electrical parameters of the vertical lines were calculated with the formulas proposed by Gutierrez *et al.* [50]. The tower data necessary for the simulation is listed in Table 2.3. The connection of the tower to ground was made using a lumped impedance of 17Ω . In Fig. 2.7, a comparison of the measured voltage waveform at the injection point of the tower with the calculated waveform is presented. The simulation of this case with the NLT program took 2.45 seconds.

2.6 Conclusions

Two methods for analyzing electromagnetic transients in non-uniform multiconductor transmission lines using the Numerical Laplace Transform have been presented and compared. From the results, it can be concluded that the cascaded connection method is more efficient than the chain matrix derivation in accuracy and computer time. The examples reveal a high effectiveness of the methods to reproduce practical cases with different non-uniformity conditions, showing a very good agreement with the ATP/EMTP and experimental results. The differences in the waveforms of Figs. 2.4 stress the importance of including frequency dependent effects in some cases of transient analysis of short non-uniform lines.

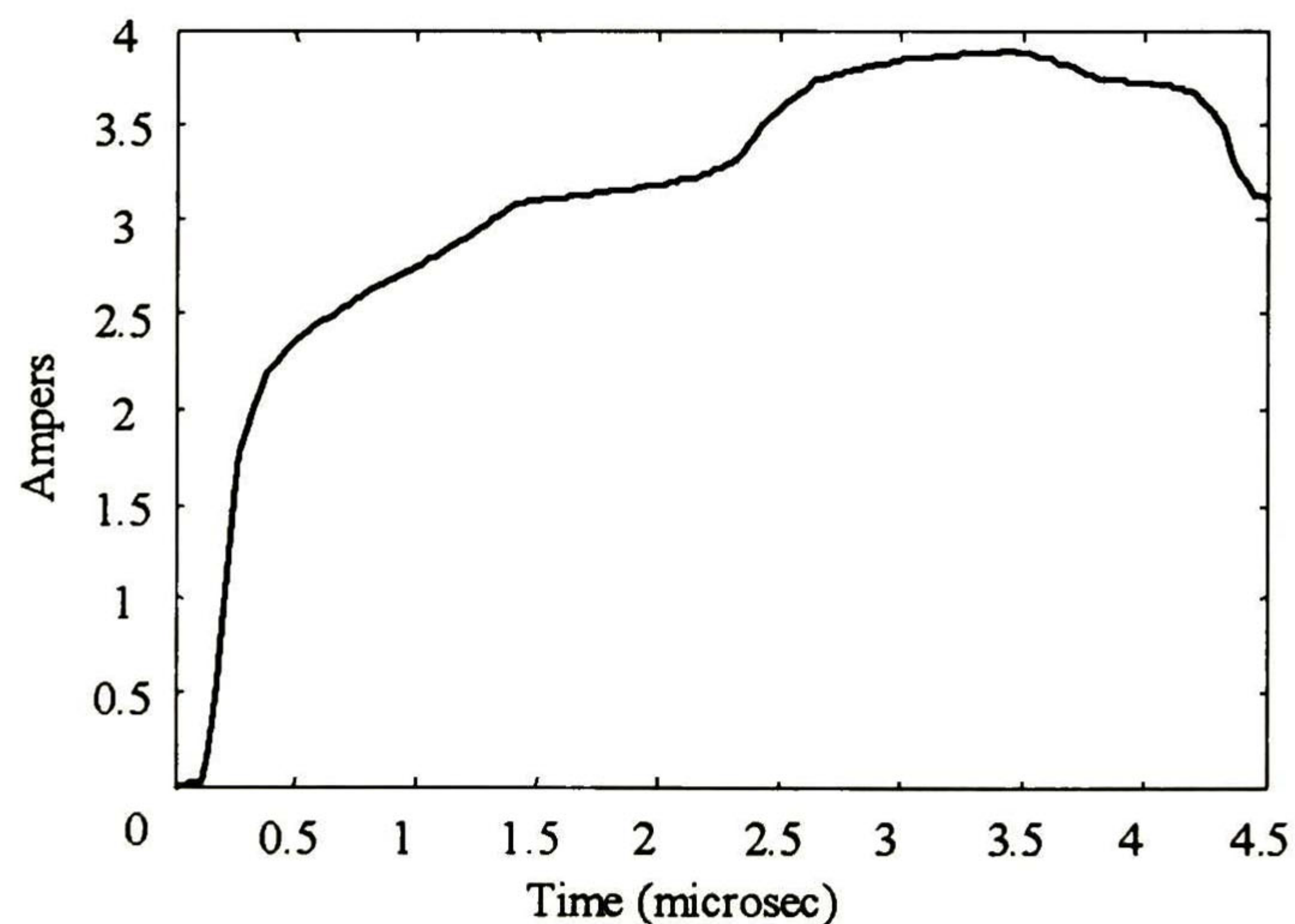


Figure 2.5. Waveform of the current source injected to the tower.

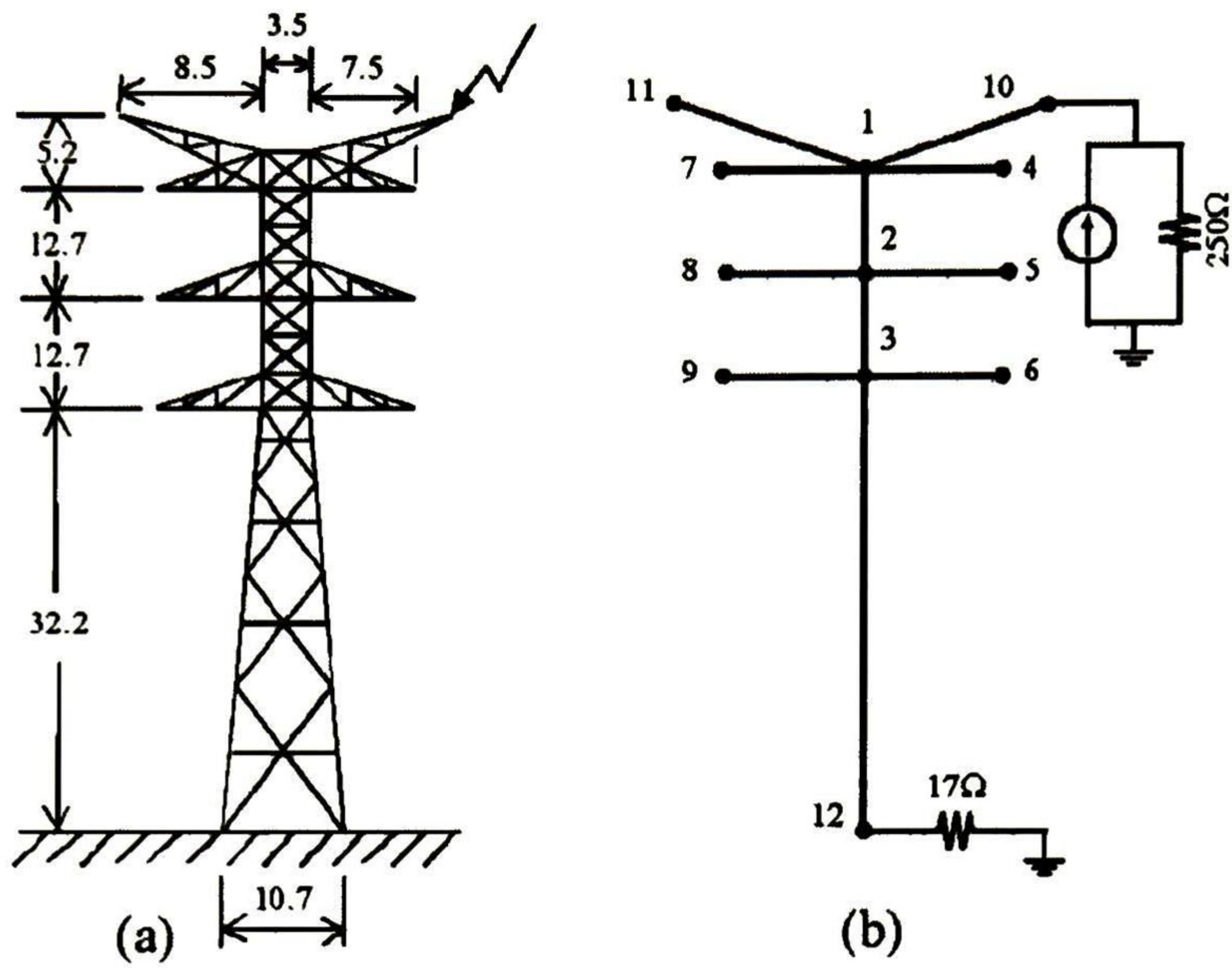


Figure 2.6. (a) Transmission tower. (b) Tower representation with non-uniform line segments.

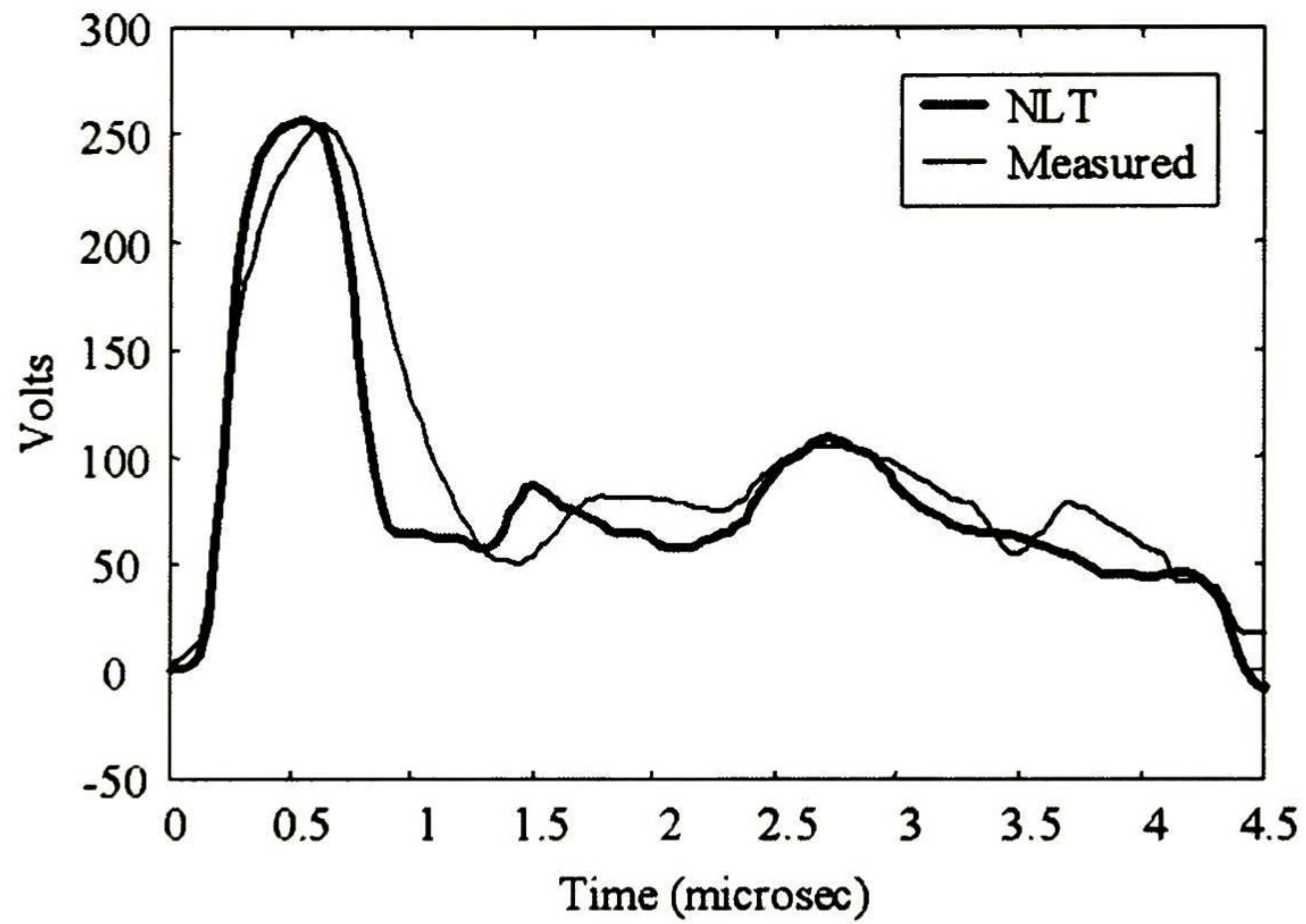


Figure 2.7. Voltage at the injection point of the tower..

Table 2.3. Tower Data

Material	Iron
Resistivity	$9.09 \times 10^{-7} \Omega\text{-m}$
Magnetic Permeability	$4\pi \times 10^{-4} \text{ H/m}$
Ground Resistivity	$30 \Omega\text{-m}$

Main structure.	
Number of columns	4
Column equivalent radius	0.1 m
Max. distance between columns	10.7 m
Min. distance between columns	3.5 m.
Tower Arms	
Number of columns	4
Column equivalent radius	0.05 m
Max. distance between columns	3.5 m
Min. distance between columns	0.0 m
Arm length (phase)	7.5 m
Arm length (ground wire)	8.5 m

3 Field Excited Lines

3.1 Introduction

One of the most important aspects in transient studies is the response of transmission lines excited by incident electromagnetic fields. These fields can be produced by distant sources such as transmitters, lightning discharges and an electromagnetic pulse (EMP) or by nearby sources such as arcing at relay contacts and other radiating structures. The determination of currents and voltages induced at the line terminals is essential to these studies. Taylor *et al.* [28] applied a quasi-TEM approach to the study of field coupling to a two-wire line. With this approach, the main propagation mode of the line is the transverse electromagnetic where the electric and magnetic fields surrounding the line lie solely in the transverse plane orthogonal to the line axis. This condition is equivalent to assume that the cross-sectional dimensions of the line are much smaller than a wavelength of the external wave. Taylor's approach was extended to multiconductor transmission lines by Paul [34]. In their formulation, the transmission line equations are expressed in terms of line total currents and voltages with the effect of the external field represented by means of distributed voltage and current sources along the line. A more practical representation in the frequency domain has been adopted in [35], in which the contribution of the external field is included by connecting equivalent lumped voltage and current sources at the receiving end of the line.

In this Chapter, the approach presented in [36] for non-uniform field excited single phase line is extended to the case of multiconductor lines, using the non-uniform line model of cascaded connection of chain matrices, discussed in Chapter 2, and including the effect of incident electromagnetic fields by means of lumped sources. Again, the solution in time domain is obtained applying the Numerical Laplace Transform (NLT) and comparisons with ATP/EMTP results are provided.

3.2 Incident Field Representation

Using Taylor's formulation of distributed sources along the line, a field excited non-uniform line model can be obtained by means of the cascaded connection of uniform line segments. The resultant model includes the effect of external fields using only lumped voltage and current sources connected at the receiving end of the line. This technique produces an important simplification in the study of the field excited line phenomenon, without losing accuracy.

3.2.1 Distributed Sources

Consider a multiconductor line excited by an incident electromagnetic field. To include the effects of this field, the line propagation equations defined in (2.1) can be modified as follows:

$$\frac{d}{dx} \begin{bmatrix} \mathbf{V}(x, s) \\ \mathbf{I}(x, s) \end{bmatrix} = \begin{bmatrix} \mathbf{0} & -\mathbf{Z} \\ -\mathbf{Y} & \mathbf{0} \end{bmatrix} \begin{bmatrix} \mathbf{V}(x, s) \\ \mathbf{I}(x, s) \end{bmatrix} + \begin{bmatrix} \mathbf{V}_F(x, s) \\ \mathbf{I}_F(x, s) \end{bmatrix} \quad (3.1)$$

where

$$\mathbf{V}_F(x, s) = s \begin{bmatrix} \vdots \\ \int_0^{h_i} \mathbf{B}_z dy \\ \vdots \end{bmatrix} \quad (3.2a)$$

$$\mathbf{I}_F(x, s) = -\mathbf{Y} \begin{bmatrix} \vdots \\ \int_0^{h_i} \mathbf{E}_y dy \\ \vdots \end{bmatrix} \quad (3.2b)$$

In (3.2a) and (3.2b), h_i refers to the height of the i -th conductor, \mathbf{B}_z is the incident magnetic field in the z direction and \mathbf{E}_y is the incident electric field in the y direction, according to the coordinate system shown in Fig. 3.1. Using the matrix exponential function, solution of (3.1) for a short line segment of length Δx can be written as

$$\begin{bmatrix} \mathbf{V}'(x, s) \\ \mathbf{I}'(x, s) \end{bmatrix} = \mathbf{\Phi}(\Delta x, s) \begin{bmatrix} \mathbf{V}(x - \Delta x, s) \\ \mathbf{I}(x - \Delta x, s) \end{bmatrix} + \int_{x-\Delta x}^x \mathbf{\Phi}(x - \tau, s) \begin{bmatrix} \mathbf{V}_F(\tau, s) \\ \mathbf{I}_F(\tau, s) \end{bmatrix} d\tau \quad (3.3)$$

Illustration of Eq. (3.3) is shown in Fig. 3.2.. If the line segment is electrically short, the integral of (3.3) can be approximated as follows:

$$\int_{x-\Delta x}^x \mathbf{\Phi}(x - \tau, s) \begin{bmatrix} \mathbf{V}_F(\tau, s) \\ \mathbf{I}_F(\tau, s) \end{bmatrix} d\tau = \begin{bmatrix} \mathbf{V}_F(x, s) \Delta x \\ \mathbf{I}_F(x, s) \Delta x \end{bmatrix} \quad (3.4)$$

3.2.2 Lumped Sources

Comparing Eqs. (3.3) and (2.8), it can be seen that the inclusion of incident fields modifies the line representation by the addition of the distributed sources vector corresponding to each segment. The complete line representation can be obtained by adding this vector at each step of the cascaded connection defined in (2.11). This gives

$$\begin{bmatrix} \mathbf{V}'(L, s) \\ \mathbf{I}'(L, s) \end{bmatrix} = \left[\prod_{i=1}^M \Phi^{(M+1-i)} \right] \begin{bmatrix} \mathbf{V}(0, s) \\ \mathbf{I}(0, s) \end{bmatrix} + \begin{bmatrix} \mathbf{V}_{FT}(L, s) \\ \mathbf{I}_{FT}(L, s) \end{bmatrix} \quad (3.5)$$

where

$$\begin{bmatrix} \mathbf{V}_{FT}(L, s) \\ \mathbf{I}_{FT}(L, s) \end{bmatrix} = \sum_{i=1}^{M-1} \left\{ \left[\prod_{n=1}^{M-i-1} \Phi^{(M-n)} \right] \begin{bmatrix} \mathbf{V}_F(i\Delta x, s)\Delta x \\ \mathbf{I}_F(i\Delta x, s)\Delta x \end{bmatrix} \right\} \quad (3.6)$$

When $\Delta x \rightarrow 0$, Eq. (3.6) becomes

$$\begin{bmatrix} \mathbf{V}_{FT}(L, s) \\ \mathbf{I}_{FT}(L, s) \end{bmatrix} = \int_0^L \Phi(L-x, s) \begin{bmatrix} \mathbf{V}_F(x, s) \\ \mathbf{I}_F(x, s) \end{bmatrix} dx \quad (3.7)$$

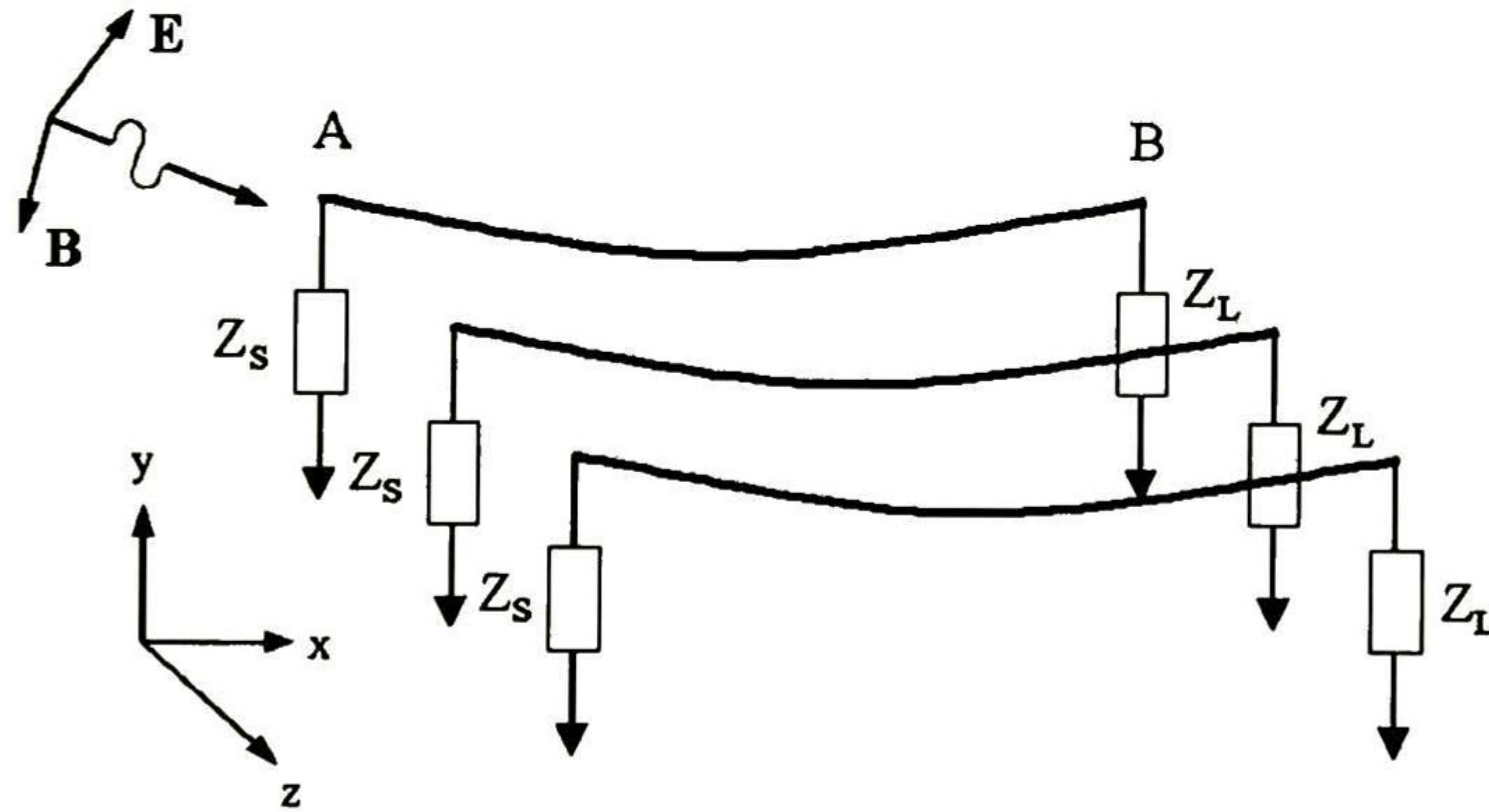


Figure 3.1. Field excited NUL configuration

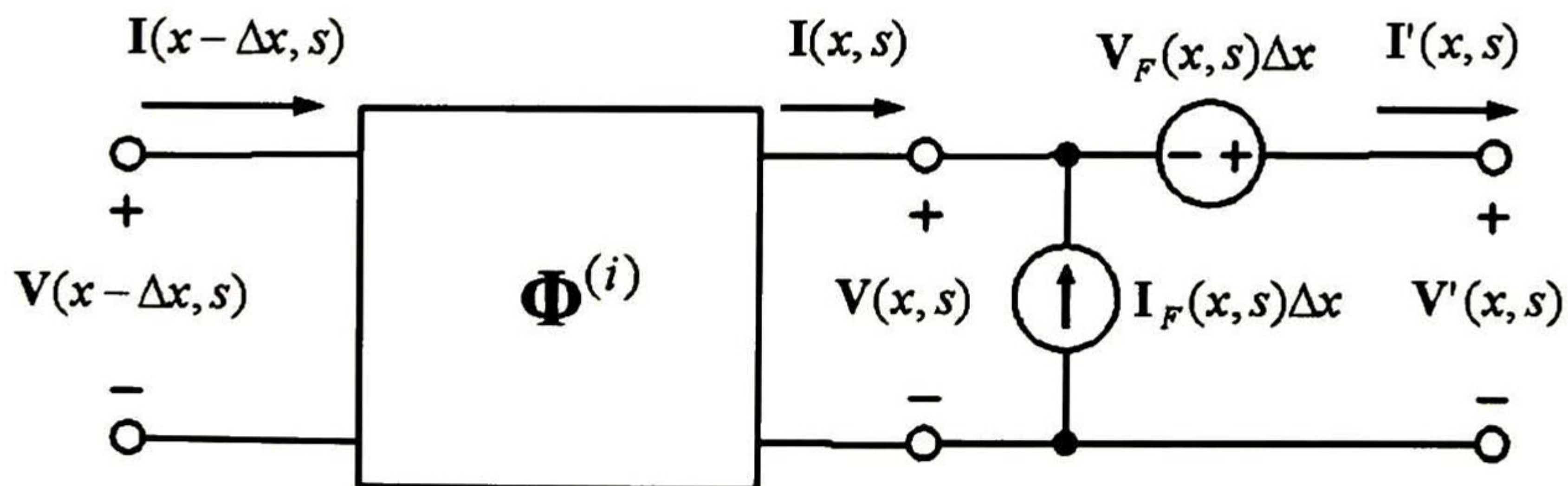


Figure 3.2. Representation of a field excited line segment

From Eq. (3.5) and (3.7), it is noticed that the incident fields add a convolution term to the cascaded connection of chain matrices. This is, the incident field excitation of the NUL can be approximated through the inclusion of the lumped sources $\mathbf{V}_{FT}(L,s)$ and $\mathbf{I}_{FT}(L,s)$ at point $x = L$ of the unexcited line, as shown in Fig. 3.3. Equation (3.5) can also be expressed in nodal form as

$$\begin{bmatrix} \mathbf{I}(0,s) \\ \mathbf{I}'(L,s) - \mathbf{I}_{FT}(L,s) \end{bmatrix} = \begin{bmatrix} \mathbf{Y}_{SS} & -\mathbf{Y}_{SR} \\ -\mathbf{Y}_{SR} & \mathbf{Y}_{RR} \end{bmatrix} \begin{bmatrix} \mathbf{V}(0,s) \\ \mathbf{V}'(L,s) - \mathbf{V}_{FT}(L,s) \end{bmatrix} \quad (3.8)$$

where

$$\mathbf{Y}_{SS} = -\Phi_{12}^{-1} \Phi_{11} \quad (3.9a)$$

$$\mathbf{Y}_{SR} = -\Phi_{12}^{-1} = \Phi_{22} \Phi_{12}^{-1} \Phi_{11} - \Phi_{21} \quad (3.9b)$$

$$\mathbf{Y}_{RR} = \Phi_{22} \Phi_{12}^{-1} \quad (3.9c)$$

and

$$\begin{bmatrix} \Phi_{11} & \Phi_{12} \\ \Phi_{21} & \Phi_{22} \end{bmatrix} = \begin{bmatrix} \prod_{i=1}^M \Phi^{(M+1-i)} \end{bmatrix} \quad (3.10)$$

3.2.3 Modified Nodal Analysis

In Eq. (3.8), $\mathbf{I}(0,s)$, $\mathbf{I}(L,s)$, $\mathbf{V}_{FT}(L,s)$ and $\mathbf{I}_{FT}(L,s)$ are known vectors, while $\mathbf{V}(0,s)$ and $\mathbf{V}(L,s)$ are unknown. Therefore, solving this equation implies a series of algebraic manipulations. An alternative way to represent the inclusion of the equivalent sources $\mathbf{V}_{FT}(L,s)$ and $\mathbf{I}_{FT}(L,s)$ is through the application of the Modified Nodal Analysis (MNA) [55]. This method, unlike the conventional nodal method, allows the direct insertion of ideal voltage sources.

Figure 3.4 shows the application of the MNA for a multiconductor transmission line with incident field excitation. The modified nodal representation, according to Figs. 3.4(b) and 3.4(c), is as follows:

$$\begin{bmatrix} \mathbf{0} \\ \mathbf{I}_{FT} \\ \mathbf{0} \\ \mathbf{V}_{FT} \end{bmatrix} = \begin{bmatrix} \mathbf{Y}_{SS} + \mathbf{Y}_S & -\mathbf{Y}_{SR} & \mathbf{0} & \mathbf{0} \\ -\mathbf{Y}_{SR} & \mathbf{Y}_{RR} & \mathbf{0} & \mathbf{U} \\ \mathbf{0} & \mathbf{0} & \mathbf{Y}_L & -\mathbf{U} \\ \mathbf{0} & \mathbf{U} & -\mathbf{U} & \mathbf{0} \end{bmatrix} \begin{bmatrix} \mathbf{V}_1 \\ \mathbf{V}_2 \\ \mathbf{V}_3 \\ \mathbf{J}_{FT} \end{bmatrix} \quad (3.11)$$

where \mathbf{Y}_{SS} , \mathbf{Y}_{SR} and \mathbf{Y}_{RR} are defined by (3.9); \mathbf{V}_1 , \mathbf{V}_2 and \mathbf{V}_3 are voltage vectors for the nodes indicated by their subscripts; \mathbf{J}_{FT} is the vector of currents flowing through the ideal voltage

source vector \mathbf{V}_{FT} , \mathbf{Y}_S and \mathbf{Y}_L are the source and load admittance matrices, as shown in Fig. 3.4. Notice that (3.11) complies with

$$\mathbf{V}_{FT} = \mathbf{V}_2 - \mathbf{V}_3 \tag{3.12}$$

3.3 Applications

Simulation of two application examples was performed. First, a 3-phase distribution line excited by an electromagnetic field propagating in the $-y$ direction was analyzed. Then, the same line was excited by a field propagating in the x direction. Results were compared with those obtained using ATP/EMTP. Simulations were conducted using the same PC of section 2.5.

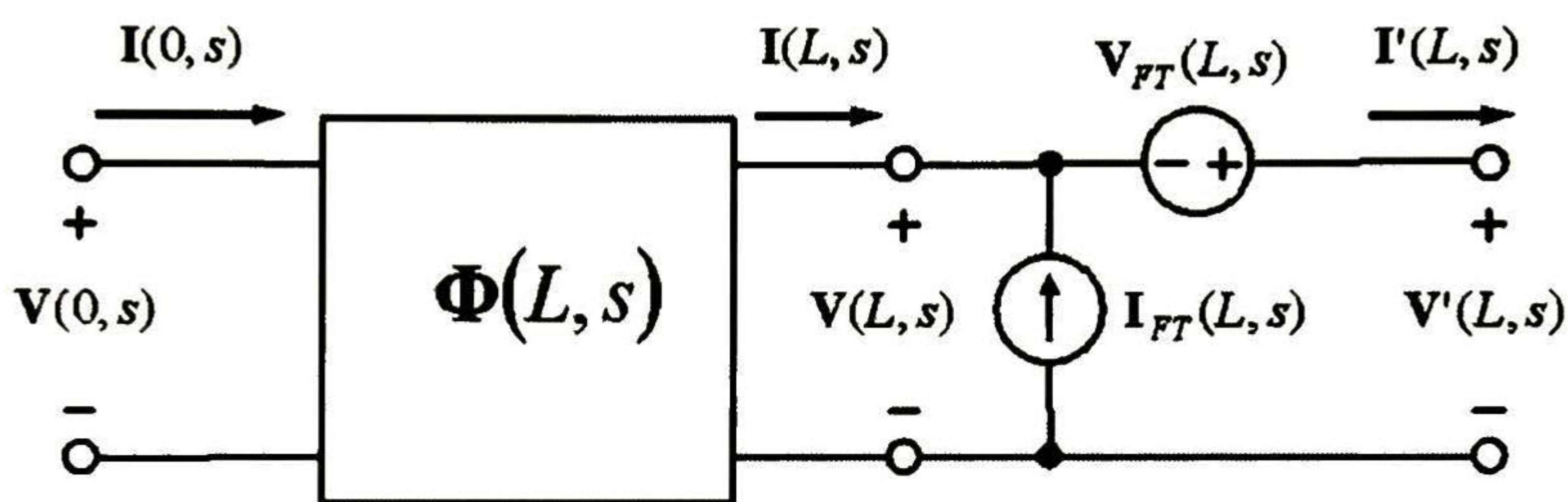


Figure 3.3. Field excited line representation through equivalent sources.

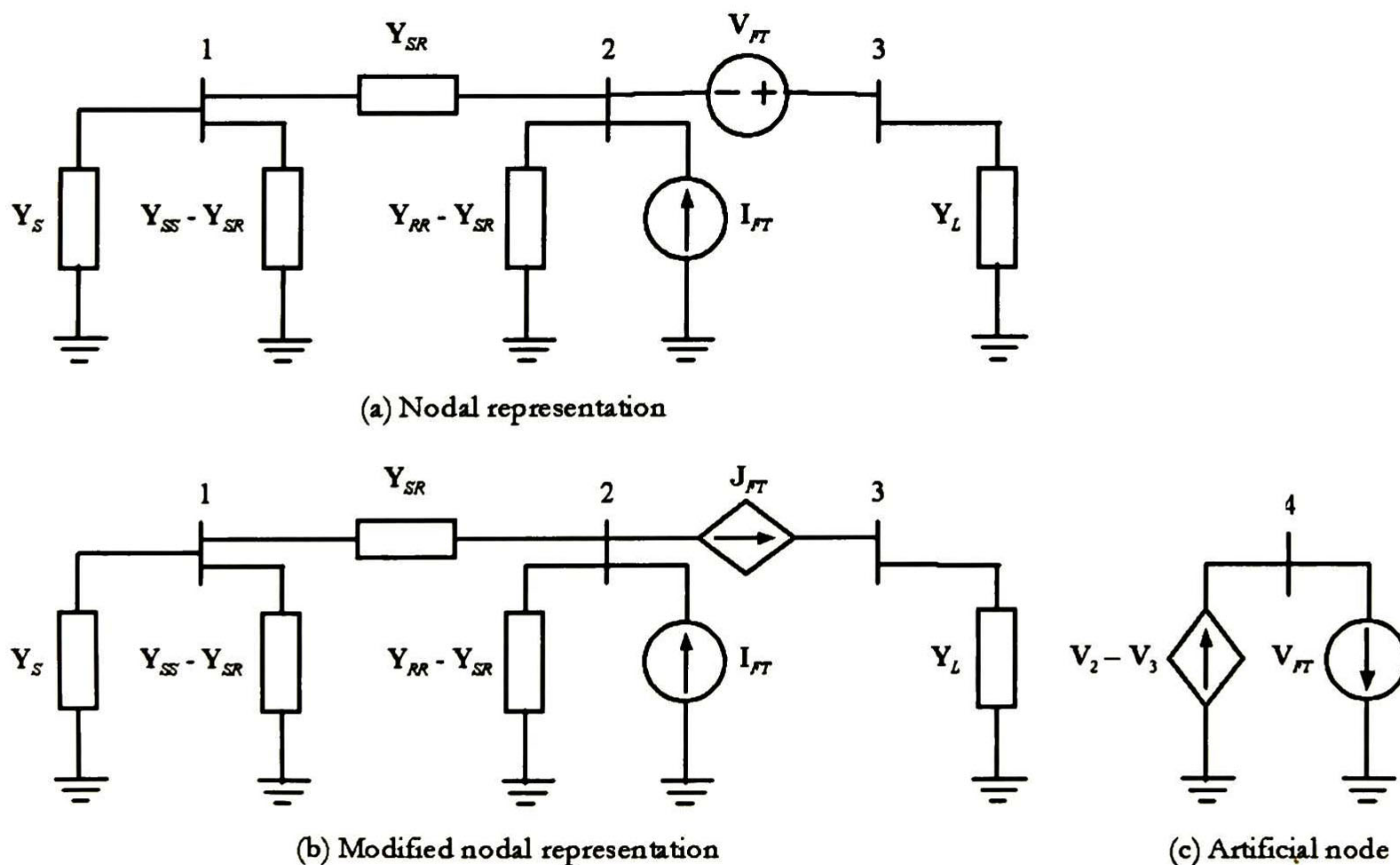


Figure 3.4. Representation of a transmission line with incident field excitation through MNA.

3.3.1 Field excited Distribution Line with Propagation in the $-y$ Direction

A 3-phase line of 100m excited by a plane wave propagating in the $-y$ direction is presented, as shown in Fig. 3.1. The only field components with non-zero value are \mathbf{B}_z and \mathbf{E}_x . Therefore, from (3.2b), $\mathbf{I}_F(x,s) = 0$, while the elements of the series voltage source $\mathbf{V}_F(x,s)$ are determined as follows:

$$V_{Fi}(x,s) = h_i(x)F(s) \quad (3.13)$$

where $F(s)$ is the Laplace transform of a uniform linear double ramp [1(V/m)/10ns/90ns] and $h_i(x)$ is a function that represents the height variations due to sagging of the i -th conductor. The line maximum and minimum heights are 10m and 5m, respectively. The 3 phases are connected to resistances of 523Ω at both ends. Distance between phases is 0.3 m. Results obtained when applying the proposed technique were compared with EMTP/ATP, using the J. Marti line model [6]. In both cases, the line was divided in 20 equal segments. Fig. 3.5 shows the induced voltages at ends A and B of the central conductor of the line. For this case, the simulation with the ATP took 5.76 seconds plus 2.66×20 required for the J. Martí fitting routine. The complete simulation with the NLT program took 8.34 seconds. This example was repeated including one neutral wire located 1.8m below the central phase (radius = 1.25cm, resistivity = $2 \times 10^{-7}\Omega\text{-m}$, relative permeability = 1000). Results using frequency dependent electrical parameters and constant electrical parameters are shown in Fig. 3.6. Although both waveforms are very similar, the difference is readily seen. As in example 2.5.1, computer times when using frequency dependent parameters were very close to those of constant parameters.

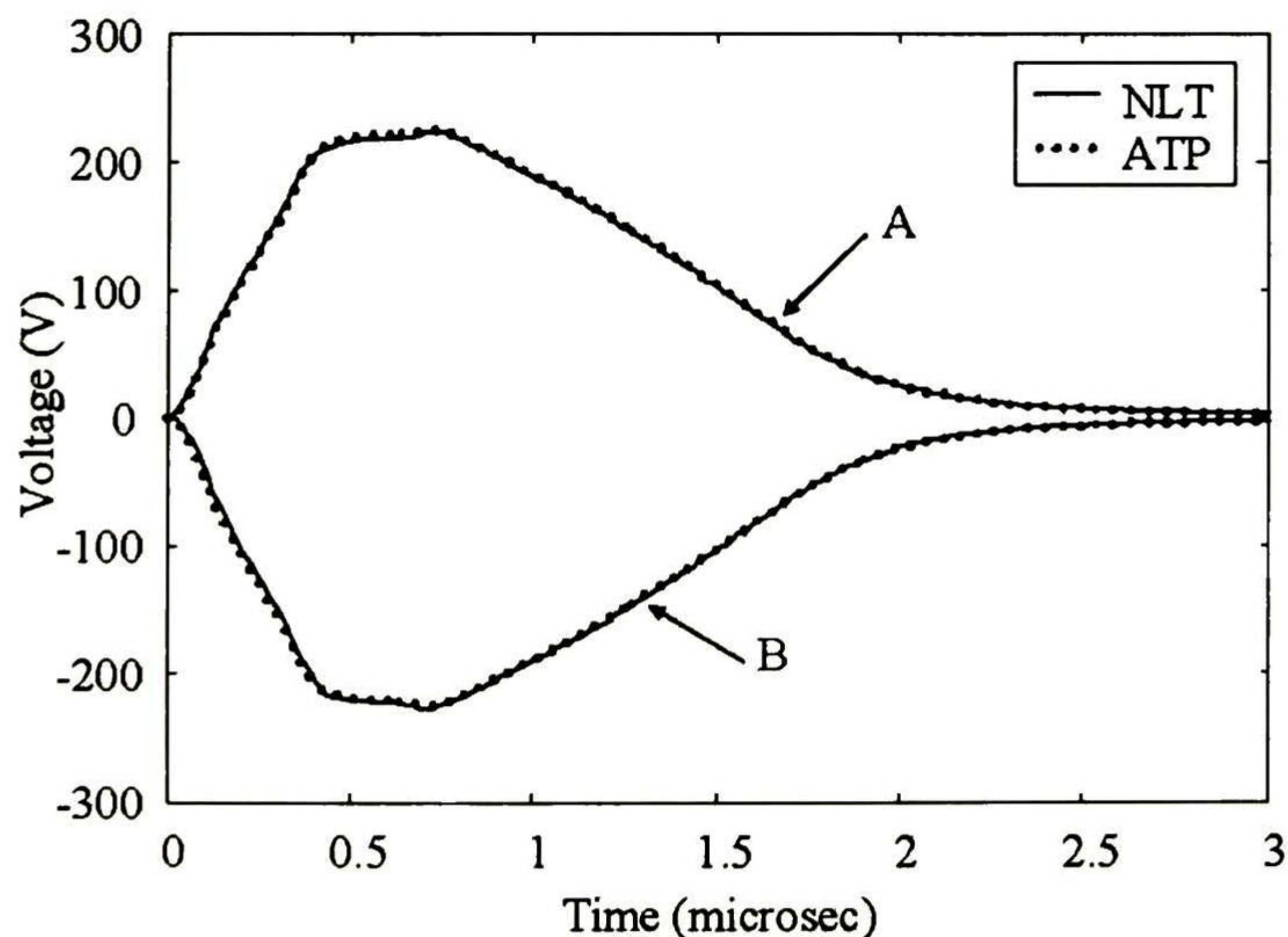


Figure 3.5. Induced voltages at the ends of the line central conductor.

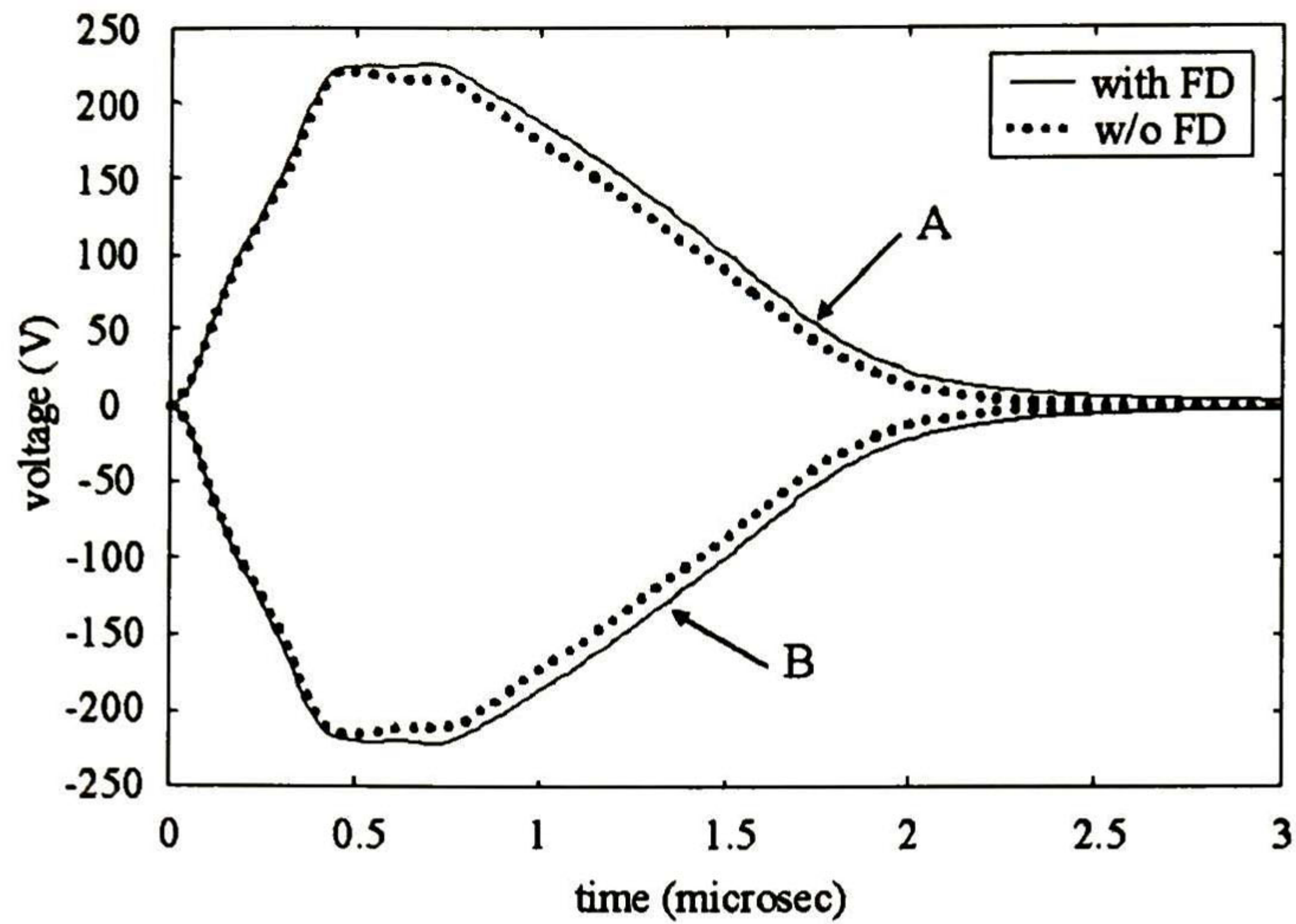


Figure 3.6. Induced voltages at the ends of the line central conductor (including a neutral wire below phase conductors).

3.3.2 Incident Field with Propagation in the x Direction

The same line of section 3.3.1 is now excited by a plane wave propagating in the x direction. $V_F(x,s)$ is determined as in the previous example, while $I_F(x,s)$ is computed using (3.2b). Fig. 3.7 shows the induced voltages at ends A and B of the central conductor, computed with the NLT program.

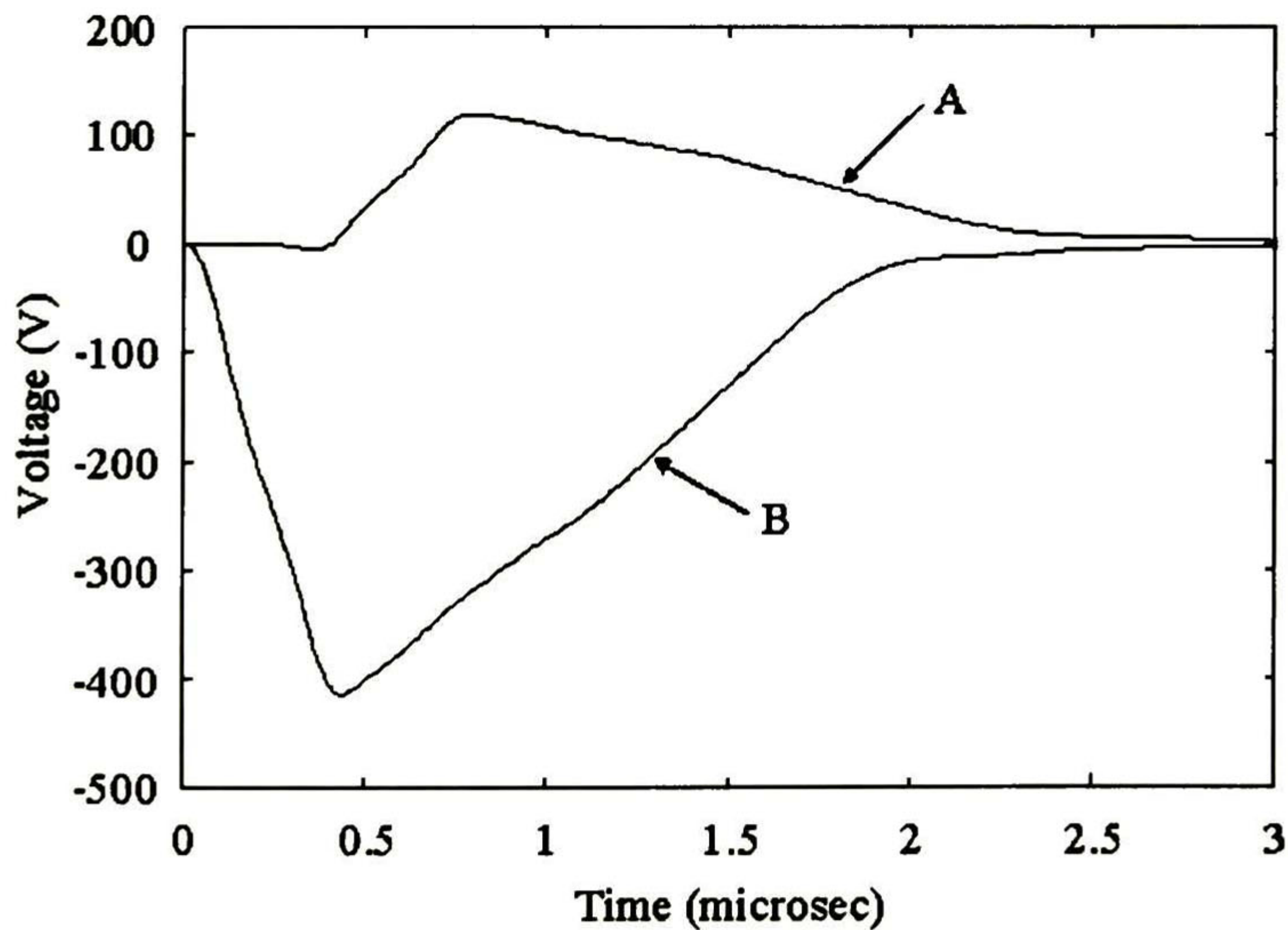


Figure 3.7. Induced voltages at the ends of the line central conductor.

3.4 Conclusions

A method for analyzing electromagnetic transients in field excited non-uniform multiconductor transmission lines using the Numerical Laplace Transform has been presented. The examples reveal a high agreement with the ATP/EMTP results. As in Chapter 2, the importance of including frequency dependence of the line parameters has been analyzed. The amplitude difference of the waveforms shown in Fig. 3.6 with and without including frequency dependent effects could be of importance for the design and coordination of line protections.

4 Time Domain Analysis of Non-uniform Lines

4.1 Introduction

In Chapter 2, a frequency domain model for non-uniform lines has been presented. It has been shown that the inclusion of frequency dependence in the line electrical parameters is a straightforward process in this domain. In the other hand, the inclusion of these effects in time domain adds considerable complications to the general, time domain solution of the transmission line equations.

In this Chapter, a new time domain model for single phase non-uniform transmission lines with frequency dependent electrical parameters is presented. The proposed model is based on synthesizing an equivalent uniform transmission line from the chain matrix of the NUL. The frequency and the space dependence of the electrical parameters of the NUL are introduced into the equivalent uniform line model by means of a transient resistance and a transient conductance. The resulting modified transmission line equations are solved by using the Method of Characteristics.

The Method of Characteristics, one of several finite difference methods, has been used successfully in calculating transients on lines with non-uniformities and nonlinear effects, due to its effectiveness in solving propagation equations of hyperbolic type, such as the transmission line equations [23, 24]. It has been reported that this method does not present the numerical oscillations that are very common in finite difference methods [51-54]. In this thesis, a new single-interior point procedure for this method is presented.

Results obtained with the proposed method are compared with those obtained with the Numerical Laplace Transform method.

4.2 Transient Parameters of a Non-uniform Line

Consider the 2-port model for non-uniform transmission lines defined in (2.11). For a single phase line, this model can be written as follows:

$$\begin{bmatrix} V(L,s) \\ I(L,s) \end{bmatrix} = \left[\prod_{i=1}^M \Phi^{(M+1-i)} \right] \begin{bmatrix} V(0,s) \\ I(0,s) \end{bmatrix} = \begin{bmatrix} \Phi_{11} & \Phi_{12} \\ \Phi_{21} & \Phi_{22} \end{bmatrix} \begin{bmatrix} V(0,s) \\ I(0,s) \end{bmatrix} \quad (4.1)$$

where $V(0,s)$ and $I(0,s)$ are the voltage and current in the Laplace domain at point $x = 0$ of the line, respectively, while $V(L,s)$ and $I(L,s)$ are the analogous values at point $x = L$. For a symmetrical non-uniform line (non-uniformities are symmetric with respect to the center of the line), the values of Φ_{11} , Φ_{12} , Φ_{21} and Φ_{22} of Eq. (4.1) can be defined as

$$\Phi_{11} = \cosh(\gamma_{nu} L) \quad (4.2a)$$

$$\Phi_{12} = \frac{1}{Y_{0,nu}} \sinh(\gamma_{nu} L) \quad (4.2b)$$

$$\Phi_{21} = Y_{0,nu} \sinh(\gamma_{nu} L) \quad (4.2c)$$

$$\Phi_{22} = \Phi_{11} \quad (4.2d)$$

being γ_{nu} the propagation constant and $Y_{0,nu}$ the characteristic admittance corresponding to the complete non-uniform line. These values are defined by the following equations:

$$\gamma_{nu} = \sqrt{Z_{nu} Y_{nu}} \quad (4.3a)$$

$$Y_{0,nu} = \sqrt{\frac{Y_{nu}}{Z_{nu}}} \quad (4.3b)$$

where Z_{nu} and Y_{nu} are the longitudinal impedance and transversal admittance of the complete non-uniform line, respectively. From (4.2b) and (4.2c), the following equality can be found:

$$Y_{0,nu} \Phi_{12} = \frac{\Phi_{21}}{Y_{0,nu}} \quad (4.4)$$

Solving (4.4) for $Y_{0,nu}$ it yields

$$Y_{0,nu} = \sqrt{\frac{\Phi_{21}}{\Phi_{12}}} \quad (4.5)$$

and solving (4.2a) or (4.2d) for γ_{nu}

$$\gamma_{nu} = \frac{\text{arccosh}(\Phi_{11})}{L} = \frac{\text{arccosh}(\Phi_{22})}{L} \quad (4.6)$$

In the other hand, from (4.3a) and (4.3b)

$$Z_{nu} = \gamma_{nu} / Y_{0,nu} \quad (4.7a)$$

$$Y_{nu} = \gamma_{nu} Y_{0,nu} \quad (4.7b)$$

However, a non symmetrical line such as the one shown in Fig. 2.2 does not comply with the equality expressed in (4.2d) because of its bi-directional nature. Thus, when analyzing this type of line, if the left hand side of the line is the source side and the right hand side is the load side, the propagation constant is computed from (4.2a). Otherwise, this constant is computed from (4.2d).

Finally, a uniform line model equivalent to the non-uniform line is proposed:

$$\frac{d}{dx} \begin{bmatrix} V(x,s) \\ I(x,s) \end{bmatrix} = \begin{bmatrix} 0 & -Z_{nu} \\ -Y_{nu} & 0 \end{bmatrix} \begin{bmatrix} V(x,s) \\ I(x,s) \end{bmatrix} \quad (4.8)$$

with Z_{nu} and Y_{nu} computed from the elements of the chain matrix of the complete non-uniform line. These terms can be expressed as

$$Z_{nu} = R'(s) + sL_G \quad (4.9a)$$

$$Y_{nu} = G'(s) + sC_G \quad (4.9b)$$

where $R'(s)$ and $G'(s)$ represent the transient longitudinal resistance and shunt conductance of the line, while L_G and C_G are the geometric inductance and capacitance computed at a mean value of the line non-uniformity, respectively. From (4.9), the transient electrical parameters are given by

$$R'(s) = Z_{nu} / s - L_G \quad (4.10a)$$

$$G'(s) = Y_{nu} / s - C_G \quad (4.10b)$$

As explained in the next sections, these values can be included in time domain analysis by means of recursive convolutions using rational approximations.

4.3 Telegrapher Equations in Time Domain

The Telegrapher Equations of a single phase transmission line, including frequency dependence of the line electrical parameters, are defined as follows [44]:

$$\frac{\partial v}{\partial x} + L_G \frac{\partial i}{\partial t} + \frac{\partial}{\partial t} \int_0^t r'(t-\tau) i(\tau) d\tau = 0 \quad (4.11a)$$

$$\frac{\partial i}{\partial x} + C_G \frac{\partial v}{\partial t} + \frac{\partial}{\partial t} \int_0^t g'(t-\tau) v(\tau) d\tau = 0 \quad (4.11b)$$

where $r'(t)$ and $g'(t)$ are the time domain versions of (4.10a) and (4.10b), respectively. If $R'(s)$ and $G'(s)$ are synthesized using rational functions and applying the Leibnitz's rule [24], the line equations can be expressed as follows:

$$\frac{\partial v}{\partial x} + D \frac{\partial i}{\partial t} + R_x i + \psi = 0 \quad (4.12a)$$

$$\frac{\partial i}{\partial x} + E \frac{\partial v}{\partial t} + G_x v + \phi = 0 \quad (4.12b)$$

where

$$\psi = -\sum_{i=1}^{N_1} k_i p_i \int_0^t e^{-p_i(t-\tau)} i(\tau) d\tau \quad (4.13a)$$

$$\phi = -\sum_{i=1}^{N_2} m_i q_i \int_0^t e^{-q_i(t-\tau)} v(\tau) d\tau \quad (4.13b)$$

$$R_x = \sum_{i=0}^{N_1} k_i, \quad G_x = \sum_{i=0}^{N_2} m_i \quad (4.13c), (4.13d)$$

$$D = k_\infty + L_G, \quad E = m_\infty + C_G \quad (4.13e), (4.13f)$$

Besides, k_i and p_i are the poles and residues of the rational approximation of $R'(s)$, while m_i and q_i are the poles and residues of the rational approximation of $G'(s)$, respectively. These poles and residues are computed using the technique known as Vector Fitting [8].

4.4 Method of Characteristics

Equations (4.12a) and (4.12b) can be represented as a 2x2 set of first order partial differential equations [56]:

$$\frac{\partial}{\partial x} \mathbf{U} + \mathbf{A} \frac{\partial}{\partial t} \mathbf{U} + \mathbf{B} \mathbf{U} + \mathbf{W} = 0 \quad (4.14)$$

where

$$\mathbf{U} = \begin{bmatrix} v \\ i \end{bmatrix}, \quad \mathbf{A} = \begin{bmatrix} 0 & D \\ E & 0 \end{bmatrix}, \quad (4.15a), (4.15b),$$

$$\mathbf{B} = \begin{bmatrix} 0 & R_x \\ G_x & 0 \end{bmatrix}, \quad \mathbf{W} = \begin{bmatrix} \psi \\ \phi \end{bmatrix} \quad (4.15c), (4.15d)$$

The eigenvalues of \mathbf{A} are given by

$$\lambda_{1,2} = \pm \sqrt{DE} \quad (4.16)$$

and the eigenvectors are given by

$$\mathbf{M}_L = \begin{bmatrix} 1 & Z_w \\ 1 & -Z_w \end{bmatrix}, \quad \mathbf{M}_R = \begin{bmatrix} 1 & 1 \\ Y_w & -Y_w \end{bmatrix} \quad (4.17a), (4.17b)$$

where

$$Z_w = \sqrt{D/E}, \quad Y_w = Z_w^{-1} \quad (4.18a), (4.18b)$$

Left multiplying (4.12a) and (4.12b) times \mathbf{M}_L , as defined in (4.17a), yields

$$\begin{bmatrix} \left(\frac{\partial v}{\partial x} + D \frac{\partial i}{\partial t} + R_x i + \psi \right) + Z_w \left(\frac{\partial i}{\partial x} + E \frac{\partial v}{\partial t} + G_x v + \phi \right) \\ \left(\frac{\partial v}{\partial x} + D \frac{\partial i}{\partial t} + R_x i + \psi \right) - Z_w \left(\frac{\partial i}{\partial x} + E \frac{\partial v}{\partial t} + G_x v + \phi \right) \end{bmatrix} = \begin{bmatrix} 0 \\ 0 \end{bmatrix} \quad (4.19)$$

Regrouping (4.19) and applying (4.16) and (4.18a)

$$\begin{bmatrix} \left(\frac{\partial}{\partial x} + \lambda_1 \frac{\partial}{\partial t} \right) v + Z_w \left(\frac{\partial}{\partial x} + \lambda_1 \frac{\partial}{\partial t} \right) i + R_x i + Z_w G_x v + \psi + Z_w \phi \\ \left(\frac{\partial}{\partial x} + \lambda_2 \frac{\partial}{\partial t} \right) v - Z_w \left(\frac{\partial}{\partial x} + \lambda_2 \frac{\partial}{\partial t} \right) i + R_x i - Z_w G_x v + \psi - Z_w \phi \end{bmatrix} = \begin{bmatrix} 0 \\ 0 \end{bmatrix} \quad (4.20)$$

Along the characteristic curves defined by $\lambda = \pm dt/dx$, the following equivalence can be applied:

$$\left(\frac{\partial}{\partial x} + \lambda_1 \frac{\partial}{\partial t} \right) \Leftrightarrow \frac{d}{dx} \quad \text{and} \quad \left(\frac{\partial}{\partial x} + \lambda_2 \frac{\partial}{\partial t} \right) \Leftrightarrow \frac{d}{dx} \quad (4.21a), (4.21b)$$

Finally, using (4.21) in (4.20), it can be written

$$\begin{bmatrix} dv + Z_w di + R_x i dx + Z_w G_x v dx + (\psi + Z_w \phi) dx \\ dv - Z_w di + R_x i dx - Z_w G_x v dx + (\psi - Z_w \phi) dx \end{bmatrix} = \begin{bmatrix} 0 \\ 0 \end{bmatrix} \quad (4.22)$$

4.5 Numerical Solution

In order to deal with the convolution terms of Eq. (4.22), these terms are numerically solved using backward Euler rule when the poles and residues are real and central differences rule when the poles and residues are complex pairs, as detailed in section 4.5.1. Complete numerical solution of Eq. (4.22) is found applying finite differences, as explained in sections 4.5.2 and 4.5.3.

4.5.1 Numerical Treatment of the Recursive Convolutions

4.5.1.1 Real Poles and Residues

If $\Psi(s)$ is the Laplace domain spectrum of the recursive convolution ψ given in (4.13a), the rational approximation of $\Psi(s)$ is given by the following expression:

$$\Psi(s) = -\sum_{i=1}^{N_1} \Psi_i, \quad i = 1, 2, \dots, N_1 \quad (4.23)$$

where N_1 is the order of the approximation. For real poles and residues

$$\Psi_i = \frac{k_i p_i}{s + p_i} I(s) \quad (4.24)$$

Equation (4.24) can be written as

$$s\Psi_i + p_i \Psi_i = k_i p_i I(s) \quad (4.25)$$

or in time domain

$$\frac{d\psi_i}{dt} + p_i \psi_i = k_i p_i i(t) \quad (4.26)$$

Applying backward Euler rule to Eq. (4.26)

$$\psi_{i,n+1} = \frac{\Delta t}{1 + p_i \Delta t} \left(\frac{\psi_{i,n}}{\Delta t} + k_i p_i i_{n+1} \right) \quad (4.27)$$

with $\psi_{i,n}$ denoting $\psi_{i(n\Delta t)}$. According to (4.23), the total convolution can be expressed as follows:

$$\psi_{n+1} = -\sum_{i=1}^{N_1} \psi_{i,n+1} = -\sum_{i=1}^{N_1} \frac{\Delta t}{1 + p_i \Delta t} \left(\frac{\psi_{i,n}}{\Delta t} + k_i p_i i_{n+1} \right) \quad (4.28)$$

and similarly for ϕ

$$\phi_{n+1} = -\sum_{i=1}^{N_2} \phi_{i,n+1} = -\sum_{i=1}^{N_2} \frac{\Delta t}{1 + q_i \Delta t} \left(\frac{\phi_{i,n}}{\Delta t} + m_i q_i v_{n+1} \right) \quad (4.29)$$

being N_2 the order of the approximation.

4.5.1.2 Complex Poles and Residues

If the rational approximation of $\Psi(s)$ is computed using complex pairs of poles and residues, Eq. (4.24) is modified as follows:

$$\Psi_i = \left(\frac{k_i p_i}{s + p_i} + \frac{k_i^* p_i^*}{s + p_i^*} \right) I(s) \quad (4.30)$$

which is equivalent to

$$\Psi_i = \left(\frac{a_i s + b_i c_i}{s^2 + d_i s + b_i} \right) I(s) \quad (4.31)$$

where

$$a_i = k_i p_i + k_i^* p_i^* \quad (4.32a)$$

$$b_i = p_i p_i^* \quad (4.32b)$$

$$c_i = k_i + k_i^* \quad (4.32c)$$

$$d_i = p_i + p_i^* \quad (4.32d)$$

The coefficients a_i , b_i , c_i and d_i defined in (4.32) are always real. Eq. (4.31) can be written as

$$s^2 \Psi_i + d_i s \Psi_i + b_i \Psi_i = a_i s I(s) + b_i c_i I(s) \quad (4.33)$$

or in time domain

$$\frac{d^2 \psi_i}{dt^2} + d_i \frac{d\psi_i}{dt} + b_i \psi_i = a_i \frac{di(t)}{dt} + b_i c_i i(t) \quad (4.34)$$

Applying the central differences rule to (4.34) and in accordance to (4.23), the total convolution is expressed as follows:

$$\psi_{n+1} = -\sum_{i=1}^{N_1} \frac{\Delta t}{1 + d_i \Delta t / 2} \left[\frac{a_i}{2} (i_{n+1} - i_{n-1}) + b_i c_i \Delta t i_n + \frac{\psi_{i,n} (2 - b_i \Delta t^2) - \psi_{i,n-1} (1 - d_i \Delta t / 2)}{\Delta t} \right] \quad (4.35)$$

and similarly for ϕ

$$\phi_{n+1} = -\sum_{i=1}^{N_2} \frac{\Delta t}{1 + h_i \Delta t / 2} \left[\frac{e_i}{2} (v_{n+1} - v_{n-1}) + f_i g_i \Delta t v_n + \frac{\phi_{i,n} (2 - f_i \Delta t^2) - \phi_{i,n-1} (1 - h_i \Delta t / 2)}{\Delta t} \right] \quad (4.36)$$

where

$$e_i = m_i q_i + m_i^* q_i^* \quad (4.37a)$$

$$f_i = q_i q_i^* \quad (4.37b)$$

$$g_i = m_i + m_i^* \quad (4.37c)$$

$$h_i = q_i + q_i^* \quad (4.37d)$$

4.5.2 Internal Points

A numerical form of (4.22) can be found using finite differences:

$$\begin{bmatrix} \Delta v + Z_w \Delta i + R_x i \Delta x + Z_w G_x v \Delta x + (\psi + Z_w \phi) \Delta x \\ \Delta v - Z_w \Delta i + R_x i \Delta x - Z_w G_x v \Delta x + (\psi - Z_w \phi) \Delta x \end{bmatrix} = \begin{bmatrix} 0 \\ 0 \end{bmatrix} \quad (4.38)$$

Supposing that v and i are known values at points Q and Q' of Fig. 4.1, the solution can be extended to point P as follows:

$$(v_P - v_Q) + Z_w (i_P - i_Q) + \frac{R_x \Delta x}{2} (i_P + i_Q) + \frac{Z_w G_x \Delta x}{2} (v_P + v_Q) + \frac{\Delta x}{2} (\psi_P + \psi_Q) + \frac{Z_w \Delta x}{2} (\phi_P + \phi_Q) = 0 \quad (4.39a)$$

$$(v_P - v_Q) - Z_w (i_P - i_Q) - \frac{R_x \Delta x}{2} (i_P + i_Q) + \frac{Z_w G_x \Delta x}{2} (v_P + v_Q) - \frac{\Delta x}{2} (\psi_P + \psi_Q) + \frac{Z_w \Delta x}{2} (\phi_P + \phi_Q) = 0 \quad (4.39b)$$

Rearranging (4.39)

$$G_1 v_P + Z_1 i_P - G_2 v_Q - Z_2 i_Q + \frac{\Delta x}{2} (\psi_P + \psi_Q) + \frac{Z_w \Delta x}{2} (\phi_P + \phi_Q) = 0 \quad (4.40a)$$

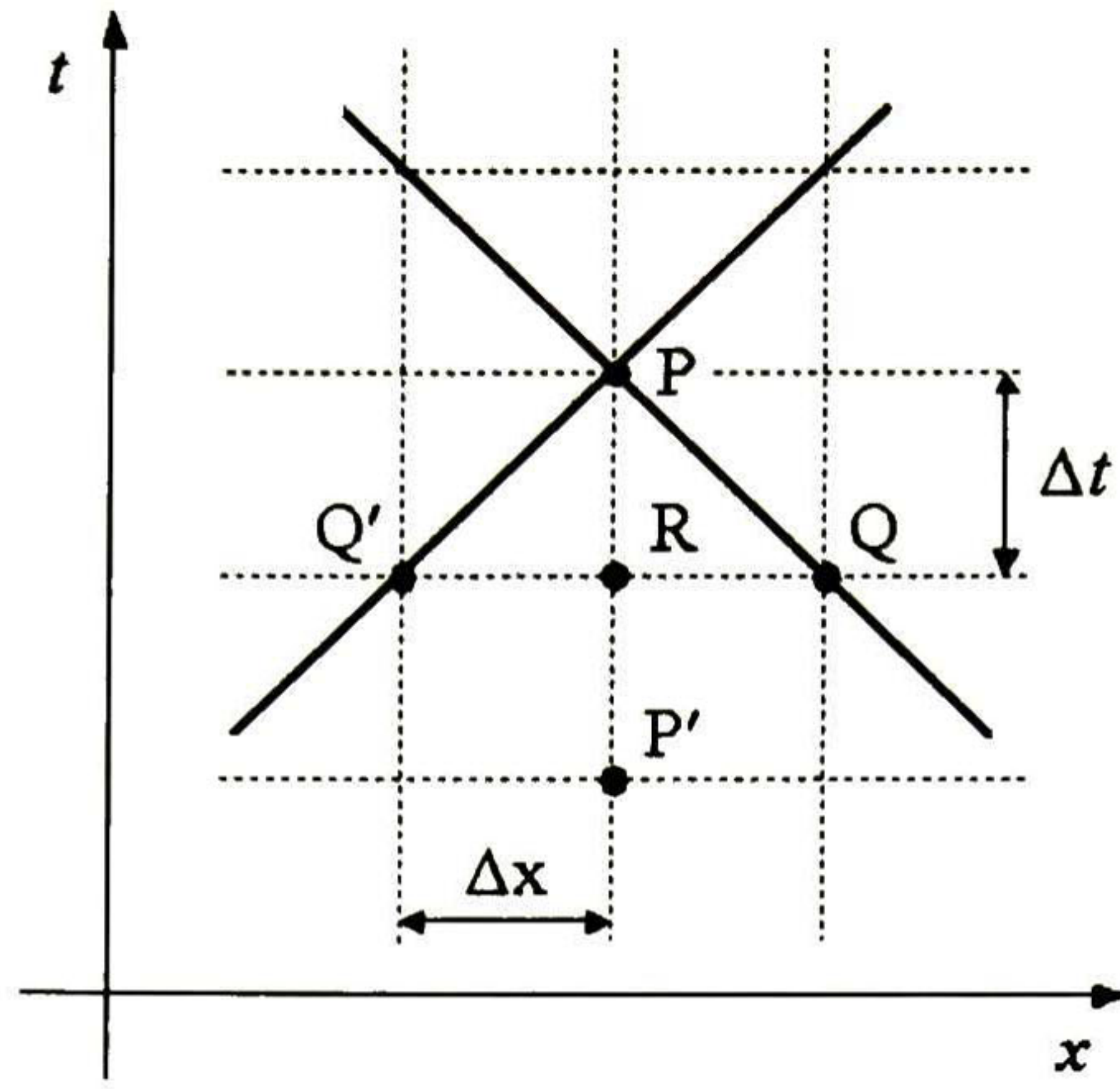


Figure 4.1. Characteristics grid – Internal points.

$$G_1 v_P - Z_1 i_P - G_2 v_Q + Z_2 i_Q - \frac{\Delta x}{2} (\psi_P + \psi_Q) + \frac{Z_W \Delta x}{2} (\phi_P + \phi_Q) = 0 \quad (4.40b)$$

where

$$G_1 = 1 + \frac{Z_W G_X \Delta x}{2}, \quad G_2 = 1 - \frac{Z_W G_X \Delta x}{2} \quad (4.41a), (4.41b)$$

$$Z_1 = Z_W + \frac{R_X \Delta x}{2}, \quad Z_2 = Z_W - \frac{R_X \Delta x}{2} \quad (4.41c), (4.41d)$$

Addition of (4.40a) and (4.40b) yields

$$2G_1 v_P - G_2 (v_{Q'} + v_Q) - Z_2 (i_{Q'} - i_Q) + \frac{\Delta x}{2} (\psi_{Q'} - \psi_Q) + \frac{Z_W \Delta x}{2} (2\phi_P + \phi_{Q'} + \phi_Q) = 0 \quad (4.42)$$

while the subtraction of the same equations gives

$$2Z_1 i_P - G_2 (v_{Q'} - v_Q) - Z_2 (i_{Q'} + i_Q) + \frac{\Delta x}{2} (2\psi_P + \psi_{Q'} + \psi_Q) + \frac{Z_W \Delta x}{2} (\phi_{Q'} - \phi_Q) = 0 \quad (4.43)$$

4.5.2.1 Computation of v_P and i_P with Real Poles and Residues

The voltage at point P can be computed from Eq. (4.42):

$$v_P = \frac{1}{2G_1} \left[G_2 (v_{Q'} + v_Q) + Z_2 (i_{Q'} - i_Q) - \frac{\Delta x}{2} (\psi_{Q'} - \psi_Q) - \frac{Z_W \Delta x}{2} (2\phi_P + \phi_{Q'} + \phi_Q) \right] \quad (4.44)$$

However, according to (4.29), ϕ_P is a function of v_P :

$$\phi_P = -\sum_{i=1}^{N_2} \frac{\Delta t}{1+q_i \Delta t} \left(\frac{\phi_{i,R}}{\Delta t} + m_i q_i v_P \right) \quad (4.45)$$

Hence, the following expression is defined instead of (4.44):

$$v_P = \frac{1}{2G_1'} \left[G_2 (v_{Q'} + v_Q) + Z_2 (i_{Q'} - i_Q) - \frac{\Delta x}{2} (\psi_{Q'} - \psi_Q) - \frac{Z_W \Delta x}{2} (2\phi_P' + \phi_{Q'} + \phi_Q) \right] \quad (4.46)$$

where ϕ_P' and G_1' are given by

$$\phi_P' = -\sum_{i=1}^{N_2} \frac{\phi_{i,R}}{1+q_i \Delta t} \quad (4.47a)$$

$$G_1' = G_1 - \frac{Z_W \Delta x \Delta t}{2} \sum_{i=1}^{N_2} \frac{m_i q_i}{1+q_i \Delta t} \quad (4.47b)$$

The current at point P, i_P , can be obtained from Eq. (4.43). Since now ψ_P is a function of i_P , this current is computed as

$$i_P = \frac{1}{2Z_1'} \left[G_2 (v_{Q'} - v_Q) + Z_2 (i_{Q'} + i_Q) - \frac{\Delta x}{2} (2\psi_P' + \psi_{Q'} + \psi_Q) - \frac{Z_W \Delta x}{2} (\phi_{Q'} - \phi_Q) \right] \quad (4.48)$$

where and ψ_P and Z_1' are given by

$$\psi_P' = -\sum_{i=1}^{N_1} \frac{\psi_{i,R}}{1+p_i \Delta t} \quad (4.49a)$$

$$Z_1' = Z_1 - \frac{\Delta x \Delta t}{2} \sum_{i=1}^{N_1} \frac{k_i p_i}{1+p_i \Delta t} \quad (4.49b)$$

4.5.2.2 Computation of v_P and i_P with Complex Poles and Residues

If ϕ_P is computed from (4.36) with complex poles and zeros, this convolution term is a function not only of v_P , but also of v_R and $v_{P'}$:

$$\phi_P = -\sum_{i=1}^{N_2} \frac{\Delta t}{1+h_i \Delta t / 2} \left[\frac{e_i}{2} (v_P - v_{P'}) + f_i g_i \Delta t v_R + \frac{\phi_{i,R} (2 - f_i \Delta t^2) - \phi_{i,P'} (1 - h_i \Delta t / 2)}{\Delta t} \right] \quad (4.50)$$

Similarly, if ψ_P is computed from (4.35) with complex poles and zeros, this term is a function of i_P , i_R and $i_{P'}$:

$$\psi_P = -\sum_{i=1}^{N_1} \frac{\Delta t}{1+d_i \Delta t/2} \left[\frac{a_i}{2} (i_P - i_{P'}) + b_i c_i \Delta t i_R + \frac{\psi_{i,R} (2 - b_i \Delta t^2) - \psi_{i,P'} (1 - d_i \Delta t/2)}{\Delta t} \right] \quad (4.51)$$

Therefore, v_P is computed from Eq. (4.42) as

$$v_P = \frac{1}{2G_1'} \left[-G_2' v_R - G_3' v_{P'} + G_2 (v_{Q'} + v_Q) + Z_2 (i_{Q'} - i_Q) - \frac{\Delta x}{2} (\psi_{Q'} - \psi_Q) - \frac{Z_W \Delta x}{2} (2\phi_{P'} + \phi_{Q'} + \phi_Q) \right] \quad (4.52)$$

while i_P is computed from Eq. (4.43) as

$$i_P = \frac{1}{2Z_1'} \left[-Z_2' i_R - Z_3' i_{P'} + G_2 (v_{Q'} - v_Q) + Z_2 (i_{Q'} + i_Q) - \frac{\Delta x}{2} (2\psi_{P'} + \psi_{Q'} + \psi_Q) - \frac{Z_W \Delta x}{2} (\phi_{Q'} - \phi_Q) \right] \quad (4.53)$$

where

$$\phi_P' = -\sum_{i=1}^{N_2} \frac{\phi_{i,R} (2 - f_i \Delta t^2) - \phi_{i,P'} (1 - h_i \Delta t/2)}{1 + h_i \Delta t/2} \quad (4.54a)$$

$$G_1' = G_1 - \frac{Z_W \Delta x \Delta t}{2} \sum_{i=1}^{N_2} \frac{e_i}{2 + h_i \Delta t} \quad (4.54b)$$

$$G_2' = -Z_W \Delta x \Delta t^2 \sum_{i=1}^{N_2} \frac{f_i g_i}{1 + h_i \Delta t/2} \quad (4.54c)$$

$$G_3' = Z_W \Delta x \Delta t \sum_{i=1}^{N_2} \frac{e_i}{2 + h_i \Delta t} \quad (4.54d)$$

$$\psi_P' = -\sum_{i=1}^{N_2} \frac{\psi_{i,R} (2 - b_i \Delta t^2) - \psi_{i,P'} (1 - d_i \Delta t/2)}{1 + d_i \Delta t/2} \quad (4.54e)$$

$$Z_1' = Z_1 - \frac{\Delta x \Delta t}{2} \sum_{i=1}^{N_1} \frac{a_i}{2 + d_i \Delta t} \quad (4.54f)$$

$$Z_2' = -\Delta x \Delta t^2 \sum_{i=1}^{N_1} \frac{b_i c_i}{1 + d_i \Delta t/2} \quad (4.54g)$$

$$Z_3' = \Delta x \Delta t \sum_{i=1}^{N_1} \frac{a_i}{2 + d_i \Delta t} \quad (4.54h)$$

4.5.3 Boundary Points

For the source boundary point S ($x = 0$), as shown in Fig. 4.2(a), the application of an ideal voltage source $v_s = f(t)$ is considered. In this case, Eq. (4.40b) is modified as follows:

$$G_1 v_s - Z_1 i_s - G_2 V_Q + Z_2 i_Q - \frac{\Delta x}{2} (\psi_s + \psi_Q) + \frac{Z_w \Delta x}{2} (\phi_s + \phi_Q) = 0 \quad (4.55)$$

For the load boundary point L ($x = L$), as shown in Fig. 4.2(b), the connection of a resistive load R_L is considered. This yields

$$i_L = \frac{v_L}{R_L} \quad (4.56)$$

Applying (4.56), Eq. (4.40a) is modified as follows:

$$G_1 v_L + Z_1 \frac{v_L}{R_L} - G_2 V_{Q'} - Z_2 i_{Q'} + \frac{\Delta x}{2} (\psi_L + \psi_{Q'}) + \frac{Z_w \Delta x}{2} (\phi_L + \phi_{Q'}) = 0 \quad (4.57)$$

4.5.3.1 Computation of i_s and v_L with Real Poles and Residues

The current at the source boundary point S, i_s , can be computed from Eq. (4.55). However, similarly to the internal points, ψ_s is a function of i_s ; thus, this current is computed as

$$i_s = \frac{1}{Z_1'} \left[G_1 v_s - G_2 V_Q + Z_2 i_Q - \frac{\Delta x}{2} (\psi_s' + \psi_Q) + \frac{Z_w \Delta x}{2} (\phi_s + \phi_Q) \right] \quad (4.58)$$

where Z_1' is computed from (4.49b) and ψ_s' is given by

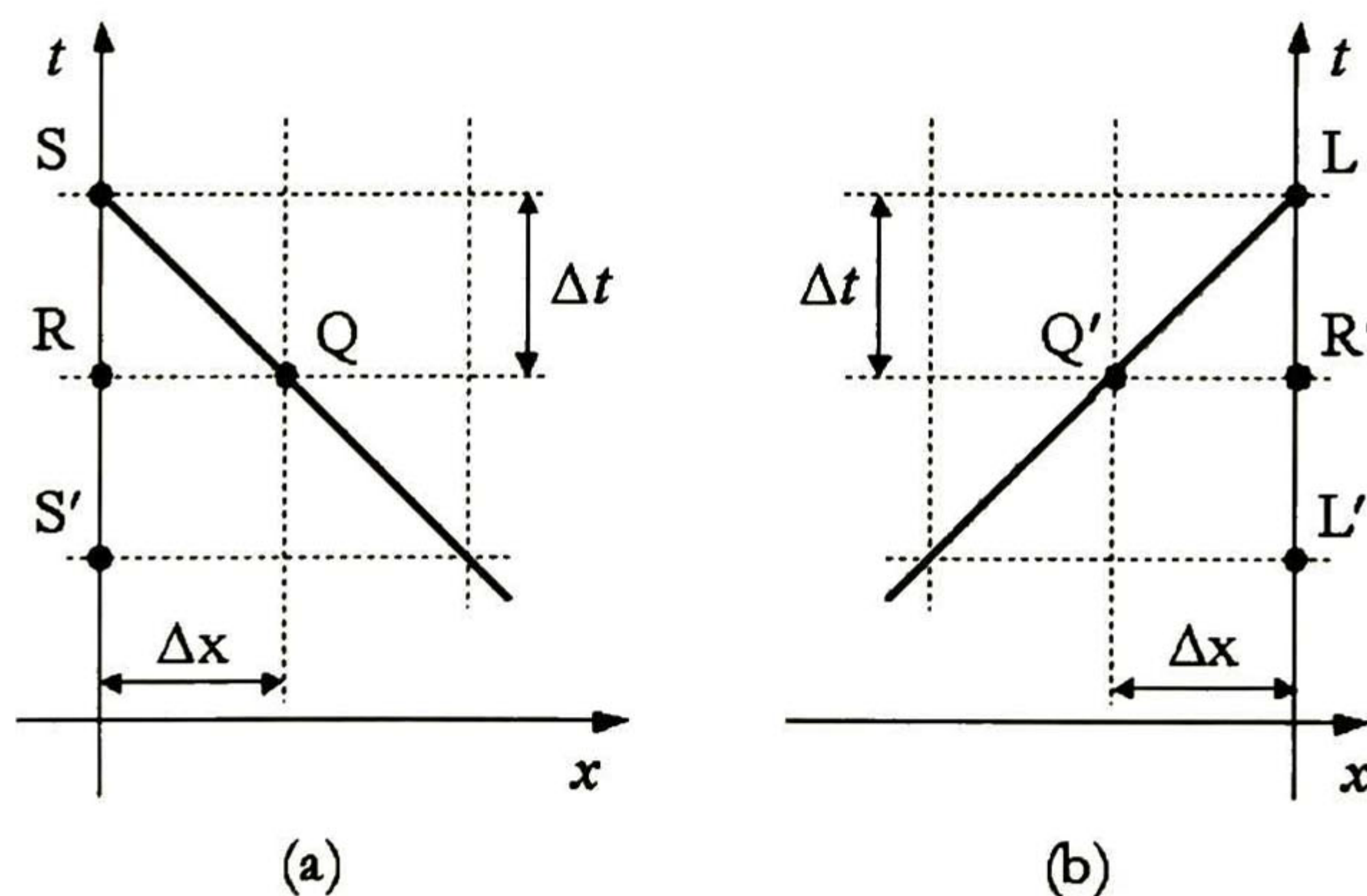


Figure 4.2. Characteristics grid: (a) source boundary, (b) load boundary.

$$\psi'_S = -\sum_{i=1}^{N_1} \frac{\psi_{i,R}}{1 + p_i \Delta t} \quad (4.59)$$

The voltage at the load boundary point L, v_L , can be computed from Eq. (4.57). But in this case ψ_L and ϕ_L are both functions of v_L and the computation of this voltage is done through the following equation:

$$v_L = \frac{R_L}{G'_1 R_L + Z'_1} \left[G_2 V_{Q'} + Z_2 i_{Q'} - \frac{\Delta x}{2} (\psi'_L + \psi_{Q'}) - \frac{Z_W \Delta x}{2} (\phi'_L + \phi_{Q'}) \right] \quad (4.60)$$

where G'_1 is computed from (4.47b) while ψ'_L and ϕ'_L are given by

$$\psi'_L = -\sum_{i=1}^{N_1} \frac{\psi_{i,R'}}{1 + p_i \Delta t} \quad (4.61a)$$

$$\phi'_L = -\sum_{i=1}^{N_2} \frac{\phi_{i,R'}}{1 + q_i \Delta t} \quad (4.61b)$$

4.5.3.2 Computation of i_S and v_L with Complex Poles and Residues

At the source boundary point S, the convolution term ψ_S is a function of i_S , i_R and $i_{S'}$; thus, the current at this point is computed from (4.55) as follows:

$$i_S = \frac{1}{Z'_1} \left[-\frac{Z'_2 i_R + Z'_3 i_{S'}}{2} + G_1 v_S - G_2 V_{Q'} + Z_2 i_{Q'} - \frac{\Delta x}{2} (\psi'_S + \psi_{Q'}) + \frac{Z_W \Delta x}{2} (\phi_S + \phi_{Q'}) \right] \quad (4.62)$$

where Z'_1 , Z'_2 and Z'_3 are computed from (4.54f), (4.54g) and (4.54h), respectively, and

$$\psi'_S = -\sum_{i=1}^{N_1} \frac{\psi_{i,R} (2 - b_i \Delta t^2) - \psi_{i,S'} (1 - d_i \Delta t / 2)}{1 + d_i \Delta t / 2} \quad (4.63)$$

At the final boundary point L, the convolution terms ψ_L and ϕ_L are both functions of v_L , $v_{R'}$ and $v_{L'}$. Again, the voltage is computed from (4.56) as follows:

$$v_L = \frac{R_L}{G'_1 R_L + Z'_1} \left[-v_{R'} \left(\frac{G'_2 R_L + Z'_2}{2 R_L} \right) - v_{L'} \left(\frac{G'_3 R_L + Z'_3}{2 R_L} \right) + G_2 v_{Q'} + Z_2 i_{Q'} - \frac{\Delta x}{2} (\psi'_L + \psi_{Q'}) - \frac{Z_W \Delta x}{2} (\phi'_L + \phi_{Q'}) \right] \quad (4.64)$$

where G'_1 , G'_2 and G'_3 are computed from (4.54b), (4.54c) and (4.54d), respectively, and

$$\psi_L = -\sum_{i=1}^{N_1} \frac{\psi_{i,R'}(2 - bi \Delta t^2) - \psi_{i,L'}(1 - d_i \Delta t / 2)}{1 + d_i \Delta t / 2} \quad (4.65a)$$

$$\phi'_L = -\sum_{i=1}^{N_2} \frac{\phi_{i,R'}(2 - f_i \Delta t^2) - \phi_{i,L'}(1 - h_i \Delta t / 2)}{1 + h_i \Delta t / 2} \quad (4.65b)$$

4.5.4 Applications

The method proposed in this section was validated by means of 3 application examples. First, a symmetrical sagging between 2 towers was analyzed. As second example, an unsymmetrical sagging, consisting of the same river crossing line presented in Chapter 2 was presented. Finally, a machine winding was modeled by means of transmission line segments. Results were compared with those obtained with the NLT method.

4.5.4.1 Sagging Between Towers

A single-phase line 600m long with a sagging between towers is analyzed. The line maximum and minimum heights are 28m at the towers and 8m at the middle span. A unit step voltage source is connected to the sending node, while the receiving node is left open. Fig. 4.3 shows the voltage at the receiving end of the line, comparing the results obtained with the Numerical Laplace Transform and the Method of Characteristics. Results when the line presents no sagging (UL) are also included. Figs. 4.4 and 4.5 show a comparison of frequency spectrums of the transient resistance and conductance of the NUL, computed using Eqs. (4.10a) and (4.10b), against those spectrums obtained with the Vector Fitting technique. In Fig 4.5, the transient conductance is zero for the uniform line.

4.5.4.2 River Crossing

As second application example, a single-phase line with an unsymmetrical sagging, consisting of the same river crossing line of section 2.5.1, is analyzed. In this case, the right hand side of the line is connected to a unit step voltage source while the left hand side is left open. The voltage waveform at this side is shown in Fig. 4.6. A comparison between the exact frequency spectrums of the transient resistance and conductance of the NUL and those obtained with the Vector Fitting technique is shown in Figs. 4.7 and 4.8.

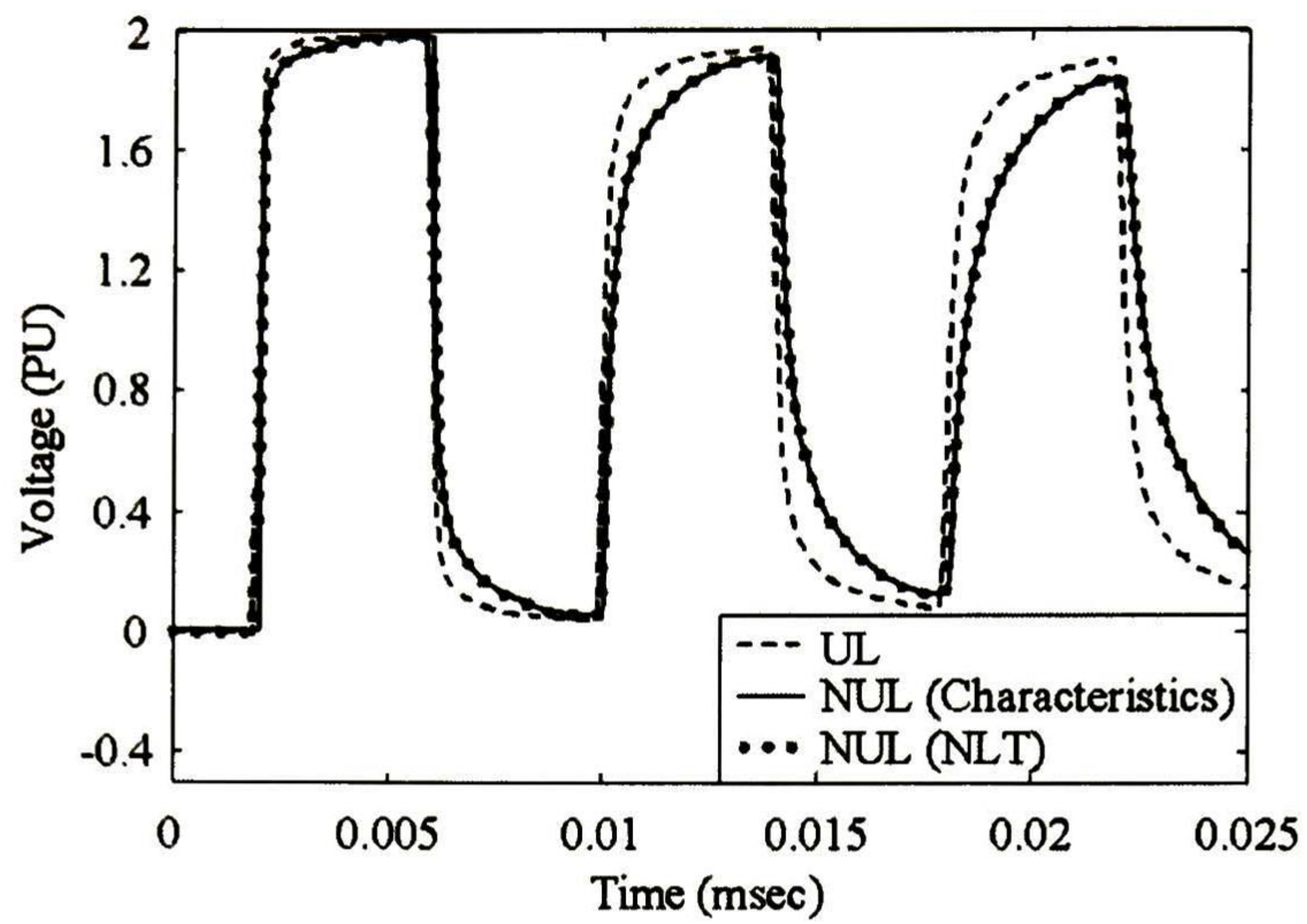


Figure 4.3. Voltage at the receiving end of the line.

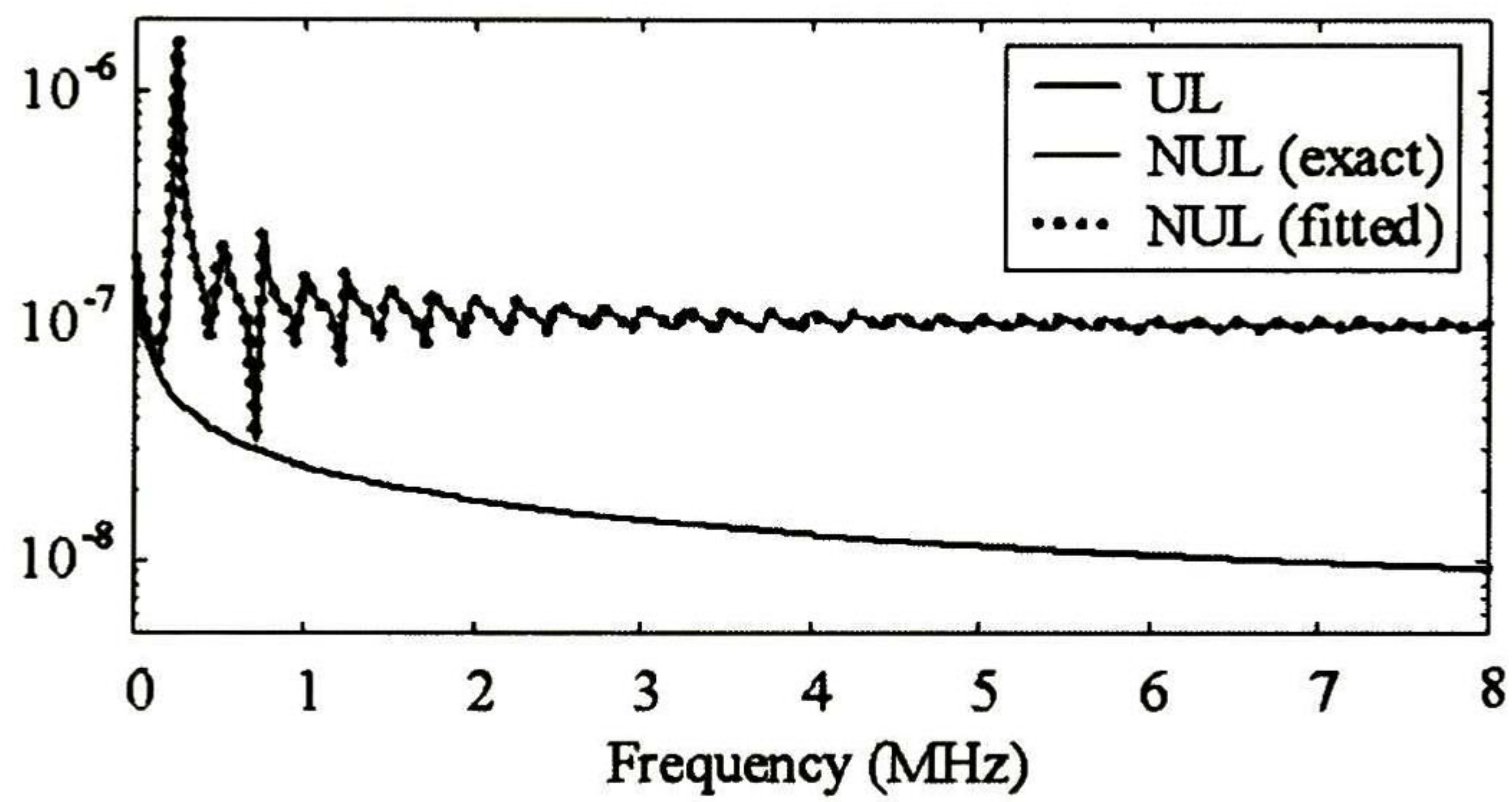


Figure 4.4. Transient resistance for the sagging between towers (in ohms).

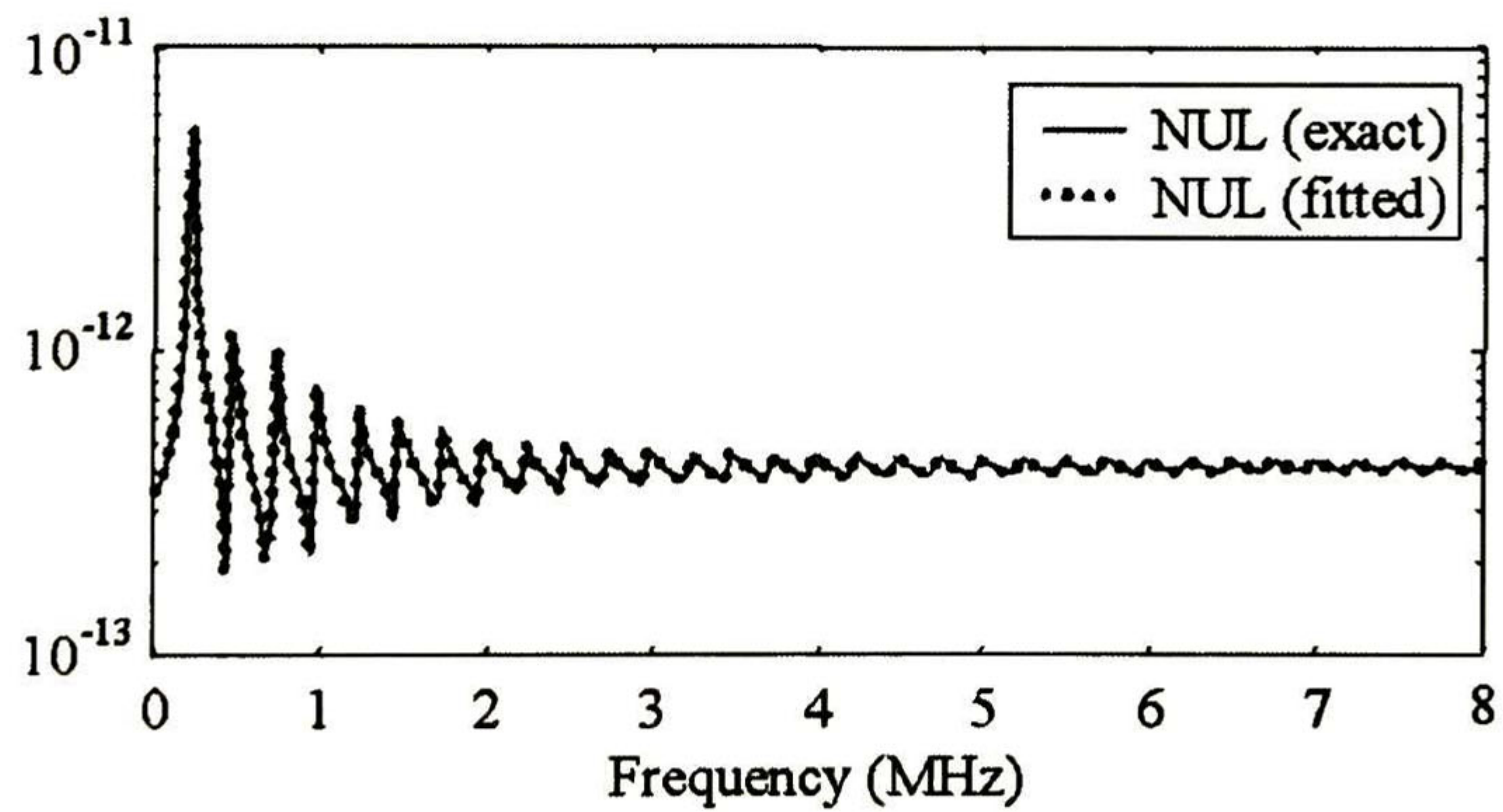


Figure 4.5. Transient conductance for the sagging between towers (in Siemens).

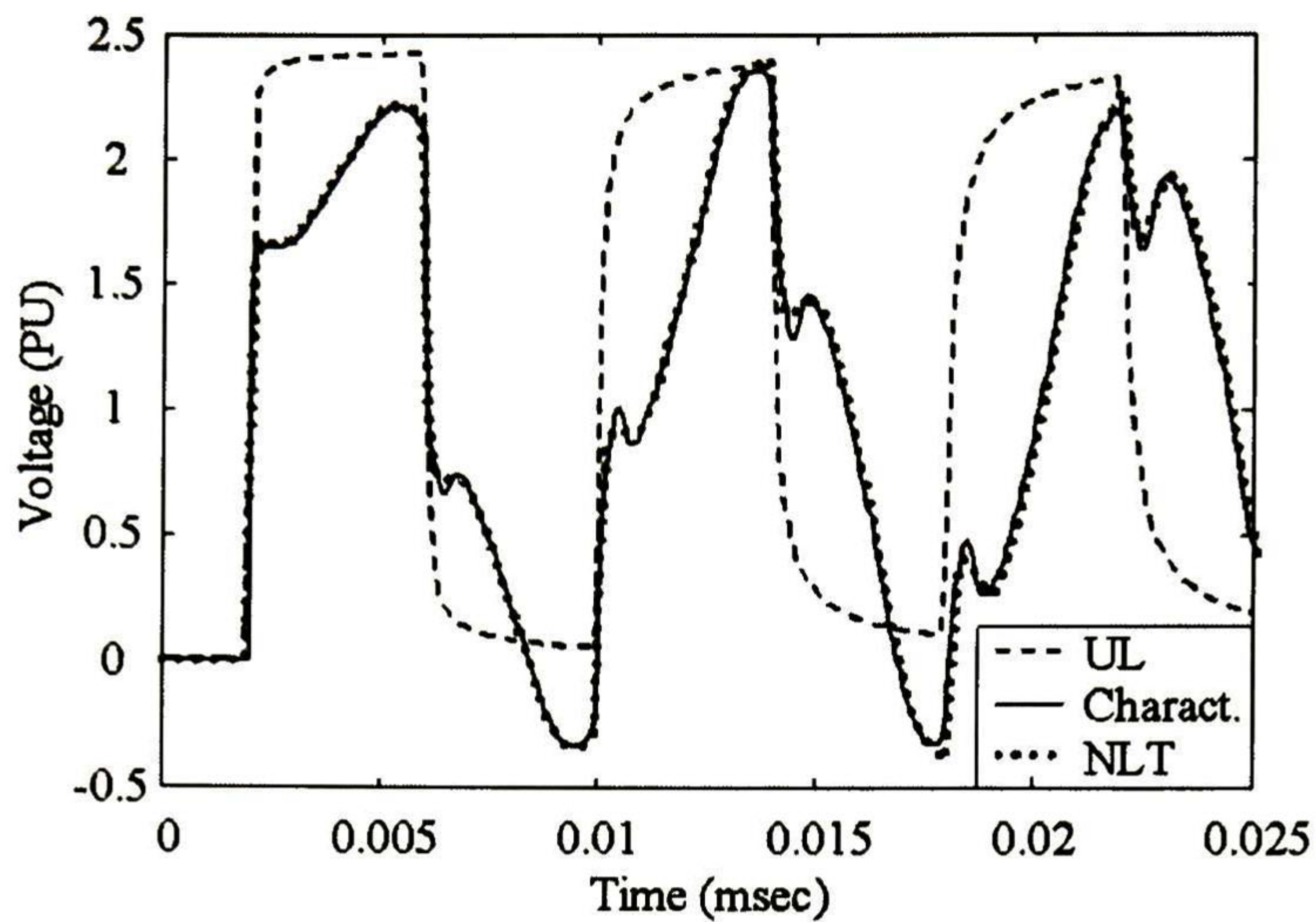


Figure 4.6. Voltage at the left hand side of the river crossing profile.

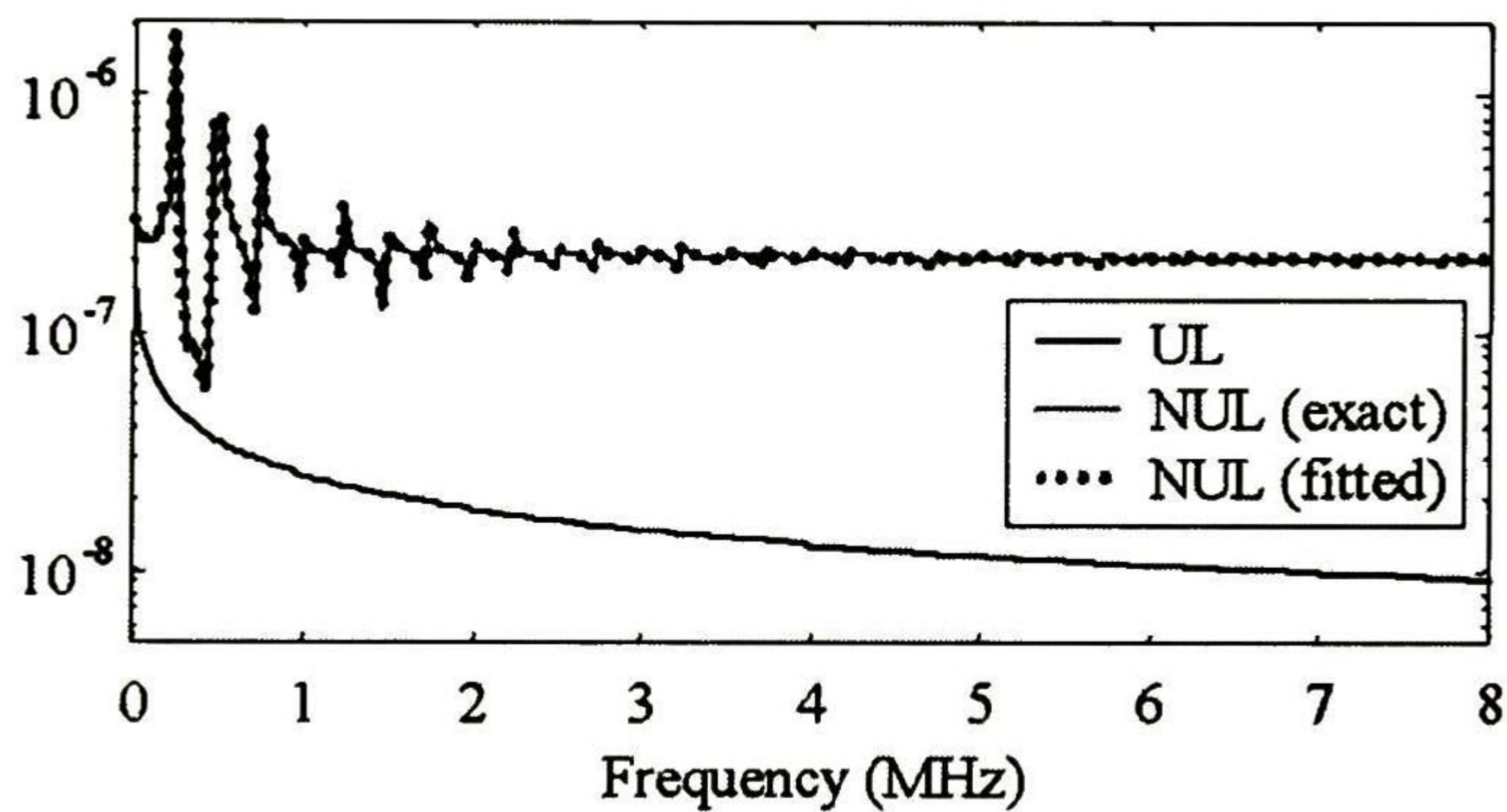


Figure 4.7. Transient resistance for the river crossing (in Ohms).

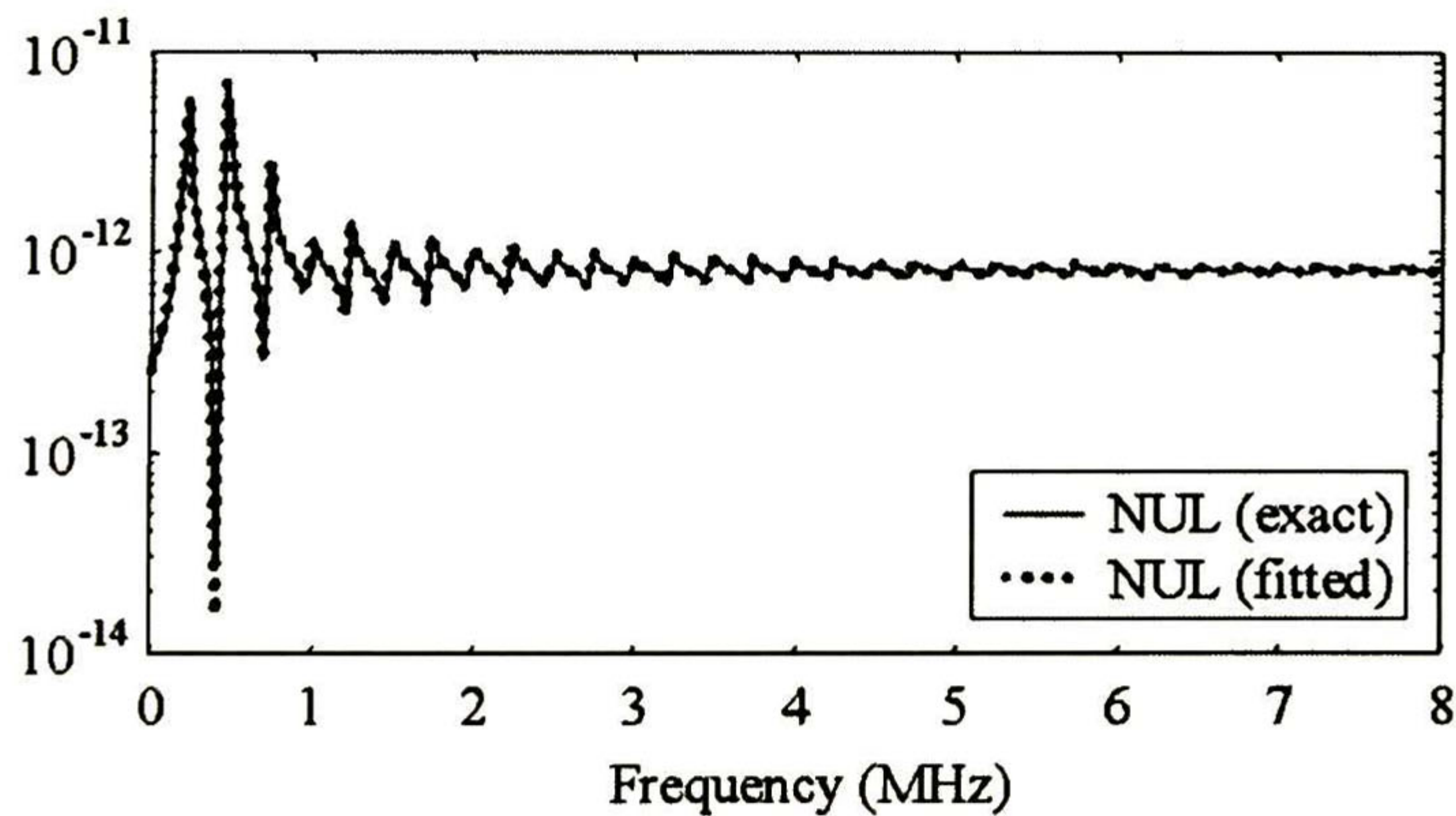


Figure 4.8. Transient conductance for the river crossing (in Siemens).

4.5.4.3 Machine Winding (Single Coil)

A machine winding is modeled using 6 transmission line segments, as shown in figure 4.9. The coil electrical parameters are computed according to [57] and the data listed in Table 4.1. Chain matrices of all segments are computed and connected in cascade to get an equivalent matrix for the complete winding. A unit step voltage source is connected to node A, while node B is left open. Figure 4.10 shows the voltage waveform at node B.

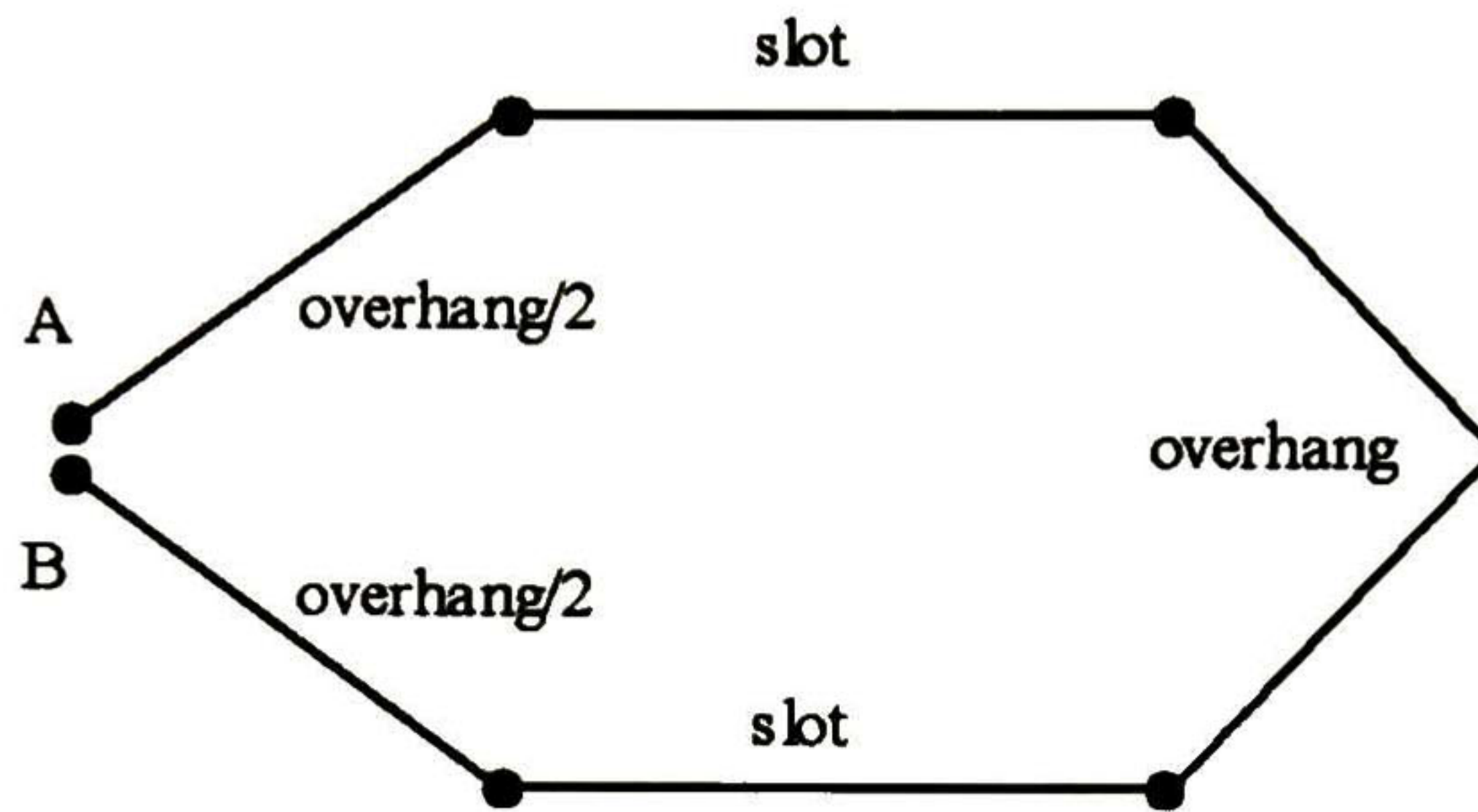


Figure 4.9. Winding representation using line segments.

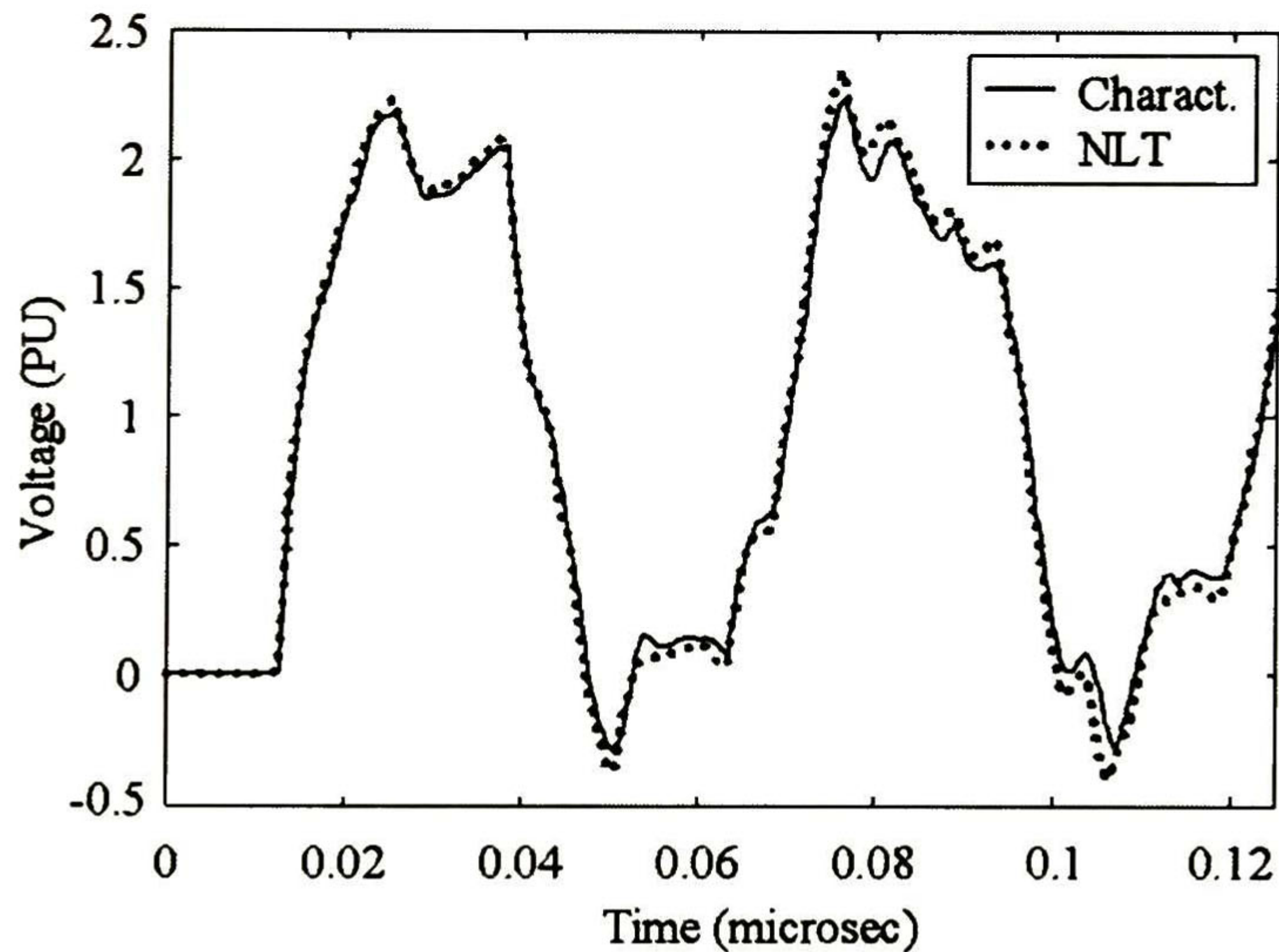


Figure 4.10. Voltage at node B of the winding.

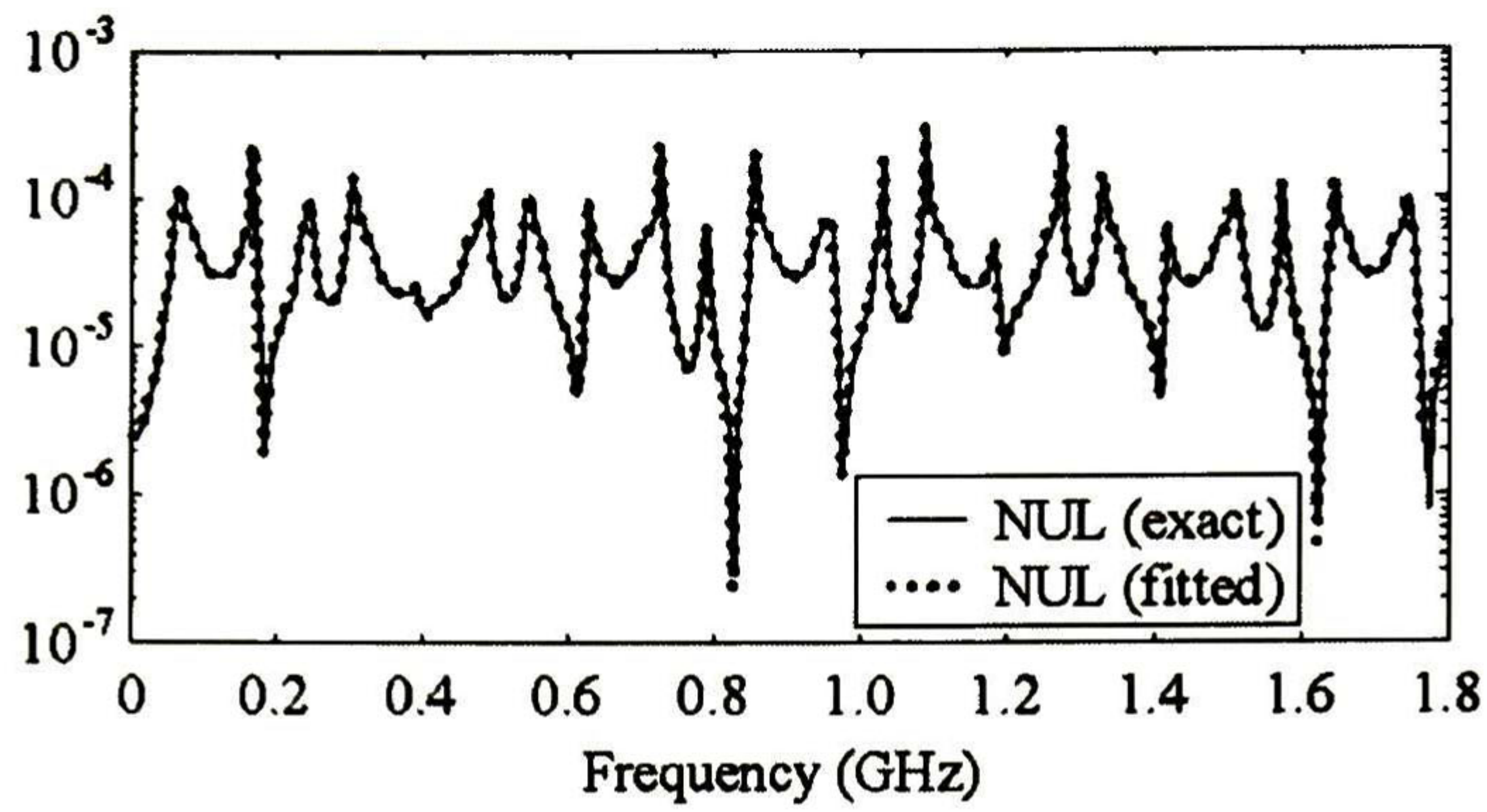


Figure 4.11. Transient resistance for the machine winding (in Ohms).

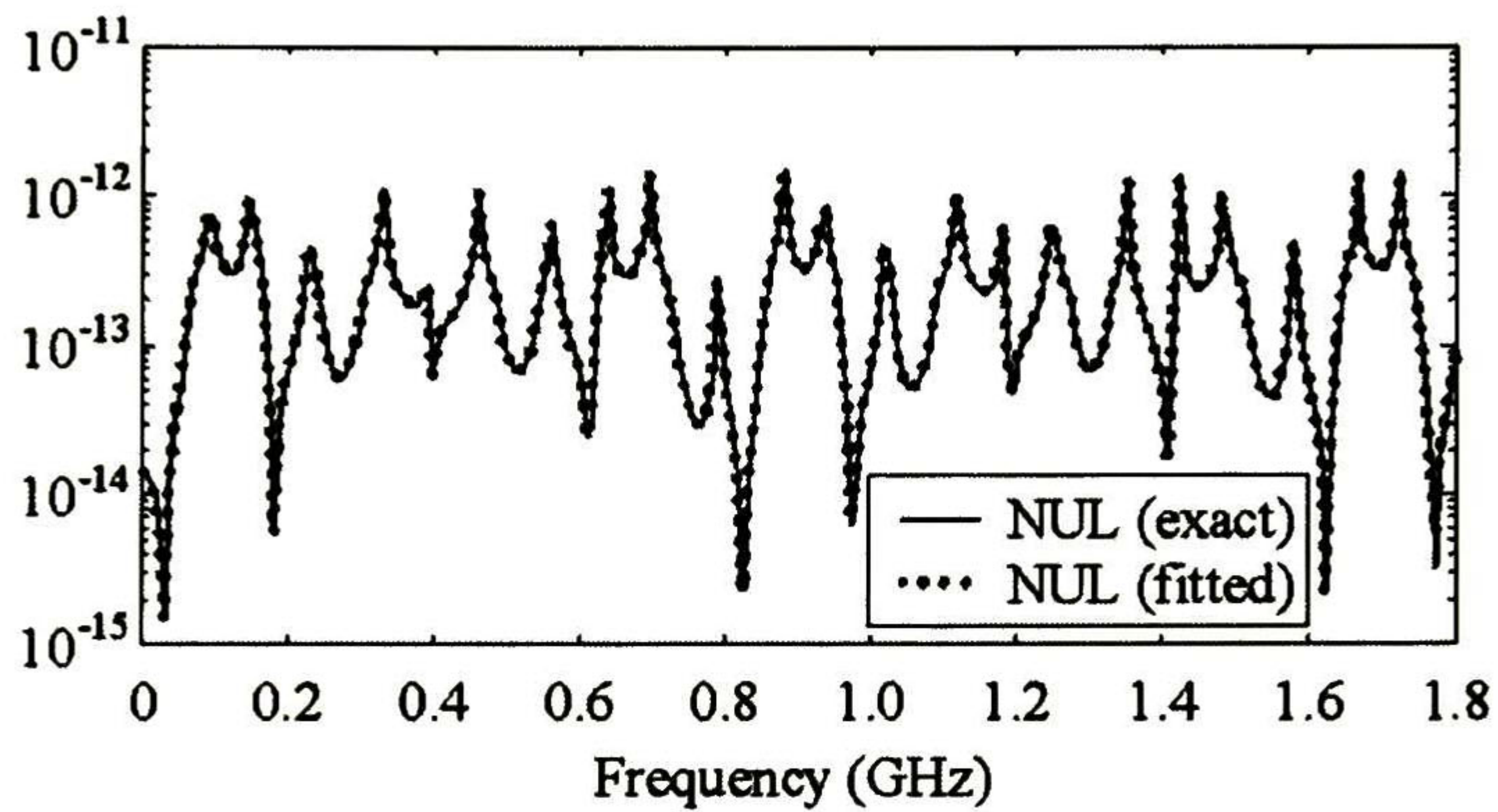


Figure 4.12. Transient conductance for the machine winding (in Siemens).

Table 4.1. Winding Data

Slot width	0.75m
Slot material	Iron
Turn area	3 x 9 mm
Turn length	3.8 m
Slot length	0.75 m
Overhang length	1.15 m
Conductor material	Copper

For this example, the numerical solution of the convolutions applying central differences presented oscillations. Thus, Gear 2nd order method was used instead. Equations (4.35) and (4.36) were replaced by the following:

$$\psi_{n+1} = -\sum_{i=1}^{N_1} \frac{\Delta t}{4 + 3d_i \Delta t + 2b_i \Delta t^2} \left[(3a_i + b_i c_i \Delta t) i_{n+1} - a_i (4i_n - i_{n-1}) + \frac{2\psi_{i,n} (5 + 2d_i \Delta t) - \psi_{i,n-1} (8 + d_i \Delta t) + 2\psi_{i,n-2}}{\Delta t} \right] \quad (4.66)$$

$$\phi_{n+1} = -\sum_{i=1}^{N_2} \frac{\Delta t}{4 + 3h_i \Delta t + 2f_i \Delta t^2} \left[(3e_i + f_i g_i \Delta t) v_{n+1} - e_i (4v_n - v_{n-1}) + \frac{2\phi_{i,n} (5 + 2h_i \Delta t) - \phi_{i,n-1} (8 + h_i \Delta t) + 2\phi_{i,n-2}}{\Delta t} \right] \quad (4.67)$$

4.6 Numerical Solution with One Internal Point

In the characteristics grid presented in Figs. 4.1 and 4.2, there are $n-1$ internal points, i. e., the line is divided in n segments of length Δx . If the grid presented in Fig. 4.13 is considered instead, only one internal point must be taken into account. In this figure, τ is the one-way time delay given by $\tau = L/v$, being L the line length and v the line propagation velocity.

4.6.1 Internal Point

Supposing that v and i are known values at points S' and L' of Fig. 4.13, the solution can be extended to point P as follows:

$$(v_P - v_{S'}) + Z_W (i_P - i_{S'}) + \frac{R_X L}{4} (i_P + i_{S'}) + \frac{Z_W G_X L}{4} (v_P + v_{S'}) + \frac{L}{4} (\psi_P + \psi_{S'}) + \frac{Z_W L}{4} (\phi_P + \phi_{S'}) = 0 \quad (4.68a)$$

$$(v_P - v_{L'}) - Z_W (i_P - i_{L'}) - \frac{R_X L}{4} (i_P + i_{L'}) + \frac{Z_W G_X L}{4} (v_P + v_{L'}) - \frac{L}{2} (\psi_P + \psi_{L'}) + \frac{Z_W L}{4} (\phi_P + \phi_{L'}) = 0 \quad (4.68b)$$

Rearranging (4.68)

$$G_1 v_P + Z_1 i_P - G_2 v_{S'} - Z_2 i_{S'} + \frac{L}{4} (\psi_P + \psi_{S'}) + \frac{Z_W L}{4} (\phi_P + \phi_{S'}) = 0 \quad (4.69a)$$

$$G_1 v_P - Z_1 i_P - G_2 v_{L'} + Z_2 i_{L'} - \frac{L}{4} (\psi_P + \psi_{L'}) + \frac{Z_W L}{4} (\phi_P + \phi_{L'}) = 0 \quad (4.69b)$$

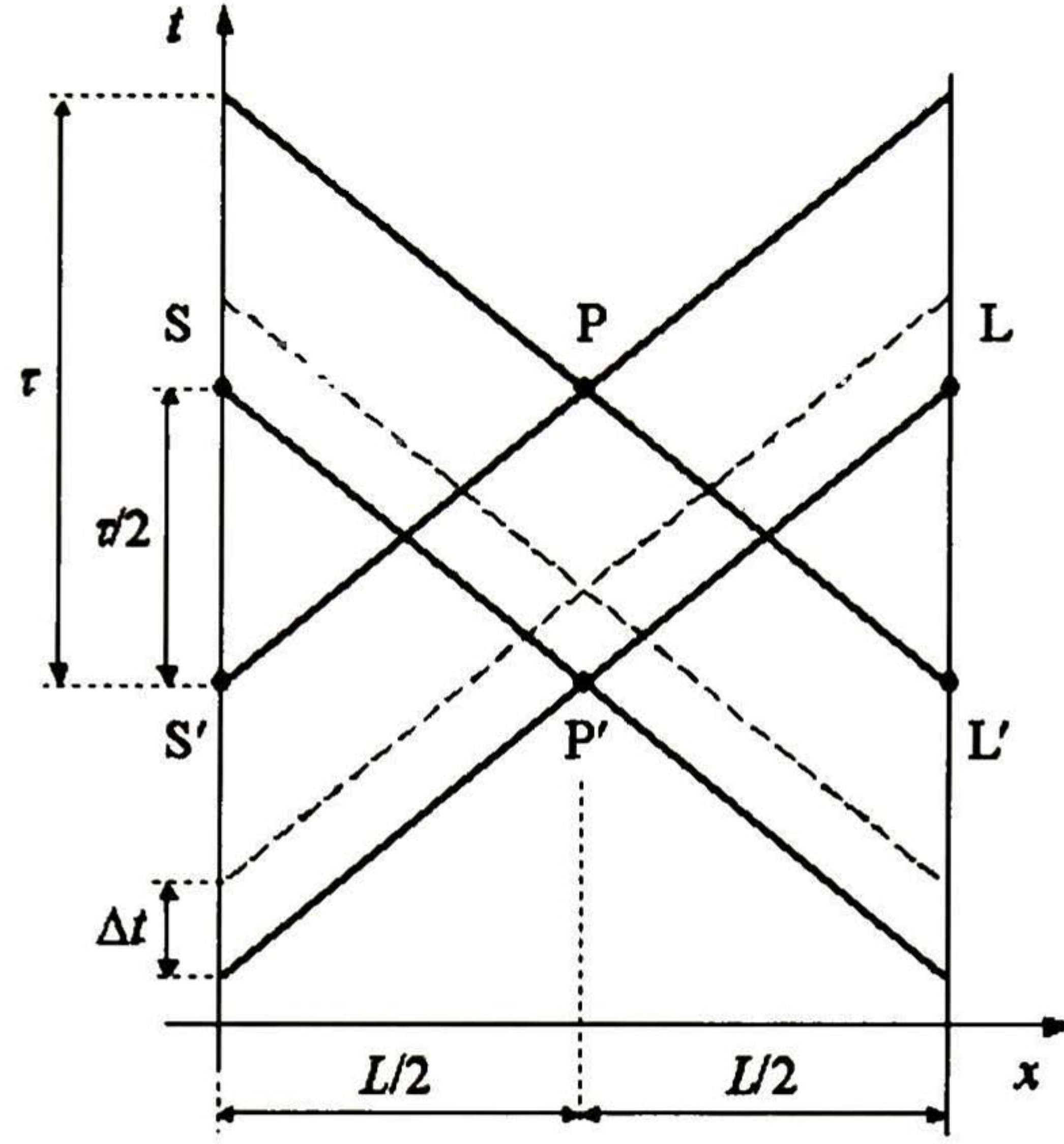


Figure 4.13. Characteristics grid with one internal point.

where

$$G_1 = 1 + \frac{Z_w G_X L}{4}, \quad G_2 = 1 - \frac{Z_w G_X L}{4} \quad (4.70a), (4.70b)$$

$$Z_1 = Z_w + \frac{R_X L}{4}, \quad Z_2 = Z_w - \frac{R_X L}{4} \quad (4.70c), (4.70d)$$

Addition of (4.69a) and (4.69b) gives the following:

$$2G_1 v_P - G_2 (v_{S'} + v_{L'}) - Z_2 (i_{S'} - i_{L'}) + \frac{L}{4} (\psi_{S'} - \psi_{L'}) + \frac{Z_w L}{4} (2\phi_P + \phi_{S'} + \phi_{L'}) = 0 \quad (4.71)$$

while the subtraction of the same equations yields

$$2Z_1 i_P - G_2 (v_{S'} - v_{L'}) - Z_2 (i_{S'} + i_{L'}) + \frac{L}{4} (2\psi_P + \psi_{S'} + \psi_{L'}) + \frac{Z_w L}{4} (\phi_{S'} - \phi_{L'}) = 0 \quad (4.72)$$

4.6.1.1 Computation of v_P and i_P with Real Poles and Residues

If ϕ_P is computed from (4.29) with real poles and residues, this term is a function of v_P ; thus, this voltage is computed from (4.42) as

$$v_P = \frac{1}{2G_1} \left[G_2 (v_{S'} + v_{L'}) + Z_2 (i_{S'} - i_{L'}) - \frac{L}{4} (\psi_{S'} - \psi_{L'}) - \frac{Z_w L}{4} (2\phi_P + \phi_{S'} + \phi_{L'}) \right] \quad (4.73)$$

where G_1' and ϕ_P' are given by

$$\phi_P' = -\sum_{i=1}^{N_2} \frac{\phi_{i,P-\Delta t}}{1+q_i \Delta t} \quad (4.74a)$$

$$G_1' = G_1 - \frac{Z_w L \Delta t}{4} \sum_{i=1}^{N_2} \frac{m_i q_i}{1+q_i \Delta t} \quad (4.74b)$$

The subscript $P-\Delta t$ denotes values corresponding to one time step prior to point P.

The current at point P, i_P , can be obtained from Eq. (4.43). But since ψ_P is computed from (4.28), this term is a function of i_P , so this current is computed as

$$i_P = \frac{1}{2Z_1'} \left[G_2 (v_{S'} - v_{L'}) + Z_2 (i_{S'} + i_{L'}) - \frac{L}{4} (2\psi_P' + \psi_{S'} + \psi_{L'}) - \frac{Z_w L}{4} (\phi_{S'} - \phi_{L'}) \right] \quad (4.75)$$

where Z_1' and ψ_P' are given by

$$\psi_P' = -\sum_{i=1}^{N_1} \frac{\psi_{i,P-\Delta t}}{1+p_i \Delta t} \quad (4.76a)$$

$$Z_1' = Z_1 - \frac{L \Delta t}{4} \sum_{i=1}^{N_1} \frac{k_i p_i}{1+p_i \Delta t} \quad (4.76b)$$

4.6.1.2 Computation of v_P and i_P with Complex Poles and Residues

If now ϕ_P is computed from (4.36) with complex pairs of poles and residues, this term is a function of v_P and the voltages 1 and 2 time steps prior to point P, $v_{P-\Delta t}$ and $v_{P-2\Delta t}$; thus, v_P is computed from (4.42) as

$$v_P = \frac{1}{2G_1'} \left[-G_2' v_{P-\Delta t} - G_3' v_{P-2\Delta t} + G_2 (v_{S'} + v_{L'}) + Z_2 (i_{S'} - i_{L'}) - \frac{L}{4} (\psi_{S'} - \psi_{L'}) - \frac{Z_w L}{4} (2\phi_P' + \phi_{S'} + \phi_{L'}) \right] \quad (4.77)$$

where

$$\phi_P' = -\sum_{i=1}^{N_2} \frac{\phi_{i,P-\Delta t} (2 - f_i \Delta t^2) - \phi_{i,P-2\Delta t} (1 - h_i \Delta t / 2)}{1 + h_i \Delta t / 2} \quad (4.78a)$$

$$G_1' = G_1 - \frac{Z_w L \Delta t}{4} \sum_{i=1}^{N_2} \frac{e_i}{2 + h_i \Delta t} \quad (4.78b)$$

$$G_2' = -\frac{Z_w L \Delta t^2}{2} \sum_{i=1}^{N_2} \frac{f_i g_i}{1 + h_i \Delta t / 2} \quad (4.78c)$$

$$G_3' = \frac{Z_w L \Delta t}{2} \sum_{i=1}^{N_2} \frac{e_i}{2 + h_i \Delta t} \quad (4.78d)$$

Similarly, if ψ_P is computed from (4.35), this term is a function of i_P , $i_{P-\Delta t}$ and $i_{P-2\Delta t}$. thus, i_P is computed from (4.43) as

$$i_P = \frac{1}{2Z_1'} \left[-Z_2' i_{P-\Delta t} - Z_3' i_{P-2\Delta t} + G_2 (v_{S'} - v_{L'}) + Z_2 (i_{S'} + i_{L'}) - \frac{L}{4} (2\psi_{P'} + \psi_{S'} + \psi_{L'}) - \frac{Z_w L}{4} (\phi_{S'} - \phi_{L'}) \right] \quad (4.79)$$

where

$$\psi_{P'} = -\sum_{i=1}^{N_2} \frac{\psi_{i,P-\Delta t} (2 - b_i \Delta t^2) - \psi_{i,P-2\Delta t} (1 - d_i \Delta t / 2)}{1 + d_i \Delta t / 2} \quad (4.80a)$$

$$Z_1' = Z_1 - \frac{L \Delta t}{4} \sum_{i=1}^{N_1} \frac{a_i}{2 + d_i \Delta t} \quad (4.80b)$$

$$Z_2' = -\frac{L \Delta t^2}{2} \sum_{i=1}^{N_1} \frac{b_i c_i}{1 + d_i \Delta t / 2} \quad (4.80c)$$

$$Z_3' = \frac{L \Delta t}{2} \sum_{i=1}^{N_1} \frac{a_i}{2 + d_i \Delta t} \quad (4.80d)$$

4.6.2 Boundary Points

For the source boundary point S ($x = 0$), as shown in Fig. 4.8, the application of an ideal voltage source $v_S = f(t)$ is considered. In this case, Eq. (4.69b) is modified as follows:

$$G_1 v_S - Z_1 i_S - G_2 V_{P'} + Z_2 i_{P'} - \frac{L}{4} (\psi_S + \psi_{P'}) + \frac{Z_w L}{4} (\phi_S + \phi_{P'}) = 0 \quad (4.81)$$

For the load boundary point L ($x = L$), the connection of a resistive load R_L is considered. Applying (4.56), Eq. (4.69a) is modified as follows:

$$G_1 v_L + Z_1 \frac{v_L}{R_L} - G_2 V_{P'} - Z_2 i_{P'} + \frac{L}{4} (\psi_L + \psi_{P'}) + \frac{Z_w L}{4} (\phi_L + \phi_{P'}) = 0 \quad (4.82)$$

4.6.2.1 Computation of i_S and v_L with real Poles and Residues

The current at the source boundary, i_S , is computed from Eq. (4.81), taking into account that ψ_S is a function of i_S :

$$i_S = \frac{1}{Z_1'} \left[G_1 v_S - G_2 V_{P'} + Z_2 i_{P'} - \frac{L}{4} (\psi_S' + \psi_{P'}) + \frac{Z_w L}{4} (\phi_S + \phi_{P'}) \right] \quad (4.83)$$

Z_1' is computed from (4.76b) and ψ_S' is given by

$$\psi_S' = - \sum_{i=1}^{N_1} \frac{\psi_{i,S-\Delta t}}{1 + p_i \Delta t} \quad (4.84)$$

The voltage at the load boundary, v_L , is computed from Eq. (4.82) taking into account that ψ_L and ϕ_L are both functions of v_L :

$$v_L = \frac{R_L}{G_1' R_L + Z_1'} \left[G_2 V_{P'} + Z_2 i_{P'} - \frac{L}{4} (\psi_L' + \psi_{P'}) - \frac{Z_w L}{4} (\phi_L' + \phi_{P'}) \right] \quad (4.85)$$

G_1' is computed from (4.74b) while ψ_L' and ϕ_L' are given by

$$\psi_L' = - \sum_{i=1}^{N_1} \frac{\psi_{i,L-\Delta t}}{1 + p_i \Delta t} \quad (4.86a)$$

$$\phi_L' = - \sum_{i=1}^{N_2} \frac{\phi_{i,L-\Delta t}}{1 + q_i \Delta t} \quad (4.86b)$$

4.6.2.2 Computation of i_S and v_L with Complex Poles and Residues

In this case, the convolution term ψ_S is a function of i_S , $i_{S-\Delta t}$ and $i_{S-2\Delta t}$, thus

$$i_S = \frac{1}{Z_1'} \left[- \frac{Z_2' i_{S-\Delta t} + Z_3' i_{S-2\Delta t}}{2} + G_1 v_S - G_2 V_{P'} + Z_2 i_{P'} - \frac{L}{4} (\psi_S' + \psi_{P'}) + \frac{Z_w L}{4} (\phi_S + \phi_{P'}) \right] \quad (4.87)$$

Z_1' , Z_2' and Z_3' are computed from (4.80b), (4.80c) and (4.80d), respectively, and

$$\psi_S' = - \sum_{i=1}^{N_1} \frac{\psi_{i,S-\Delta t} (2 - b_i \Delta t^2) - \psi_{i,S-2\Delta t} (1 - d_i \Delta t / 2)}{1 + d_i \Delta t / 2} \quad (4.88)$$

Besides, ψ_L and ϕ_L are both functions of v_L , $v_{L-\Delta t}$ and $v_{L-2\Delta t}$, so v_L is computed as

$$v_L = \frac{R_L}{G_1' R_L + Z_1'} \left[-v_{L-\Delta t} \left(\frac{G_2' R_L + Z_2'}{2R_L} \right) - v_{L-2\Delta t} \left(\frac{G_3' R_L + Z_3'}{2R_L} \right) + G_2' v_P + Z_2' i_P - \frac{L}{4} (\psi_L' + \psi_P') - \frac{Z_W L}{4} (\phi_L' + \phi_P') \right] \quad (4.89)$$

where G_1' , G_2' and G_3' are computed from (4.78b), (4.78c) and (4.78d), respectively, and

$$\psi_L' = -\sum_{i=1}^{N_1} \frac{\psi_{i,L-\Delta t} (2 - b_i \Delta t^2) - \psi_{i,L-2\Delta t} (1 - d_i \Delta t / 2)}{1 + d_i \Delta t / 2} \quad (4.90a)$$

$$\phi_L' = -\sum_{i=1}^{N_2} \frac{\phi_{i,L-\Delta t} (2 - f_i \Delta t^2) - \phi_{i,L-2\Delta t} (1 - h_i \Delta t / 2)}{1 + h_i \Delta t / 2} \quad (4.90b)$$

4.6.3 Applications

The new formulation to solve the Method of Characteristics with one internal point was validated by means of two application examples. In the first one, example 4.5.4.1. was repeated to compare the results and the computer times of the conventional grid and the one-internal point grid. Then, a field experiment consisting of seven equal NUL's was reproduced.

4.6.3.1 Practical Comparison of Methods

The conventional and one-internal-point Methods of Characteristics were compared using the same application example of section 4.5.4.1. As seen in Fig. 4.14, both methods had equivalent results but, as could be supposed, the simulation with the one-internal-point method was several times faster than the conventional one; between 5 and 6 time faster using the same PC of Chapters 2 and 3.

4.6.3.2 Simulation of a Field Experiment

As second application example, the proposed one-internal-point method is applied to the simulation of a field experiment performed by Wagner, et al. [59]. The experiment consists on injecting a step like wave at one end of a 2185.4m long line divided in 7 equal segments, as shown in Fig. 5. Each segment has a length of 312.2m. The line maximum and minimum heights are 26.2m at the towers and 15.24m at the middle span. The 3 line conductors are ACSR with radius of 2.54cm. The injected wave is applied simultaneously to the 3 conductors at the sending node, while the receiving node is left open. The voltage at the receiving end of the line is shown

in Fig. 4.16, comparing the experimental results and those obtained with the Method of Characteristics. Waveforms were plotted as half of their actual magnitude, as done in [57], to remove the doubling due to the open circuit. For the simulation, the line is represented by a single-phase equivalent.

4.7 Conclusions

A time domain model for analyzing single phase non-uniform transmission lines with frequency dependent electrical parameters has been presented. The model is based on synthesizing an equivalent uniform transmission line from the chain matrix of the NUL. The application examples have shown very good agreement between the results obtained with the proposed method and those produced by the Numerical Laplace Transform program and a field experiment. Besides, a new procedure to solve the Method of Characteristics with one interior point has been presented and tested with very good results and an significant improvement in computer times.

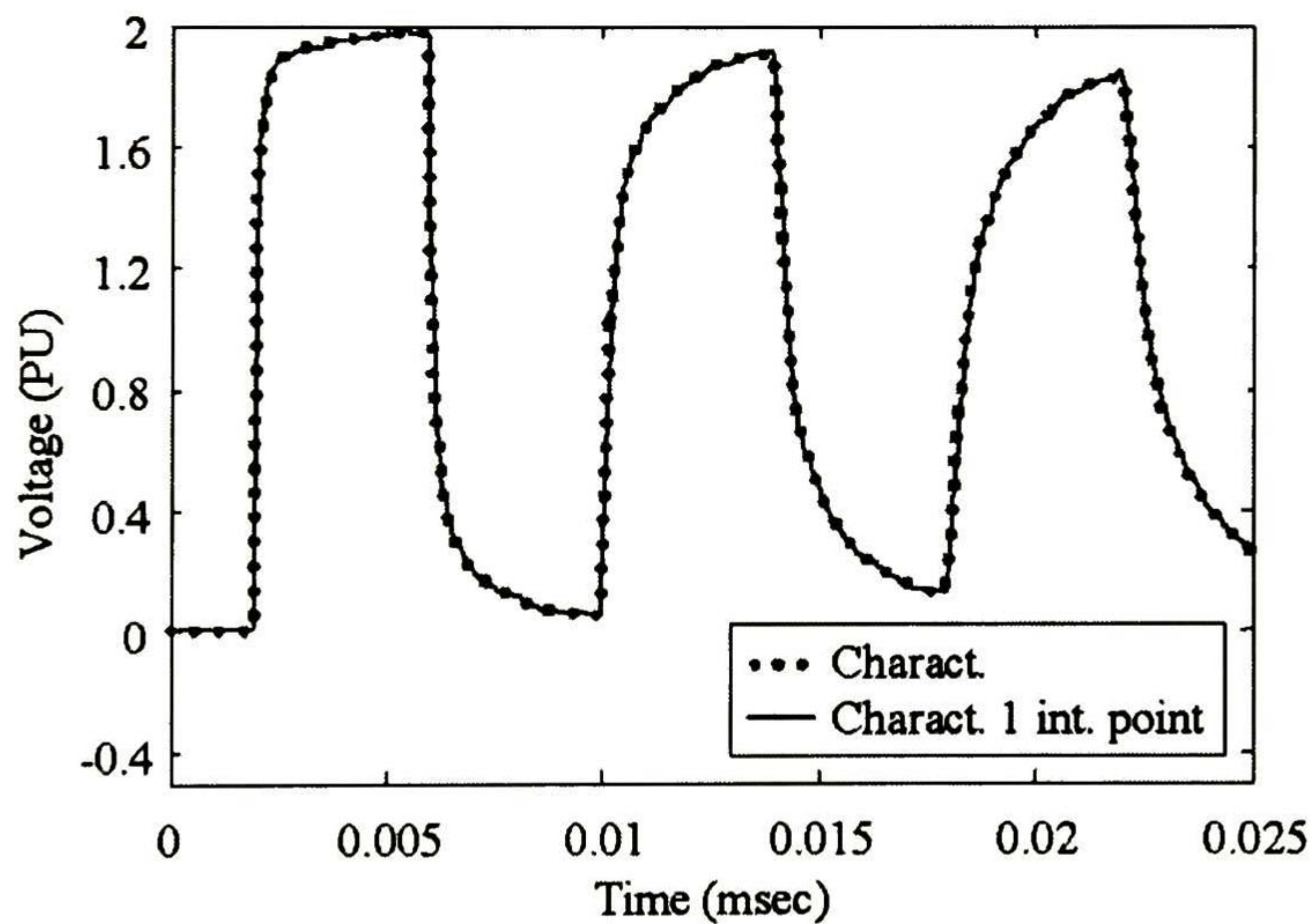


Figure 4.14. Comparison of methods.

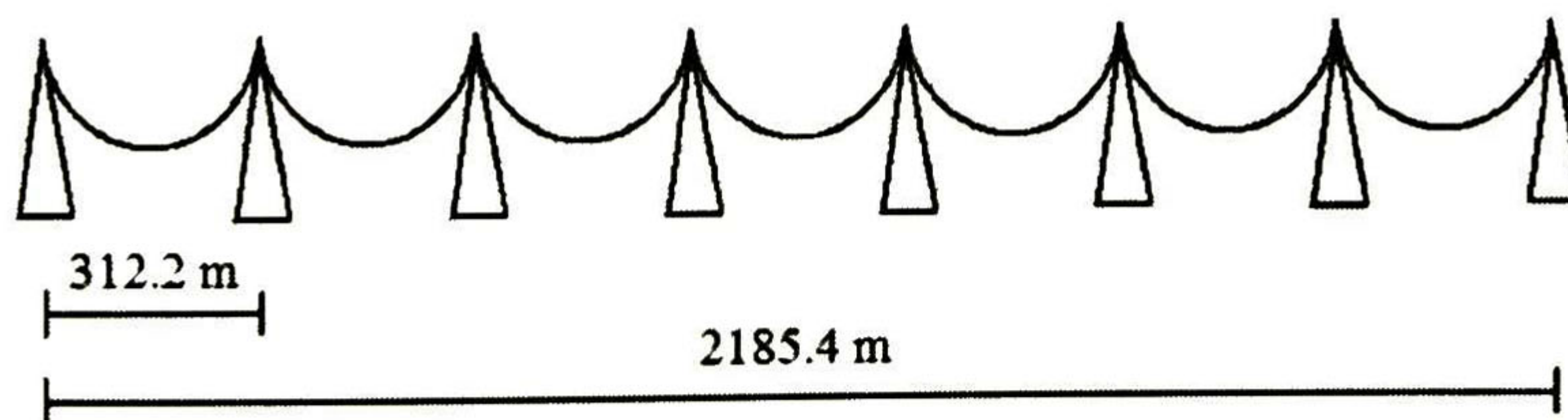


Figure 4.15. Configuration of the NUL.

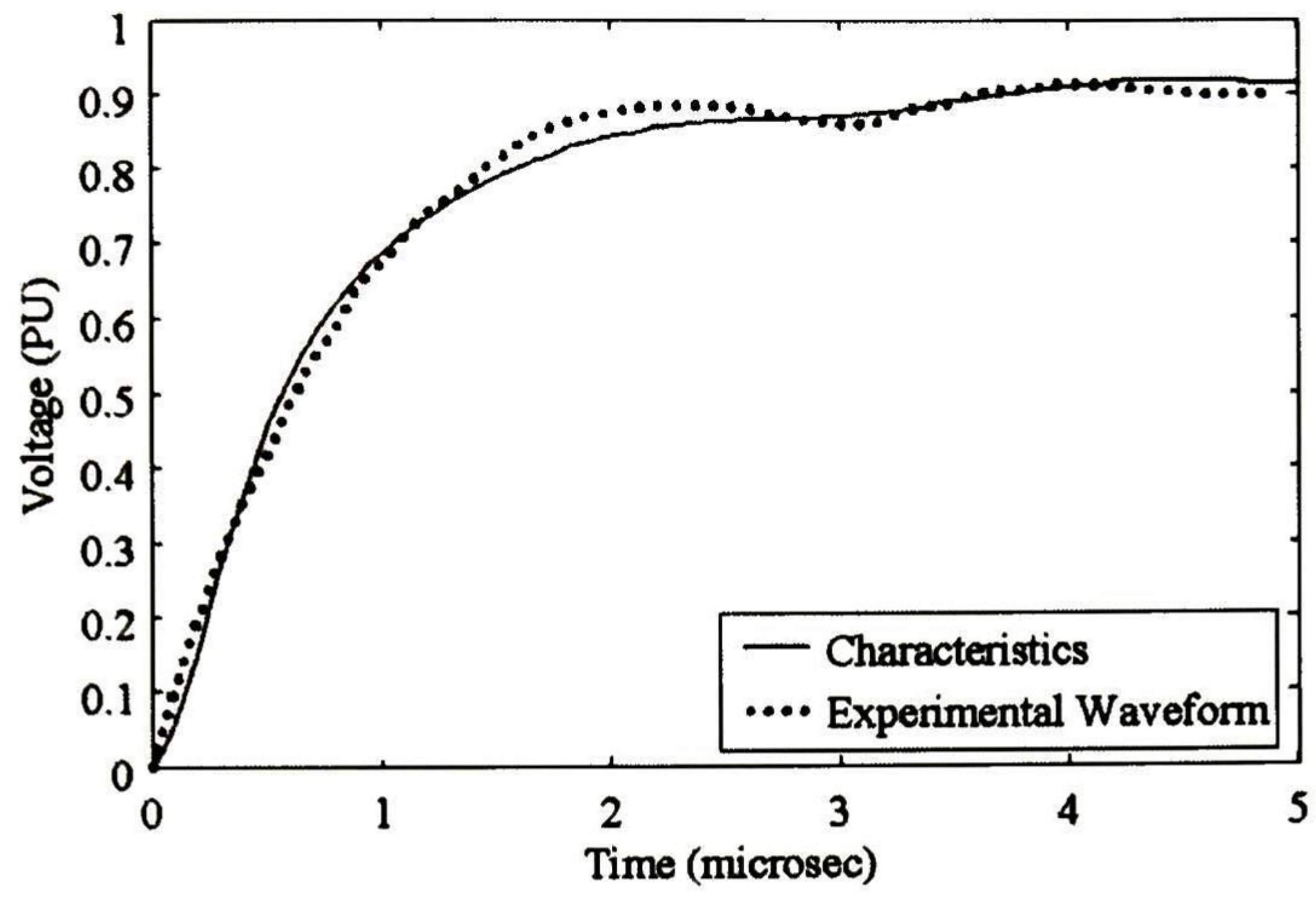


Figure 4.16. Voltage at the receiving end of the line.

5 Conclusions

5.1 Summary of Results

In this thesis, two of the most important aspects in the analysis of electromagnetic transients on transmission systems have been discussed:

- Space dependence of the line electrical parameters.
- Incident field excitation.

Solutions to these problems have been proposed and tested. For the Non-uniform Line problem, two approaches have been presented. The first one is based on the frequency domain modeling of multiconductor lines a cascaded connection of chain matrices. The time domain solution has been obtained by applying the Numerical Laplace Transform. The second approach is also frequency domain based, but in this case a time domain model for single-phase lines is obtained. This model includes transient parameters that modify the conventional transmission line equations to take into account both the space and the frequency dependence of the line electrical parameters. The resulting modified transmission line equations are solved with the Method of Characteristics.

In the case of adding the effect of incident fields on the NUL, the problem has been solved in the frequency domain by the inclusion of equivalent lumped sources connected at the receiving end of the unexcited line. The developed procedures extends the work done in [34] for single phase lines to the case of multiconductor lines. Again, the Numerical Laplace Transform was applied to get the time domain solution.

The importance of the frequency dependence of the line parameters has been shown through two different cases of short lines, a NUL and a field excited line, both simulated with the Numerical Laplace Transform program. In both cases, results have shown important

differences in the waveforms with or without frequency dependence, although computer times are very similar.

Several application examples have been presented in this thesis:

- A river crossing 3-phase line, non-uniform and highly asymmetrical, which was also used to test the accuracy of different methods to solve the NUL problem.
- A tower model constructed with NUL segments.
- 2 field excited distribution lines with incident fields propagating in different directions.
- A single-phase line with a symmetrical sagging between two towers.
- A machine winding model.
- The simulation of a field experiment consisting of seven equal NUL's.

Results from these practical examples have been validated through comparisons with ATP and experimental waveforms. Methods based on the Numerical Laplace Transform were completely free of oscillations in all cases. In the other hand, the solution with the Method of Characteristics of a machine winding model presented oscillations, which were eliminated by changing the numerical method used to solve the convolutions from central differences to Gear 2nd order.

The methods presented in this thesis represent an important alternative to the usual commercial programs to compute electromagnetic transients on NUL and field excited lines. It has been shown the ability of these methods to deal with a variety of cases with high accuracy.

5.2 Recommendations for Future Research

A list of recommendations for further developments is proposed as a continuation to the methodologies presented in this thesis:

- Extension of the NUL solution with the Method of Characteristics, presented in Chapter 4, to the multiconductor case.
- Application of the proposed methods to the simulation of electronic and communication lines.

- Inclusion of incident field excitation to the NUL solution with the Method of Characteristics using lumped sources connected to the receiving end of the line, as done in the frequency domain solution presented in Chapter 3.
- Application of equivalent network analysis to simulate large transmission systems, reducing the non-significant parts of the system.
- Implementation of the NUL models presented in this thesis to analyze switching transients and evaluate the importance of including non-uniformities on these studies.

6 References

- [1] L. Bergeron, *Water Hammer in Hydraulics and Waves Surge in Electricity*, John Wiley, NY, 1961.
- [2] H. W. Dommel, "Digital Computer Solution of Electromagnetic Transients in Single and Multiphase Networks", *IEEE Trans. Power Apparatus and Systems*, vol. PAS-88, pp. 388-399, April 1969.
- [3] A. Budner, "Introduction of Frequency Dependent Line Parameters into an Electromagnetic Transients Program", *IEEE Trans. Power Apparatus and Systems*, vol. PAS-89, pp. 88-97, January 1970.
- [4] J. K. Snelson, "Propagation of Travelling Waves on Transmission Lines-Frequency Dependent Parameters", *IEEE Trans. Power Apparatus and Systems*, vol. PAS-91, pp. 85-91, January 1972.
- [5] W. S. Meyer and H. W. Dommel, "Numerical Modeling of Frequency-Dependent Transmission-Line Parameters in an Electromagnetic Transients Program", *IEEE Trans. Power Apparatus and Systems*, vol. PAS-93, pp. 1401-1409, September 1974.
- [6] J. R. Martí, "Accurate Modelling of Frequency-Dependent Transmission Lines in Electromagnetic Transient Simulations" *IEEE Trans. Power Apparatus and Systems*, vol. PAS-101, no. 1, pp. 147-157, January 1982.
- [7] L. Martí, "Simulation of Transients in Underground Cables with Frequency-Dependent Modal Transformation Matrices", *IEEE Trans. Power Delivery*, vol. 3, no. 3, pp. 1099-1110, July 1988.
- [8] B. Gustavsen and A. Semlyen, "Combined Phase Domain and Modal Domain Calculation of Transmission Line Transients Based on Vector Fitting", *IEEE Trans. Power Delivery*, vol. 13, no. 2, pp. 596-604, April 1998.

- [9] L. M. Wedepohl, *Theory of Natural Modes in Multiconductor Transmission Lines*, Course Notes ELEC-552, UBC, 1982.
- [10] F. J. Marcano and J. Martí, "Idempotent Line Model: Case Studies", *Proc. of the International Conference on Power Systems Transients*, Seattle, Washington, June 1997.
- [11] A. Morched, B. Gustavsen and M. Tartibi, "A Universal Model for Accurate Calculation of Electromagnetic Transients on Overhead Lines and Underground Cables", *IEEE Trans. Power Delivery*, vol. 14, no. 3, pp. 1032-1037, July 1999.
- [12] P. Gómez, P. Moreno, J. L. Naredo and M. Dávila, "Frequency Domain Transient Analysis of Transmission Networks Including Non-linear Conditions", *IEEE Bologna Power Tech International Conference*, June 23-26, 2003, Bologna Italy.
- [13] S. J. Day, N. Mullineux and J. R. Reed, "Developments in Obtaining Transient Response using Fourier Transforms. Part I: Gibbs Phenomena and Fourier Integrals" *Int. J. Elect. Enging. Educ.*, vol. 3, pp. 501-506, 1965.
- [14] L. M. Wedepohl and S. E. T. Mohamed, "Transient Analysis of Multiconductor Transmission Lines with Special Reference to Nonlinear Problems", *Proc. IEE*, vol. 117, no. 5, pp. 979-988. May 1970.
- [15] J. W. Cooley and J. W. Tukey, "An Algorithm for the Machine Computation of the Complex Fourier Series", *Mathematics of Computation*, vol. 19, pp 297-301, April 1965.
- [16] J. P. Bickford, N. Mullineux and J. R. Reed, *Computation of Power System Transients*, Peregrinus, IEEE Monograph Series, England 1976.
- [17] N. Nagaoaka and A. Ametani, "A Development of a Generalized Frequency-Domain Transient Program – FTP", *IEEE Trans. Power Delivery*, vol. 3, no. 4, pp. 1996-2004, October 1988.
- [18] P. Moreno, R. de la Rosa and J. L. Naredo, "Frequency Domain Computation of Transmission Line Closing Transients", *IEEE Trans. Power Delivery*, vol. 6, pp. 275-281, January 1991.
- [19] C. Menemenlis and Z. T. Chun, "Wave Propagation on Non-uniform Lines", *IEEE Trans. Power Apparatus and Systems*, vol. PAS-101, no. 4, pp. 833-839, April 1982.
- [20] M. Ishii, T. Kawamura, T. Kouno, E. Ohsaki, K. Murotani, and T. Higuchi, "Multistory Transmission Tower Model for Lightning Surge Analysis", *IEEE Trans. Power Delivery*, vol. 6, no. 3, pp. 1327-1335, July 1991.

- [21] E. A. Oufi, A. S. Alfuhaid, and M. M. Saied, "Transient Analysis of Lossless Singlephase Non-uniform Transmission Lines" *IEEE Trans. Power Delivery*, vol. 9, no. 3, pp. 1694-1700, July 1994.
- [22] H. V. Nguyen, H. W. Dommel, and J. R. Martí, "Modelling of Single-phase Non-uniform Transmission Lines in Electromagnetic Transient Simulations", *IEEE Trans. Power Delivery*, vol. 12, no. 2, pp. 916-921, April 1997.
- [23] J. A. Gutierrez, J. L. Naredo, L. Guardado, and P. Moreno, "Transient Analysis of Non-uniform Transmission Lines through the Method of Characteristics", *Proc. of the ISH-99, 11th International Symposium on High Voltage Engineering*, vol. 2, topic B, London, U. K., August 23-27, 1999.
- [24] M. Davila, J. L. Naredo and P. Moreno, "Transient Analysis of Power Lines Including Non-uniform and Frequency Dependent Effects", *North American Power Symposium (NAPS) 2002*, Tempe, Arizona, U.S.A., October 2002.
- [25] M. S. Mamis and M. Koksas, "Lightning Surge Analysis using Non-uniform, Single-phase Line Model", *IEE Proc. Gener. Transm. Distrib.*, vol. 148, no. 1, pp. 85-90, January 2001.
- [26] A. Semlyen, "Some Frequency Domain Aspects of Wave Propagation on Non-uniform Lines", *IEEE Trans. Power Delivery*, vol. 18, no. 1, pp. 315-322, January 2003.
- [27] A. Ramirez, A. Semlyen and R. Iravani, "Modeling Non-uniform Transmission Lines for Time Domain Simulation of Electromagnetic Transients", *IEEE Trans. Power Delivery*, vol. 18, no. 3, pp. 968-973, July 2003.
- [28] C. D. Taylor and J. P. Castillo, "On Electromagnetic-field Excitation of Unshielded Multiconductor Cables", *IEEE Trans. on Electromagnetic Compatibility*, vol. EMC-20, pp. 495-500, 1978.
- [29] A. K. Agrawal, H. J. Price, and S. H. Gurbaxani, "Transient Response of a Multiconductor Transmission Line Excited by a Non-uniform Electromagnetic Field," *IEEE Trans. on Electromagnetic Compatibility*, vol. EMC-22, pp.119-129, May 1980.
- [30] F. Rachidi, "Formulation of the Field-to-transmission Line Coupling Equations in Terms of Magnetic Excitation Field", *IEEE Trans. on Electromagnetic Compatibility*, vol. EMC-35, pp. 404-407, August 1993.
- [31] C. R. Paul, "Incorporating of Terminal Constraints in the FDTD Analysis of Transmission Lines", *IEEE Trans. on Electromagnetic Compatibility*, vol. 36, no. 2, pp. 85-91, May 1994.

- [32] E. S. M. Mok and G. I. Costache, "Skin-effect Considerations on Transient response of a Transmission Line Excited by an Electromagnetic Pulse", *IEEE Trans. on Electromagnetic Compatibility*, vol. 34, no. 3, pp. 320-329, August 1992.
- [33] T. Lapohos, J. L. Vetri and J. Seregelyi, "External Field Coupling to MTL Networks with Nonlinear Junctions: Numerical Modeling and Experimental Validation", *IEEE Trans. on Electromagnetic Compatibility*, vol. 42, no. 1, pp. 16-29, February 2000.
- [34] C. R. Paul, "Frequency Response of Multiconductor Transmission Lines Field excited by an Electromagnetic Field", *IEEE Trans. on Electromagnetic Compatibility*, vol. EMC-18,
- [35] C. R. Paul, *Analysis of Multiconductor Transmission Lines*, John Wiley & Sons, U.S.A., 1994.
- [36] M. Omid, Y. Kami and M. Hayakawa, "Field Coupling to Non-uniform and Uniform Transmission Lines", *IEEE Trans. on Electromagnetic Compatibility*, vol. 39, no. 3, pp 201-211, August 1997.
- [37] C. R. Paul, "A SPICE Model for Multiconductor Transmission Lines Excited by an Incident Electromagnetic Field", *IEEE Trans. on Electromagnetic Compatibility*, vol. 36, no. 4, pp. 42-55, November 1994.
- [38] R. Khazaka and M. Nakhla, "Analysis of High-Speed Interconnects in the Presence of Electromagnetic Interference", *IEEE Trans. Microwave Theory Tech.*, vol.46, no. 7, pp. 940-947, July 1998.
- [39] L. M. Silveira., I. M. Elfadel, J. K. White, M. Chilukuri and K. S. Kundert, "Efficient Frequency-Domain Modeling and Circuit Simulation of Transmission Lines", *IEEE Trans. Comp. Pack. And Man. Tech-Pt.B*, Vol. 17, No.4, pp. 505-513, November 1994.
- [40] D. B. Kuznetsov and J. E. Schutt-Ainé, "Optimal Ttransient Simulation of Transmission Lines", *IEEE Trans. Circ. and Systems - I*, vol. 43, no. 2, pp.110-121, February 1996.
- [41] W. T. Beyene and J. E. Schutt-Ainé, "Efficient Transient Simulation of High-Speed Interconnects Characterized by Sample Data", *IEEE Trans. Comp. Pack. And Man. Tech-Pt.B*, Vol. 21, No.1, pp. 105-114, February 1998.
- [42] R. Sanaie, E. Chiprout, M. Nakhla, and Q. J. Zhang, "A Fast Method for Frequency and Time Domain Simulation of High-Speed VLSI Interconnects", *IEEE Trans. Microwave Theory Tech.*, vol.42, no. 12, pp. 2562-2571, December 1994.
- [43] I. Erdin, A. Dounavis, R. Achar and M. S. Nakhla, "A SPICE Model For Incident Field Coupling to Lossy Multiconductor Transmission Lines", *IEEE Trans. on Electromagnetic Compatibility*, vol. 43, no. 4, pp. 585-594, November 2001.

- [44] R. Radulet, A. Timotin, A. Tugulea and A. Nica, "The Transient Response of the Electric lines Based on the Equations with Transient Line-Parameters", *Rev. Roum. Sci. Techn.*, vol. 23, no. 1, pp. 3-19, 1978.
- [45] A. Ramirez, *Advanced Models for Electromagnetic Transient Simulation of Power Transmission Lines*, Ph. D. Dissertation, CINVESTAV Guadalajara, October 2001.
- [46] J. D. Hoffman, *Numerical Methods for Engineers and Scientists*, McGraw Hill, 1992.
- [47] G. H. Golub and C. F. Van Loan, *Matrix Computation*, Johns Hopkins University Press, 1983.
- [48] C. B. Moler and C. F. Van Loan, "Nineteen Dubious Ways to Compute the Exponential of a Matrix", *SIAM Review* 20, p.p. 801-836, 1979.
- [49] F. L. Alvarado, R. H. Lasseter and J. J. Sanchez, "Testing of Trapezoidal Integration with Damping for the Solution of Power Transient Problems", *IEEE Trans. Power Apparatus and Systems*, vol. PAS-102, p.p. 3783-3790, December 1983.
- [50] J. A. Gutiérrez, P. Moreno, J. L. Naredo and L. Guardado, "Non-uniform Line Tower Model for Lightning Transient Studies", *Proceedings of the International Conference on Power Systems Transients, IPST'01*, Rio de Janeiro, Brazil, June 24-28 2001.
- [51] A. Ramírez, J. L. Naredo, P. Moreno and L. Guardado, "Electromagnetic Transients in Overhead Lines Considering Frequency Dependence and Corona Effect via the Method of Characteristics", *Int. Journal of Electrical Power and Energy Systems*, vol. 23, pp. 179-188, 2001.
- [52] J. A. Gutierrez, P. Moreno, J. L. Naredo and J. C. Gutierrez, "Fast Transients Analysis of Non-uniform Transmission Lines Through the Method of Characteristics", *Int. Journal of Electrical Power and Energy Systems*, vol. 24, pp. 781-788, 2002.
- [53] P. Moreno, A. R. Chávez, J. L. Naredo, L. Guardado, "Fast Transients Analysis of Non-Uniform Multiconductor Transmission Lines", *IEEE/PES Transmission and Distribution 2002 Latin America*, Sao Paulo, Brazil, March 18-22, 2002.
- [54] M. Dávila, J. L. Naredo, P. Moreno and A. Ramírez, "Practical Implementation of a Transmission Line Model for Transient Analysis Considering Corona and Skin Effects", *IEEE Bologna Power Tech International Conference*, June 23-26, 2003, Bologna Italy.
- [55] L. M. Wedepohl and L. Jackson, "Modified Nodal Analysis: an Essential Addition to Electrical Circuit Theory and Analysis", *Engineering Science and Education Journal*, p.p. 84-92, June 2002.

- [56] J. L. Naredo, A. C. Soudack, J. R. Marti, "Simulation of transients on transmission lines with corona via the method of characteristics", *IEE Proc. C, Gen. Trans. Dist.*, vol. 142, no.1, pp. 81-87, 1995.
- [57] J. L. Guardado, K. J. Cornick, "Calculation of Machine Winding Electrical Parameters at High Frequencies for Switching Transient Studies", *IEEE Trans. on Energy Conversion*, vol. 11, No. 1, March 1996.
- [58] F. J. Harris, "On the Use of Windows for Harmonic Analysis with the Discrete Fourier Transform", *Proc. of the IEEE*, vol. 66, no. 1. January 1978.
- [59] C. F. Wagner, I. W. Gross, and B. L. Lloyd, "High-voltage Impulse Test on Transmission Lines," *Amer. Inst. Elect. Eng. Trans.*, pt. III-A, vol. 73, pp. 196–210, April 1954.
- [60] D. J. Wilcox, "Numerical Laplace Transformation and Inversion", *Int. J. Elect. Enging. Educ.*, vol 15, pp. 247-265, 1978.
- [61] L. M. Wedepohl, "Power System Transients: Errors Incurred in the Numerical Inversion of the Laplace Transform", *Proc. of the 26th Midwest Symposium on Circuits and Systems*, August 1983.
- [62] A. Semlyen, A. Dabuleanu, "Fast and Accurate Switching Transient Calculations on Transmission Lines with Ground Return Using Recursive Convolutions", *IEEE Trans. Power Apparatus and Systems*, vol. PAS-94, pp. 561-571, March/April 1975.
- [63] T. Hosono, "Numerical Inversion of Laplace-transform and some Applications to Wave Optics", *Radio Sci.*, 1982, no. 16, pp. 1015-1019.
- [64] M. M. Saied, A. S. Alfuhaid and M. E. Elshandwily, "s-Domain Analysis of Electromagnetic Transients on Non-uniform Lines", *IEEE Trans. Power Delivery*, vol. 5, no. 4, pp. 2072-2083, 1990.

Appendix A : The Numerical Laplace Transform

A.1 Introduction

The Laplace transform is a very powerful analysis tool for the solution of ordinary differential equations. However, its application to practical problems is limited, given that the transformation from time to frequency domain and vice versa can be very difficult or even impossible. Besides, the time domain function may not be analytically defined, but through graphics, experimental measurements, sections or in discrete form. Particularly, the analytical solution of systems whose parameters depend non linearly on the frequency, such as transmission lines, is practically impossible. To overcome these situations, numerical transformations can be used instead of the analytical expressions.

A.2 Analysis of Errors

The numerical inversion of the Laplace transform introduces two kinds of errors: Gibbs oscillations due to the truncation of the integration range and aliasing due to the discretization of the frequency spectrum. Gibbs oscillations can be reduced using weighting functions known as windows. In the case of the aliasing error, this is reduced applying a damping factor $\exp(-ct)$. The exactitude of the new function depends on the correct choice of the damping constant c .

An evaluation of the effectiveness of four of the most common windows (Hanning, Lanczos, Blackman and Riesz) to reduce truncation errors was performed [58]. The window functions were applied to the numerical inversion of the Laplace transform of a delayed cosine function given by

$$f(t) = u(t - \tau) \cos[\omega(t - \tau)] \quad (\text{A.1})$$

with $\omega = 377 \text{ rad/s}$ y $\tau = 2 \text{ ms}$. The corresponding Laplace transform of (A.1) is

$$F(s) = \exp(-\tau s) \frac{s}{s^2 + \omega} \quad (\text{A.2})$$

A number of 256 samples were used for the NLT and observation times T of 1 and 3 cycles were tested (1 cycle = 16.66 ms). Fig. A.1 shows the relative error obtained with each window in one cycle, while fig. A.2 shows the error in 3 cycles. This error was computed as follows:

$$err = \frac{|f_2(t) - f(t)|}{\max[f(t)]} \quad (\text{A.3})$$

where $f_2(t)$ is the numerical approximation of the function $f(t)$ given in (A.1). All four windows gave excellent results when used in one cycle. However, as seen in fig. A.2, Lanczos and Riesz windows gave poor results with a larger observation time.

In addition, two methods based on empiric tests for calculating the damping constant c were analyzed. The first one was proposed by Wilcox [60] and is given by

$$c = 2\Delta\omega \quad (\text{A.4})$$

while the second was proposed by Wedepohl [61]:

$$c = \frac{\ln(N^2)}{T} \quad (\text{A.5})$$

The same cosine function given by (A.1) was used in this analysis. The evaluation was performed for three different numbers of samples: 2^8 , 2^{10} and 2^{12} . The errors obtained are shown in figs. A.3 and A.4. As seen in Fig. A.3, the use of Eq. (A.4) gives good results, but the error remains constant as the number of samples is increased (with the same observation time). In the other hand, applying (A.5) the error decreases when the number of samples is increased. Therefore, with Wedepohl's equation the aliasing error can be reduced by increasing the number of samples used in the simulation.

It is important to notice in figs. A.1 to A.4 the presence of an error of almost 100% at 2ms. This time instant corresponds to the cosine function delay. This is explained by the finite elevation time that results from the numerical evaluation of the inverse Laplace integral.

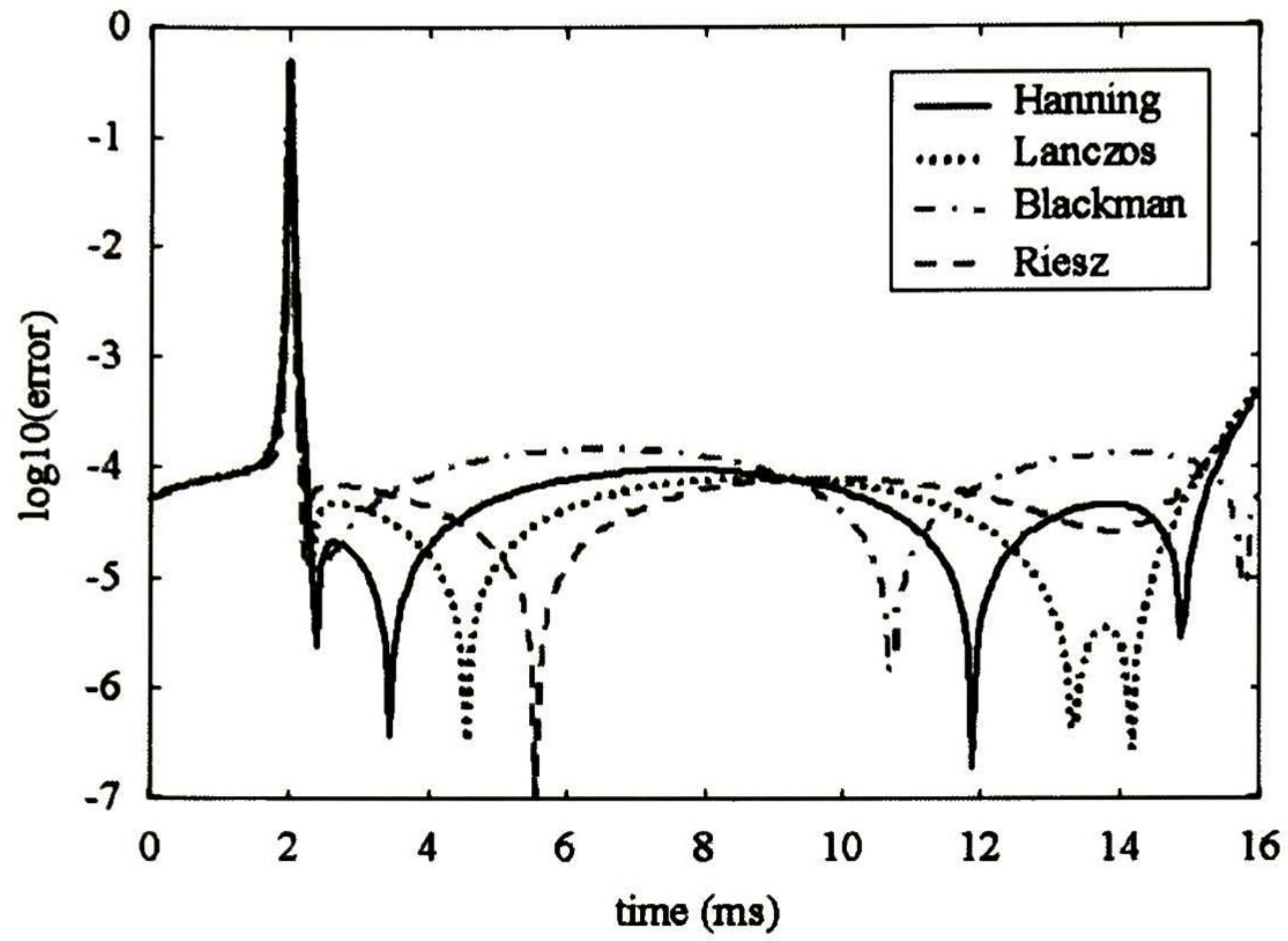


Figure A.1. Errors obtained with 4 different windows (1 cycle).

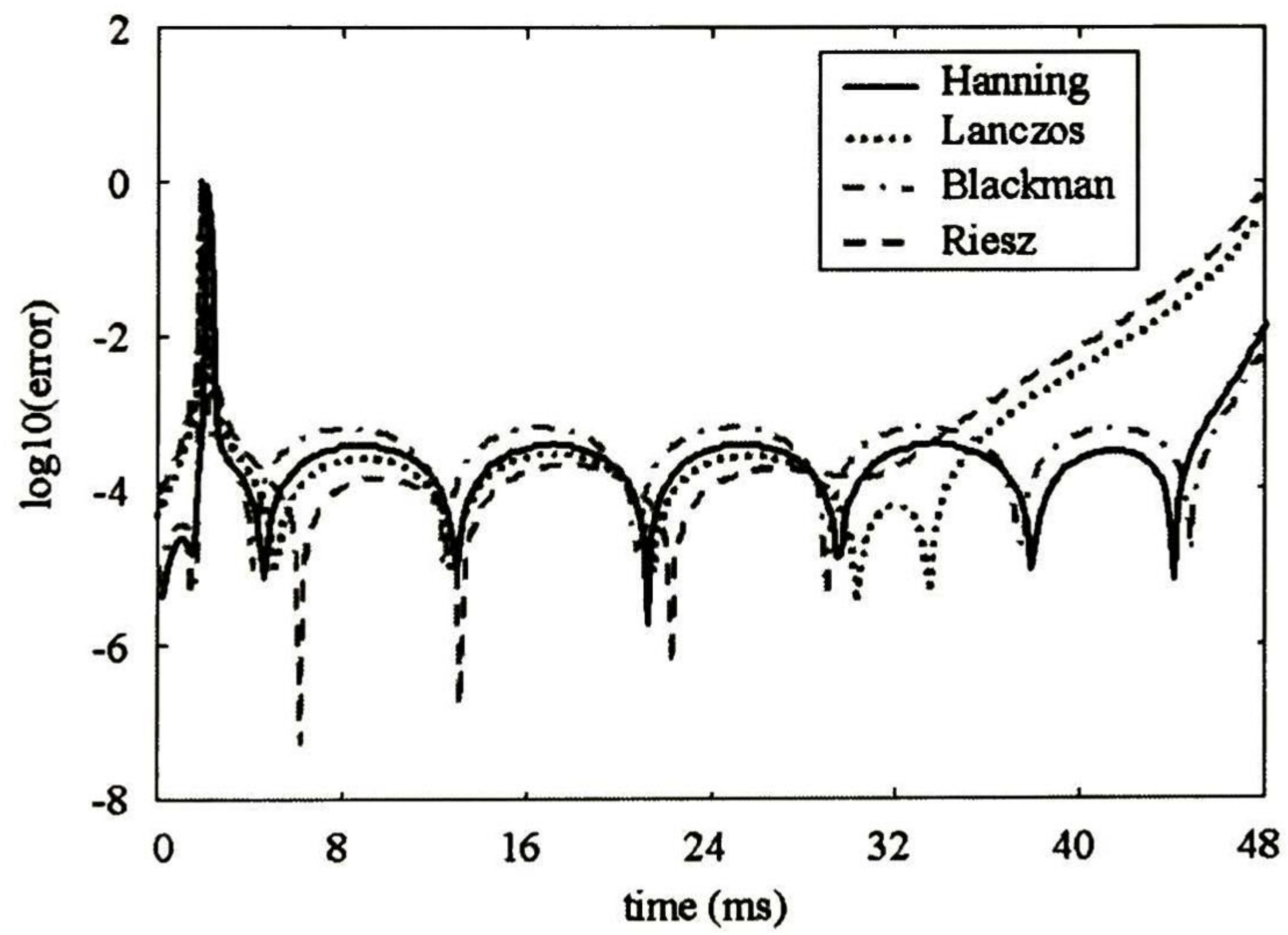


Figure A.2. Errors obtained with 4 different windows (3 cycles).

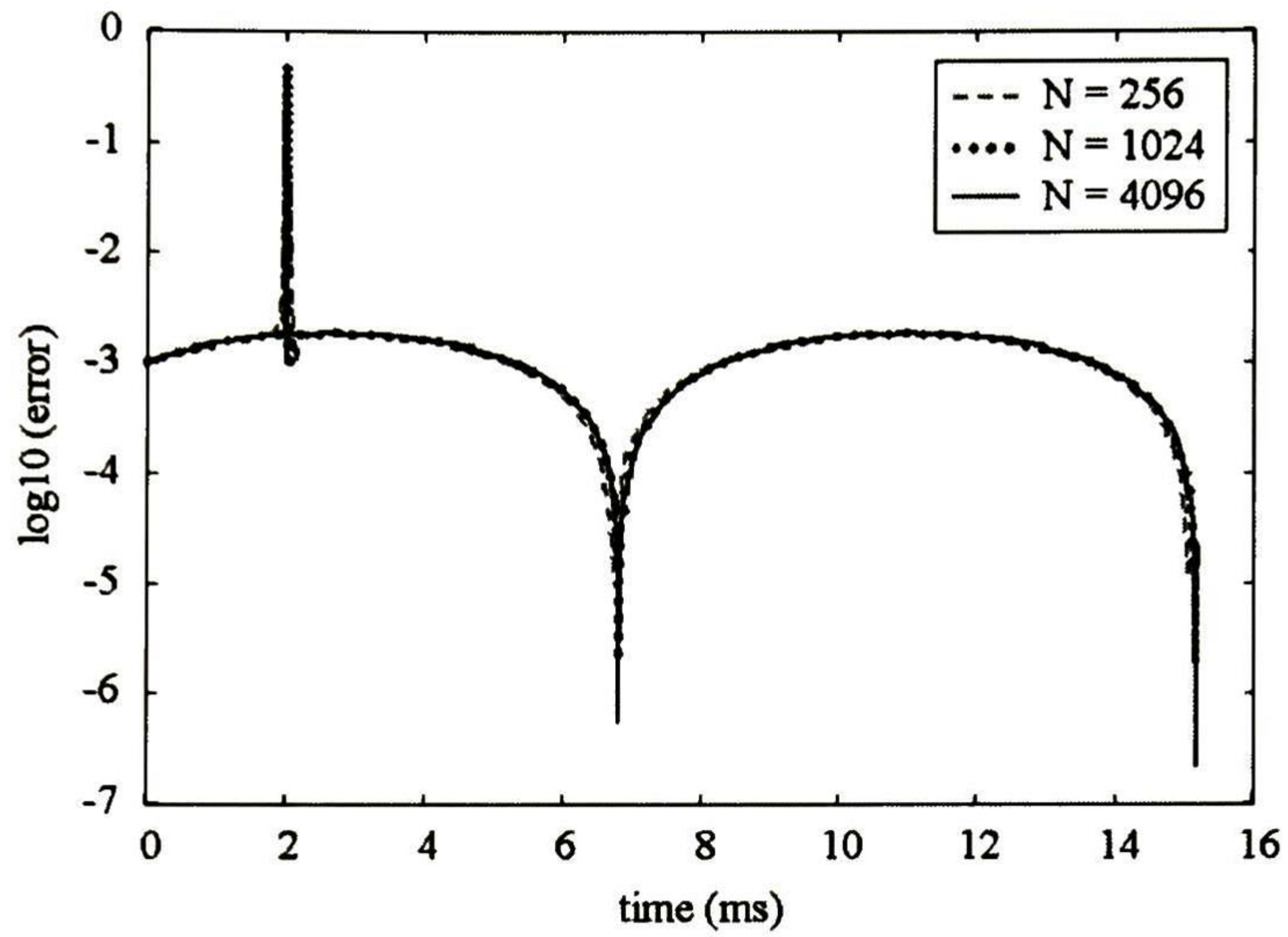


Figure A.3. Errors obtained with $\epsilon = 2\Delta\omega$ (Wilcox).

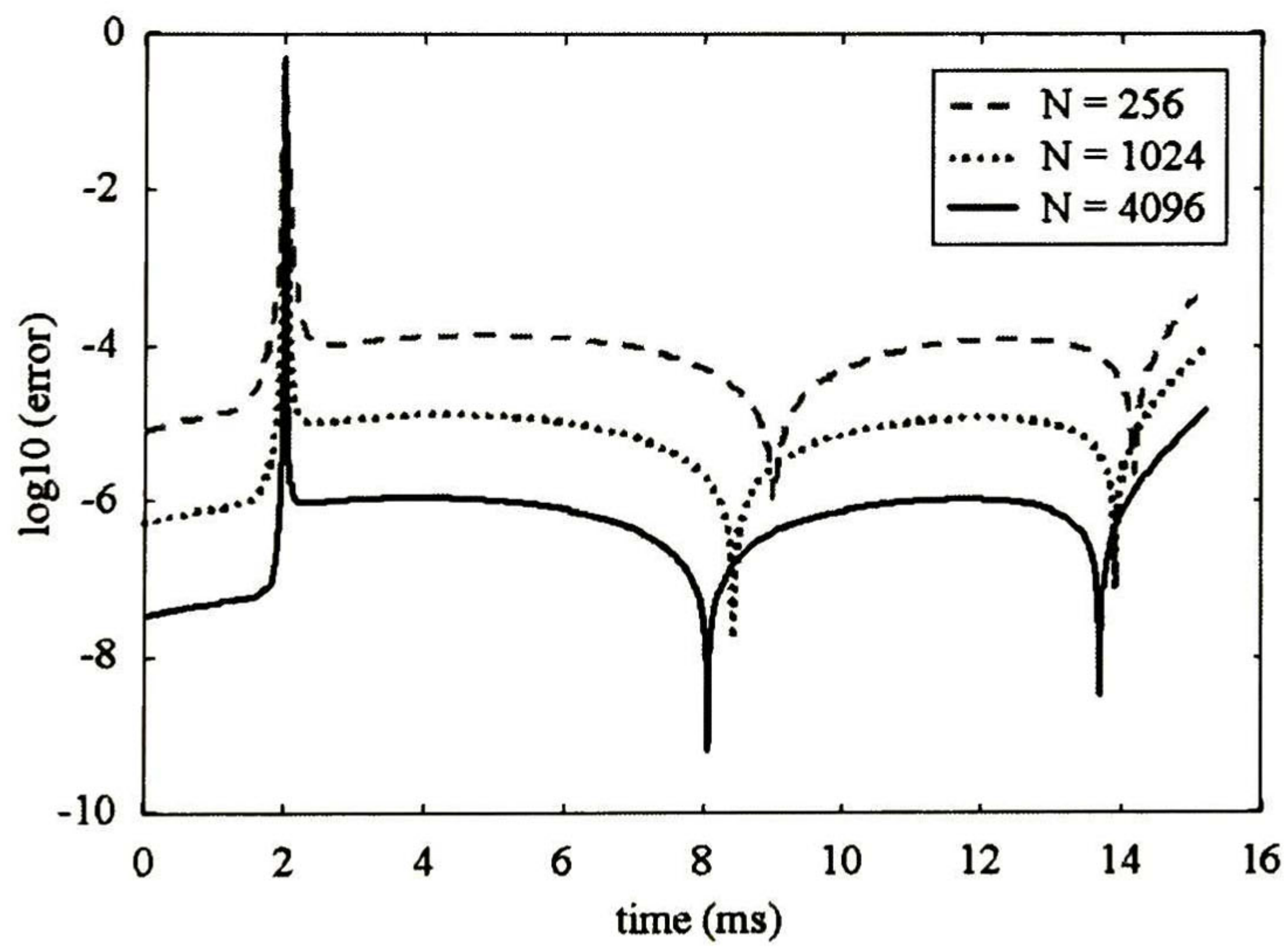


Figure A.4. Errors obtained with $\epsilon = \ln(N^2)/T$ (Wedepohl).

A.3 Discretization of the Laplace Transform Pair

Let $f(t)$ be a real and causal function of time and $F(s)$ its image in the Laplace domain. Considering a finite integration range and including a window function $\sigma(\omega)$, the inverse Laplace transforms can be written as

$$f(t) \cong \operatorname{Re} \left\{ \frac{e^{ct}}{\pi} \int_0^{\Omega} \sigma(\omega) F(c + j\omega) e^{j\omega t} d\omega \right\} \quad (\text{A.6a})$$

where $s = c + j\omega$, c is the damping constant, ω is the angular frequency and Ω is the maximum frequency. Besides, if the integration range of the direct Laplace transform is truncated, it yields

$$F(c + j\omega) \cong \int_0^T [f(t) e^{-ct}] e^{-j\omega t} dt \quad (\text{A.6b})$$

where T is the observation time. The numerical form of equations (A.6) that allows using the Fast Fourier Transform (FFT) algorithm [15] to get computer time savings is as follows:

$$f_n = \operatorname{Re} \left\{ C_n \sum_{m=0}^{N-1} F_m \exp \left(\frac{j2\pi mn}{N} \right) \right\}, \quad n = 1, 2, \dots, N-1 \quad (\text{A.7a})$$

$$F_m = \sum_{n=0}^{N-1} f_n D_n \exp \left(\frac{-j2\pi mn}{N} \right), \quad m = 1, 2, \dots, N-1 \quad (\text{A.7b})$$

where

$$f_n = f(n\Delta t) \quad (\text{A.8a})$$

$$F_m = F(c + j(2m+1)\Delta\omega) \quad (\text{A.8b})$$

$$D_n = \Delta t \exp \left(-cn\Delta t - \frac{j\pi n}{N} \right) \quad (\text{A.8c})$$

$$C_n = \frac{2\Delta\omega}{\pi} \exp \left(cn\Delta t + \frac{j\pi n}{N} \right) \quad (\text{A.8d})$$

$$\sigma_m = \sigma[(2m+1)\Delta\omega] \quad (\text{A.8e})$$

$$\Delta t = \frac{T}{N}, \quad \Delta\omega = \frac{\pi}{T} \quad (\text{A.8f}), (\text{A.8g})$$

being $\Delta\omega$ the spectrum integration step, Δt the time discretization step and N the number of samples.

Appendix B : Computation of the Line Electrical Parameters

B.1 Introduction

The electrical parameters of a transmission line are completely defined with the computation of the longitudinal impedance and transversal admittance matrices per-unit-length. These terms are the essential parameters to describe the current and voltage propagation equations along the line, as shown in Eq. (2.1).

B.2 Longitudinal Impedance Matrix

The series or longitudinal impedance matrix is computed from the geometric and electric characteristics of the transmission line. In general, it is defined as the sum of 3 matrices:

$$\mathbf{Z} = \mathbf{Z}_G + \mathbf{Z}_E + \mathbf{Z}_C \quad (\text{B.1})$$

being \mathbf{Z}_G the geometric impedance matrix, \mathbf{Z}_E the earth return impedance matrix and \mathbf{Z}_C the conductor impedance matrix.

B.2.1 Geometric Impedance

The geometric impedance matrix depends basically on the geometric configuration of the line, and is given by the following expression:

$$\mathbf{Z}_G = \frac{s\mu_0}{2\pi} \mathbf{P} \quad (\text{B.2})$$

where s is the Laplace variable, μ_0 is the free space permeability ($400\pi \eta\text{H/m}$) and \mathbf{P} is the matrix of potential coefficients, defined as

$$\mathbf{P} = \begin{bmatrix} \ln \frac{D_{11}}{R_{eq,i}} & \dots & \ln \frac{D_{1n}}{d_{1n}} \\ \vdots & & \vdots \\ \ln \frac{D_{n1}}{d_{n1}} & \dots & \ln \frac{D_{nn}}{R_{eq,i}} \end{bmatrix} \quad (\text{B.3})$$

The variables involved in the Eq. (B.3) are computed applying the method of images, as shown in Fig. B.1. This yields

$$D_{ij} = \sqrt{(x_i - x_j)^2 + (y_i + y_j)^2} \quad (\text{B.4a})$$

$$d_{ij} = \sqrt{(x_i - x_j)^2 + (y_i - y_j)^2} \quad (\text{B.4b})$$

$$R_{eq,i} = \sqrt[n]{n r_i (r_h)^{n-1}} \quad (\text{B.4c})$$

where (x_i, y_i) are the coordinates of the i th phase conductor, n is the number of conductors in a bundle, r_i is the radius of the i th phase conductor, r_h is the bundle radius and $R_{eq,i}$ is the equivalent radius of the i th phase bundle.

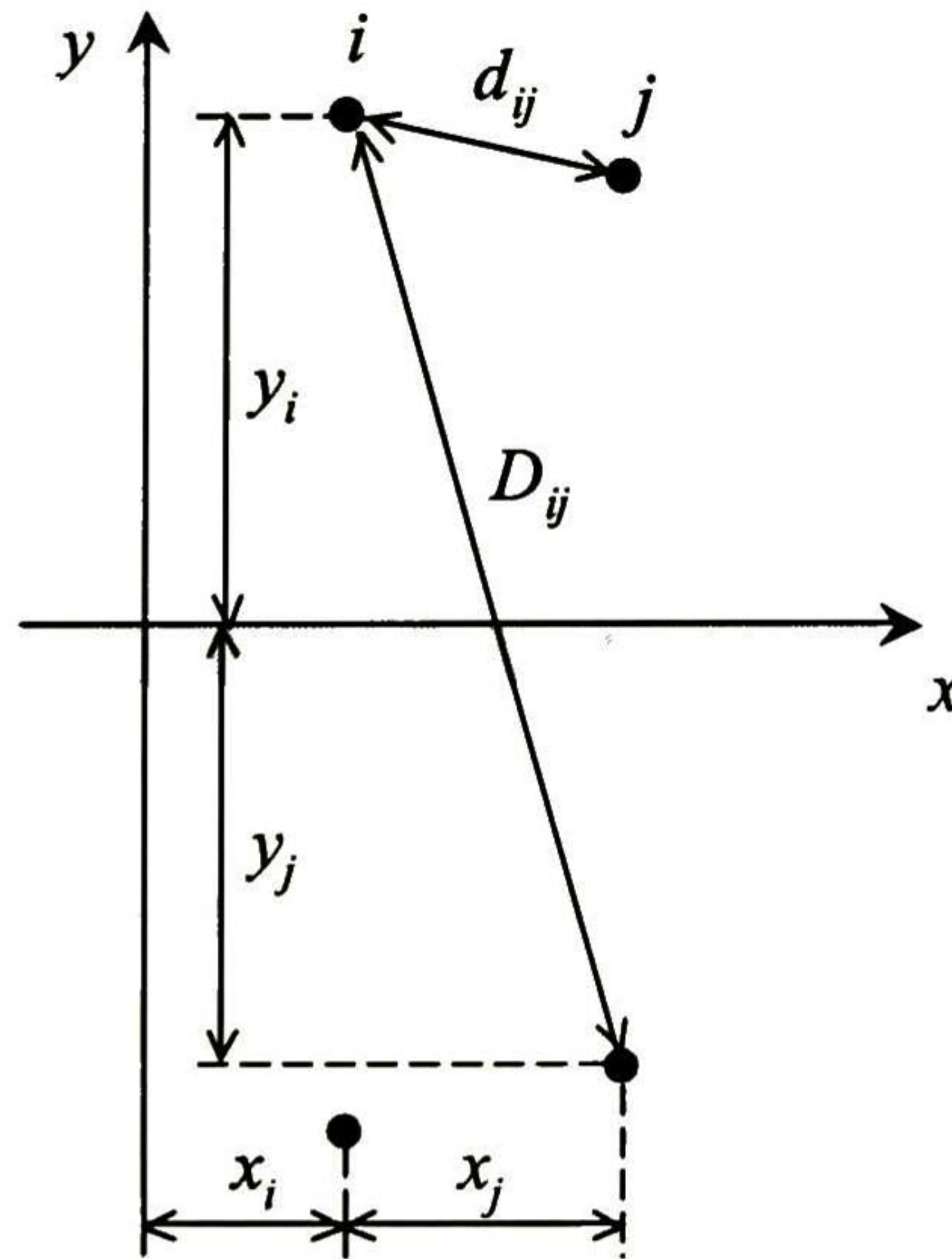


Figure B.1. Method of images.

B.2.2 Earth Return Impedance

The method of the complex penetration depth considers that the earth return currents are concentrated in a fictitious plane, parallel to the earth plane and placed at a penetration depth given by

$$p = \sqrt{\frac{\rho_e}{s\mu_e}} \quad (\text{B.5})$$

being ρ_e the ground resistivity (Ω/m) and μ_e the ground permeability (H/m). Using (B.5), it is possible to apply the method of images to compute the matrix of earth return impedances as follows:

$$\mathbf{Z}_E = \frac{s\mu_0}{2\pi} \begin{bmatrix} \ln \frac{D'_{11}}{D_{11}} & \dots & \ln \frac{D'_{1n}}{D_{1n}} \\ \vdots & & \vdots \\ \ln \frac{D'_{n1}}{D_{n1}} & \dots & \ln \frac{D'_{nn}}{D_{nn}} \end{bmatrix} \quad (\text{B.6})$$

where

$$D'_{ij} = \sqrt{(y_i + y_j + 2p)^2 + (x_i - x_j)^2} \quad (\text{B.7})$$

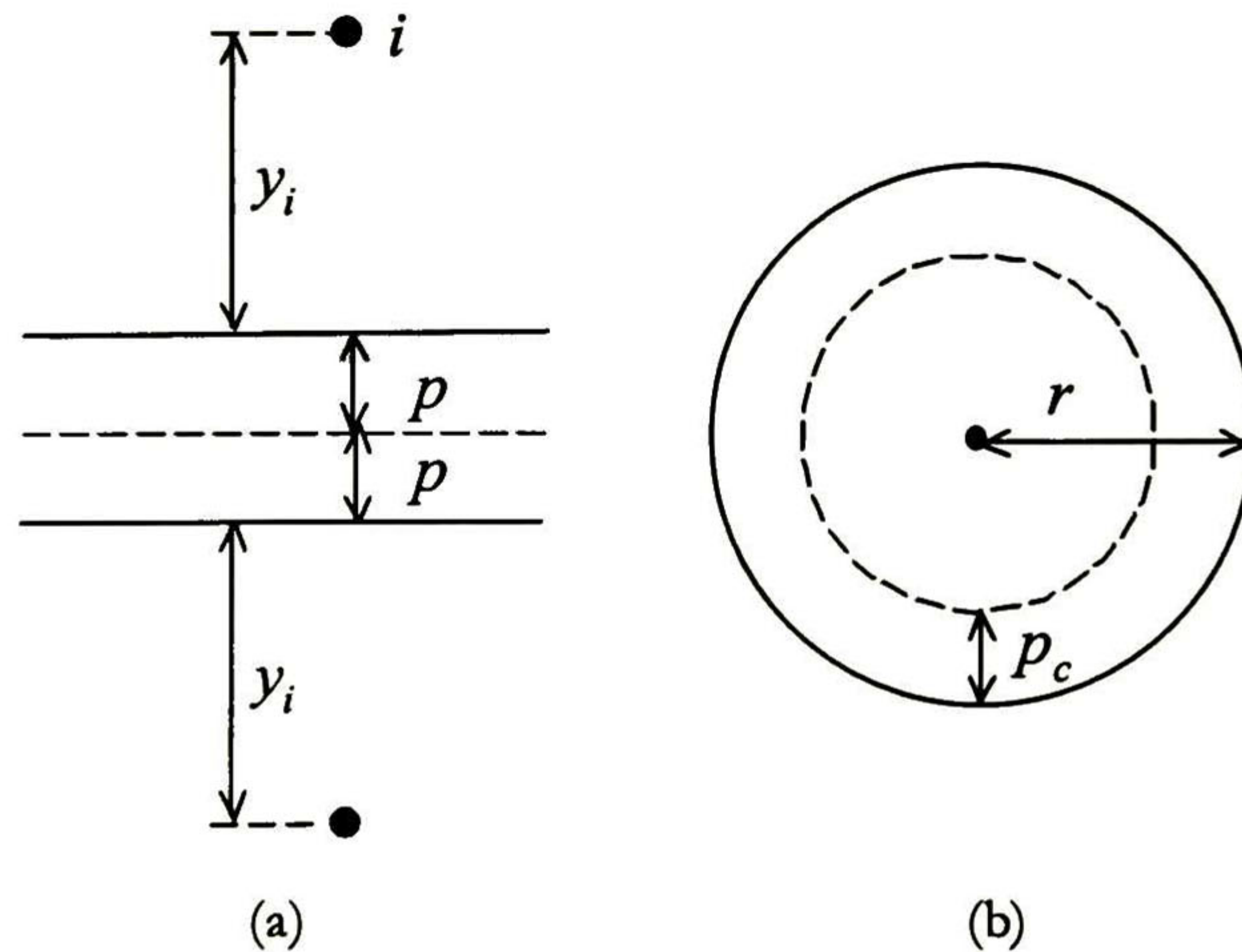


Figure B.2. Representation of the complex penetration depth: (a) earth return (b) conductor.

B.2.3 Conductor Impedance

The internal conductor impedance is produced by a phenomenon known as Kelvin or “skin” effect, which is due to the fact that the alternating current tends to flow near the conductor surface. Therefore, similarly to the earth return, a complex penetration depth can be computed for the conductors:

$$p_c = \sqrt{\frac{\rho_c}{s\mu_c}} \quad (\text{B.8})$$

Applying (B.8), the impedance of the i th phase conductor can be computed according to the following expression:

$$Z_{C,i} \cong \frac{\sqrt{R_{dc,i} + Z_{hf,i}}}{n} \quad (\text{B.9})$$

where $R_{dc,i}$ is the direct current resistance of the i th phase conductor and $Z_{hf,i}$ is its high frequency impedance. These terms are computed as

$$R_{dc,i} = \frac{\rho_{c,i}}{\pi r_i^2} \quad (\text{B.10a})$$

$$Z_{hf,i} = \frac{\rho_{c,i}}{2\pi r_i p_c} \quad (\text{B.11b})$$

where $\mu_{c,i}$ is the permeability of the i th phase conductor (H/m) and $\rho_{c,i}$ is its resistivity (Ω/m). Finally, the conductor impedance matrix for the n phases of the line is defined as

$$\mathbf{Z}_C = \text{diag}(Z_{C,1}, Z_{C,2}, \dots, Z_{C,n}) \quad (\text{B.12})$$

B.3 Transversal Admittance Matrix

Similarly to the geometric impedance matrix, the shunt or transversal admittance matrix is related to the coefficients of potential matrix. Its expression is as follows:

$$\mathbf{Y} = 2\pi\epsilon_0 s \mathbf{P}^{-1} \quad (\text{B.13})$$

where ϵ_0 is the free space permeability ($1/36\pi$ pF/m).

Appendix C : Published Work

Journal / Transaction:

1. P. Gómez, P. Moreno, J. L. Naredo, "Frequency Domain Transient Analysis of Non-Uniform Lines with Incident Field Excitation", *IEEE Trans. Power Delivery*, vol. 20, no. 3, pp. 2273-2280, July 2005.
2. P. Moreno, P. Gómez, J. L. Naredo, J. L. Guardado, "Frequency Domain Transient Analysis of Electrical Networks Including Non-linear Conditions", *ELSEVIER Int. Journal of Electrical Power & Energy Systems*, vol. 27, pp. 139-146, 2005.

Conference:

3. P. Gómez, P. Moreno, J. L. Naredo, "Modeling Non-Linear Conditions in Transmission Network Transients Using the Numerical Laplace Transform", *North American Power Symposium (NAPS) 2002*, Tempe, Arizona, U.S.A., October 2002.
4. P. Gómez, P. Moreno, J. L. Naredo, "Modelado de Condiciones No-Lineales en Redes de Transmisión Utilizando la Transformada Numérica de Laplace", *Reunión de Verano de Potencia y Aplicaciones Industriales RVP-AI/2002*, Acapulco, Gro, México, July 2002.
5. P. Gómez, P. Moreno, J. L. Naredo, M. Dávila, "Frequency Domain Transient Analysis of Transmission Networks Including Non-linear Conditions", *Proc. of IEEE Bologna Power Tech International Conference (BPT'03)*, Bologna, Italy, June 2003.
6. P. Gómez, P. Moreno, J. L. Naredo, M. Dávila, "Modeling of Non-Uniform Transmission Lines in the Frequency Domain", *North American Power Symposium (NAPS) 2003*, Saint Louis, Missouri, U.S.A., October 2003.

7. N. H. Sánchez, P. Gómez, P. Moreno, J. L. Naredo, "Frequency Domain Transient Analysis of Field excited Multiconductor Non-Uniform Lines", *North American Power Symposium (NAPS) 2004, Moscow, Idaho, U.S.A., August 2004.*
8. P. Gómez, P. Moreno, M. Dávila, J. L. Naredo, "Time Domain Analysis of Single Phase Non-uniform Lines with Frequency Dependent Electrical Parameters", *North American Power Symposium (NAPS) 2004, Moscow, Idaho, U.S.A., August 2004.*
9. P. Gómez, P. Moreno, J. L. Naredo, "Transient Analysis of Single Phase Non-uniform Lines with Frequency Dependent Electrical Parameters", *International Conference on Power Systems Transients (IPST'05), Montreal, Canada, June 2005.*



CENTRO DE INVESTIGACIÓN Y DE ESTUDIOS AVANZADOS DEL I.P.N. UNIDAD GUADALAJARA

El Jurado designado por la Unidad Guadalajara del Centro de Investigación y de Estudios Avanzados del Instituto Politécnico Nacional aprobó la tesis

Modelado de líneas de transmisión no uniformes para el análisis
de transitorios electromagnéticos

del (la) C.

Pablo GÓMEZ ZAMORANO

el día 12 de Agosto de 2005.

Dr. José Luis Naredo Villagrán
Investigador CINVESTAV 3C
CINVESTAV Unidad Guadalajara

Dr. Pablo Moreno Villalobos
Investigador CINVESTAV 3B
CINVESTAV Unidad Guadalajara

Dr. Juan Manuel Ramírez Arredondo
Investigador CINVESTAV 3B
CINVESTAV Unidad Guadalajara

Dr. Amner Israel Ramírez Vázquez
Investigador CINVESTAV 2C
CINVESTAV Unidad Guadalajara

Dr. Ricardo Octavio Mota Palomino
Profesor Investigador Titular C
Instituto Politécnico Nacional



CINVESTAV
BIBLIOTECA CENTRAL



SSIT000008393